Diffusion Dynamics of Hydronium Ions and Chlorinated Aliphatic Hydrocarbons for Microbe Encapsulating Poly(vinyl alcohol) Hydrogels

A Thesis
Presented in Partial Fulfillment of the Requirements for the
Degree of Master of Science
with a
Major in Chemical Engineering
in the
College of Graduate Studies
University of Idaho
by
Carson J. Silsby

Approved by:
Major Professor: James Moberly, Ph.D.
Committee Members: Mark Roll, Ph.D., PE; Kristopher Waynant, Ph.D.; David E. Aston, Ph.D.
Department Administrator: Dev Shrestha, Ph.D.

August 2022

Abstract

Bioremediation of chlorinated aliphatic hydrocarbons (CAHs), such as trichloroethylene (TCE), through anaerobic reductive dechlorination is one technique used to treat groundwater aquifers contaminated with CAHs. Acid generated during each dechlorination step, along with high CAH concentrations, may lead to microbial inhibition and cell death. Halting TCE reduction before complete dechlorination, for example, may leave the system more hazardous due to buildup of vinyl chloride (VC), therefore, protecting microorganisms from external inhibitory factors is crucial. Encapsulation of microorganisms in a hydrogel is one potential solution because encapsulation provides a protective barrier from inhibiting CAH concentrations and acid. The hydrogel provides a tunable environment in which microorganisms may deploy biological strategies to control local conditions, and this environment can be manipulated through engineering. However, fundamental mass transfer coefficients of these contaminants are lacking. To address this knowledge gap, mass transfer coefficients of hydronium, TCE, *cis*-1,2-dichloroethylene (cDCE), and VC, were measured in poly(vinyl alcohol) (PVA) and alginic acid (Alg) hydrogel blends at various ionic strengths. The effects of hydrogel crosslinking methods on hydronium diffusion were also investigated. Chemical crosslinking PVA with boric acid increased hydronium diffusivity by 58% while chemical crosslinking PVA / Alg with boric acid and calcium chloride decreased hydronium diffusivity by 47% when compared to the equivalent cryogel in DI water. Hydrogel blend, crosslinking method, and increases in ionic strength were found to positively affect the diffusivity of hydronium with differing magnitudes depending on the factor or combination of factors being tested. Increases in hydronium ion mass transfer were attributed to polymer contraction, increasing water fraction, solvent-polymer, and solvent-solute interactions in the hydrogel materials tested. TCE and cDCE diffusivity increased by over 100% when ionic strength was increased from 0 to 0.1 M KCl. VC saw a similar increase, but the difference was not statistically significant. A reaction-diffusion model was implemented using these diffusion coefficients to predict dechlorination in a single spherical hydrogel bead with bead radii of 0.002 – 1 cm and cell densities of $1 – 10^{12}$ cells/mL using a Monte Carlo simulation. An infinite sink was assumed outside the bead with a constant pH of 7 and a TCE concentration of 1500 ppb. This simulation found that the max molar ratio of ethylene generated per TCE degraded was 0.0005 with a bead radius of 0.2 cm and a cell density of 2.5×10^{7} cells/mL. The model predicted that microorganisms encapsulated in a single hydrogel bead could fully degrade TCE to ethylene and that the system would become pH inhibited below a pH of 5.5 due to mass transfer limitations, consistent with literature. Measured diffusion coefficients and hypothesized diffusion mechanisms in this thesis provide fundamental first-principal design information needed for future optimization of hydrogel systems.

Acknowledgements

I'd like to start by thanking my family and friends for all their love and support throughout the last three years. Especially my sister Jaclyn whose hard work, determination, and kindness inspires me every day. Without you, I wouldn't have gotten here. I'd also like to thank Charles Cornwall and Brian Petty for machining various parts for my diffusion apparatus, Thomas Williams for running XRD samples, JR Brabb and Ray Anderson for our discussions and IT support, and Benji Oswald for helping me get setup using the RCDS servers and helping debug my Slurm code.

I'd also like to thank the Department of Chemical and Biological Engineering whose faculty and staff have fostered a welcoming environment that supports collaboration and research excellence. And most of all, I'd like to thank Dr. James Moberly whose kindness, patience, and mentorship has been instrumental in my progress throughout my degree and has taught me a great deal about what it means to be a researcher and scientist. I'd also like to thank my whole committee for their support and advice throughout my degree and for pushing me to become a better researcher.

This material is based upon work supported by the National Science Foundation under Grant No. (1805358). Any opinions, findings and conclusions or recommendations expressed in this material are those of the author(s) and do not necessarily reflect the views of the National Science Foundation.

Dedication

To my parents whose love and support gave me the opportunity to seek this degree.

Table of Contents

List of Tables

List of Figures

Statement of Contribution

Chapter 2: Jonathan Counts completed multiple diffusion runs used in this section for hydronium diffusion through 10% PVA and 10% PVA / 2% Alg hydrogels in DI water and ionic solutions. The data analysis, hypotheses, conclusions, and modeling are all original work. As coauthors of the manuscript submitted to ES&T Engineering, Dr. Mark Roll and Dr. Kristopher Waynant also edited and contributed to this chapter.

Chapter 3: Jonathan Counts championed the original experimental design used in this work, but all measurements and analysis are original work. Jonathan Counts also made the base code used in the model and Dr. James Moberly and Dr. Dave MacPherson made modifications to it as well. I added pH inhibition and a steady state determination mechanism within the model to make the model more realistic to a natural system and to decrease computational time. I also developed a code to be utilized on the University of Idaho RCDS cluster to run multiple iterations of the model at one time as part of a Monte Carlo simulation.

Appendix A: Dr. James Moberly generated the sensitivity analysis plots and wrote the analysis in section 17 of Appendix A. A few plots in this appendix were also the result of work done previously by Jonathan Counts.

Chapter 1: Introduction

1.1 Chlorinated Aliphatic Hydrocarbons

Trichloroethylene (TCE) was first synthesized in Germany in 1864 and was produced on a large scale by 1910.[1,2] TCE was initially used for a variety of applications such as decaffeination, glass cleaning, metal degreasing, medical anesthetics, paint removal, and dry cleaning, eventually expanding to common household cleaners as well.[1,2] TCE toxicity was first recorded in 1916 and later in the 1920s when large scale cattle death in Europe was linked to feed treated with TCE for fat extraction.[2] Even after these initial signs of toxicity, wide spread use of TCE in industry and as a household cleaner continued with little scrutiny until 1966 when the Los Angeles county implemented emission regulations on TCE due to smog formation, which was followed by federal regulations in the 1970s.[2] In 1980, TCE was classified as a hazardous waste product,[2] and the Comprehensive Environmental Response, Compensation & Liability Act was passed, establishing funding specifically for the clean-up of hazardous chemicals, i.e. superfund sites.[1] Due to the discovery of widespread groundwater contamination at these superfund sites across the US, drinking water standards for TCE and other CAHs were established in 1989 under the Safe Drinking Water Act (1974).[1,2] It wasn't until 2011 that the EPA formally acknowledged TCE as a carcinogen. TCE is expected to cause liver and kidney cancer and has been linked to malignant lymphoma, testicular cancer, and leukemia.[3] Due to these health hazards TCE remediation has been a top priority for EPA clean-up efforts even today as new contamination sites are still identified.[4] TCE and its degradation byproduct vinyl chloride (VC) are number 16 and 4 on the ASTDR substance priority list[5] respectively.

TCE poses a serious occupational hazard via skin absorption and inhalation, but luckily some companies have opted to replace TCE with a less toxic alternative, methylene chloride.[1] Unfortunately, unsafe disposal practices and improper storage of TCE has led to numerous incidents of environmental release which can also pose a risk to both workers and the general population around the site of contamination. TCE is known as a dense nonaqueous phase liquid (DNAPL), which is meant to describe its physical properties in relation to water. TCE is more dense than water (1.46 g/mL) and has a low solubility limit.[6] In the case of a large spill, due to its high density and low solubility, TCE will accumulate on bed rock at the bottom of groundwater aquifers, slowly dissolving into the flowing ground water stream.[6] A large spill may lead to widespread contamination if TCE is allowed to migrate from the source plume to adjacent areas by groundwater flow, which may include rivers, lakes, or drinking water sources.[6] There have been multiple instances where TCE has been detected in residential wells, leading to major health consequences to its residence.[3,7] Contaminated aquifers may also lead to long term inhalation exposure since CAH fumes may evaporate from the water column and escape

through topsoil into the air, and potentially into the airspace of residential homes, a process called vapor intrusion[3], similar to radon gas intrusion. CAHs absorbed into the walls and foundation of residential homes may also lead to long term exposure of CAHs.[7] To limit the transport and spread of contaminants such as TCE in groundwater sources, quick identification and source-based remediation technologies are needed. There is no universal treatment option for contamination clean up due to biogeochemical variability between sites. Each contamination site has a unique location with geological and geographical challenges, as well as logistical challenges such as distance to available power, distance to public water sources (e.g., rivers, lakes, ocean), and completion requirements depending on regulation, financial timelines, or construction. Source based remediation technologies currently being utilized and investigated are pump and treat, air sparging, biosparging, in situ thermal treatment, oxidation processes, phytoremediation, zero valent metals (ZVMs), and activated carbon.[8] Each contamination site is unique with various biogeochemical, physical, and logistical factors that may ease or complicate remediation efforts, therefore each specific site must be thoroughly evaluated to determine the best course of action for remedial treatment.

1.2 Current Remediation Technologies

1.2.1 Direct CAH removal

Limiting the migration of CAH contaminants in ground water systems is the primary goal of remediation efforts to contain the affected area and to limit the overall impact of contamination. This objective can be accomplished by directly removing CAHs from the contaminated aquifer, assuming the exact location of the source plume is known. Extraction of the CAH source plume removes the most contaminated area of the aquifer therefore limiting contaminant migration, making it easier to utilize other remediation techniques on lower concentration areas. The use of other remediation technologies after direct CAH removal is often necessary because additional CAHs are likely absorbed into the soil surrounding the aquifer and will require in situ treatment. Additionally, migration of contaminants downstream or deeper within the aquifer may have already occurred and therefore contamination may exist in the aquifer requiring further treatment.

CAHs may be directly removed from the contaminant site by drilling a well over the contaminant plume and pumping the contaminated water out of the aquifer into a storage tank or onsite treatment system.[6] Ground water pumped out of the aquifer will need to be treated to remove CAHs and other contaminants before being injected back into the aquifer. In the case where the spill is found early or when the majority of CAH's are above the water column, vacuum extraction can be used to volatilize the CAH's from the top soil.[6] The resulting vapors are recovered at the surface and further treated.[6] The downside of direct CAH removal is the risk and cost of either further storage (and another potential spill) or

additional downstream processes for treatment. Some treatment options include combustion, oxidation, and adsorption.

The removal of contaminated soil by excavation comes with additional challenges. Moving and digging up contaminated soil could lead to accidental contamination of nearby areas that were previously uncontaminated due to contaminated dirt particles entrained in the air, missed by excavation and retained in the environment, or from contaminated solids spilling out of storage trucks during transport. Additionally, excavation could also increase the risk of exposure to all workers due to the inevitable volatilization of CAHs.

1.2.2 Thermal treatment

Combustion of liquid CAHs is an energy intensive thermal remediation method to completely decompose all contaminants after first pumping contaminated water out of the aquifer and separating the CAHs from water. Combustion products of CAHs include CO_2, H_2O, and HCl, which must be further treated to limit environmental release of acidic vapors and CO_2 into the enviroment.[8] Catalytic combustion has become the preferred method of combustion as opposed to thermal combustion due to low conversion and generation of toxic biproducts in thermal incinerators.[8,9] Mixed oxide catalysts such as cerium-zirconium, chromium-cerium, titanium-vanadium, and nanocrystalline cobalt(II,III) oxide have been utilized to increase conversion of CAHs such as TCE and 1,2-*cis*-dichloroethylene (cDCE) to combustion products.[8] Mixed titanium-zirconium-montmorillonite clays have also been found to aid in the catalytic combustion of TCE.[8] The need for further downstream treatment and separation can drive up the cost of catalytic and noncatalytic combustion, making this treatment option less viable for long term use. Generation of large quantities of CO_2 is also unavoidable, so other forms of CAH treatment should be investigated to limit further environmental pollution. This treatment option is limited since it requires pumping water out of the aquifer before treatment and therefore is unable to treat soil or other contaminated solids, unless the soil is removed and shipped offsite for treatment.

Smoldering is an option for treatment of contaminated soils using the STAR technology.[10] For in situ treatment, STAR utilizes air pumped into the aquifer and a heating source which starts the smoldering reaction by oxidizing the soil surrounding the heat source. While there is no literal combustion, the smoldering heats the soil enough to release contaminants and has been shown to be very effective with greater than 98% removal of organic contaminants.[10] Smoldering is also energy efficient, because the heat generated during oxidation of the soil keeps the reaction going, as long as there is continuous air flow, requiring little energy input after the initial startup.[10] The rate of smoldering is controlled by the air flow. If air flow is stopped, smoldering will die out quickly due to heat loss to the surrounding soil.[10] Smoldering can also be used for treatment of excavated soil, but there is considerable risk of

contaminate exposure to workers during the excavation process, so in situ treatments are preferred. One major drawback of smoldering is that it kills off biological life within the soil.

1.2.3 Adsorption

Carbon based adsorption materials such as activated carbon[11] and carbon nanotubes[12] can be used to soak up TCE and other CAHs from either a liquid or gas stream in an adsorption column.[8] Adsorbents do not degrade the CAHs on their own so further modification or downstream processes are required to remove CAHs.[8,13] Even though further treatment is needed, this method is useful for limiting the spread of CAHs in ground water aquifers by trapping the CAHs in a stable solid material. Additional work has been done by Zhou et al. to add activated carbon to other remediation techniques (e.g., bioremediation) to increase the dechlorination efficiency of that technique.[13]

1.2.4 Phytoremediation

Phytoremediation is a remediation technique which uses plants to remove contaminants from soil. Various plants such as poplars,[14,15] tobacco,[16] leguminous trees,[17] fruit trees,[18,19] willows,[20] and alfalfa[21] have been shown to be effective at removing TCE from soil. When choosing a plant to achieve remediation goals, several factors should be considered: the local climate and geology, the concentration of contaminants to be remediated, the plant's resistance to that concentration of contaminant, and the plant's uptake or degradation rate of the contaminant of interest.[22] Phytoremediation is a time intensive remediation technique and is dependent on how fast a plant can absorb and degrade the contaminants of interest. Additionally, the plants are often toxic after the remediation process due to absorption of contaminants and therefore require safe disposal once removed.[22,23]

1.2.5 Oxidation

Oxidation of TCE has been shown to be an effective form or remediation using compounds such as potassium permanganate, hydrogen peroxide, persulfate, and ozone. When TCE is oxidized by potassium permanganate, carboxylic acids and permanganate ions are the main products, and the carboxylic acids can be further oxidized to CO_2 as well.[24] H_2O_2 has been shown to degrade TCE by a Fenton reaction using pyrite as a catalyst, achieving 97% conversion.[8,25] Hydrogen peroxide has also been used in addition to ozone for the remediation of TCE since a small amount of peroxide (2% v/v) can extend ozone's' lifetime in aqueous solutions, and therefore increasing the amount of TCE that can be oxidized. Oxidation of TCE by persulfate is a common remediation technique which can be done in acidic, basic, or neutral conditions.[26] Persulfate generates sulfate and hydroxyl free radicals, which can oxidize TCE. Sulfate free radicals oxidize TCE into harmless products (CO_2, SO_4^{2-}, H^+, and Cl^-) and hydroxyl free radicals oxidize TCE into dichloroacetic acid.[26]

1.2.6 Electrochemical degradation

Electrochemical reductive dechlorination has been shown to efficiently degrade trichloroethylene to ethylene and ethane on a copper cathode and iron anode with greater than 95% conversion.[8,27] Additionally, an iron-nitrogen doped carbon cathode used with a platinum anode yielded over 95% removal of TCE during five reuse cylces.[28] Electrochemical degradation methods are still being developed and show promise for the remediation of CAHs but are energy intensive and possess safety challenges due to the generation of hydrogen and oxygen typical of electrochemical processes.

1.2.7 Zero valent metals

Iron, zinc, and magnesium are common ZVMs used for TCE remediation.[29] ZVMs are currently deployed in two main forms, as a permeable reactive barrier or by direct injection. Permeable reactive barriers are generally used to treat a contaminated area downstream from the source by placing a large permeable membrane in front of the contaminant plume. This procedure stops the plume from spreading further downstream while also using groundwater flow to drive the contaminant through the membrane.[30] Zero valent metal granular particles can be used in the membrane as the reactive component. For direct injection, smaller ZVM particles (micro or nano) are used to increase reactivity and to allow for easy transport through the aquifer.[30] Nanoparticles, in particular, show promise due to their large surface area to volume ratio which may improve reactivity and limit the need for the injection of large quantities of ZVM, but nanoparticles are still being actively researched and little is known about their impacts on the environment. Zero valent iron (ZVI) is the most common ZVM currently deployed for TCE remediation. ZVI degrades TCE by β-elimination and a study done by Farrell et al.[31] found that acetylene was the main byproduct, accounting for 90% of the reaction byproducts in their study. The application of ZVI in conjunction with biodegradation has also been investigated and shows that when coupled, increases the dechlorination efficiency of ZVI.[8,30,32] Zero valent zinc was also investigated by Cheng and Wu[33] who found that zinc lasted longer and could degrade 10x more TCE compared to ZVI. Zero valent magnesium was investigated by Marshall and Pensini[34] who found that magnesium could degrade TCE, but without the presence of a catalyst (e.g., platinum, activated carbon, vitamin B_{12}) the reaction would be inefficient in comparison to ZVI. Magnesium holds many desirable characteristics including a high reduction potential.[34]

1.2.8 Air sparging / biosparging

Air sparging is an in-situ groundwater remediation technique which utilizes air injection to partition CAHs, and other volatile organic compounds, out of groundwater and into the gas phase.[35] Pressurized air travels from the injection point (in the water table) up the aquifer, volatizing CAHs, and is collected near the surface using a vacuum extraction system. Air sparging can be modified to increase CAH

removal by adding microbial substrates such as butane or propane into the inlet pressurized air stream to enhance natural bioremediation.[36] One downside to air sparging is that it is completely dependent on soil permeability and can therefore be ineffective when used in sites with tightly packed soil,[35] and should therefore only be used when the geology of the contaminant site can be well characterized to ensure successful remediation efforts.

Biosparging is similar to air sparging, but in biosparging, air is injected below the water column to avoid contaminant vaporization and subsequent release. The air injected during biosparging is meant to stimulate aerobic microbial activity by supplying microorganisms with a constant source of oxygen. This process has been shown to effectively boost microbial co-metabolism of TCE.[37] Similar to air sparging, biosparging can only be utilized when the soil conditions under the aquifer are favorable. If the soil is not compact, the air pumped in will travel up and release CAHs into the environment causing a hazard to workers and the public. In this case, biosparging is also useless because a majority of the oxygen released in the system will likely be unavailable to microorganisms, therefore geological conditions must be extensively characterized before biosparging is implemented for CAH remediation.

1.2.9 Bioremediation

Bioremediation of CAHs can be completed by reductive dechlorination utilizing anaerobic microorganisms (see **Figure 1.1**) or aerobic co-metabolism. Bioremediation can be divided into two categories: biostimulation and bioaugmentation. Biostimulation utilizes existing microbial populations in a contaminated aquifer by injecting compounds such as substrates and electron donors, which encourage and drive reductive dechlorination processes as well as other microbial activity.[38,39] Biostimulation is often unreliable and gives inconsistent results due to inter-microbial interactions, resource competition, and biogeochemical factors.[39] An example of biostimulation would be the direct injection of substrates like emulsified vegetable oil, formate, or lactate which lowers the oxidation/reduction potential and generates hydrogen, an electron donor, during fermentation in anaerobic systems. Bioaugmentation is similar to biostimulation, but specific organisms are added to the aquifer instead to efficiently degrade CAHs.[39] By specifically targeting CAHs, a larger degree of control is achieved. In some cases, competition between naturally occurring microorganisms and the added microorganisms can severely deplete the available nutrients, negatively impacting degradation efficiency.[38] Often, the generation of electron donors such as molecular hydrogen will aid in increasing the efficiency of microbial degradation after injection of substrates.[40]

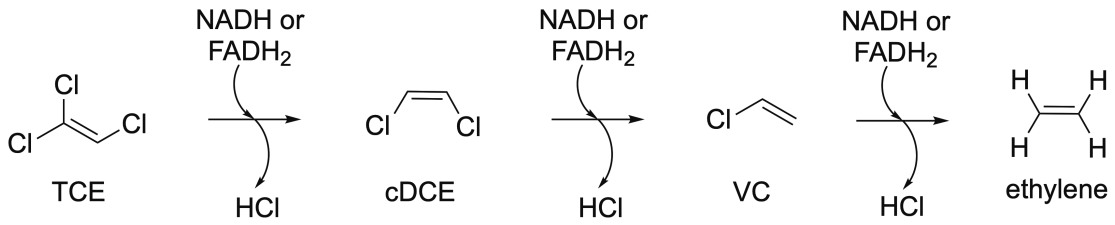

Figure 1.1: *Anaerobic reductive dechlorination mechanism of TCE to a nontoxic compound, ethylene. Hydrogen is the electron donor used by microbes to complete dechlorination.*

Bioremediation is a cost-effective method for TCE clean-up efforts,[41] but if done improperly, may leave the system in a more toxic state due to the degradation biproducts of TCE. When TCE is anaerobically reduced by microorganisms, it is first reduced to cDCE, then VC, and finally ethylene. Ethylene is the only nontoxic biodegradation biproduct, cDCE is the least toxic, and VC is the most toxic. For reference, the drinking water standards for TCE, cDCE, and VC are 5 ppb, 70 ppb, and 2 ppb respectively.[42] The detection limit for TCE and VC is 1 ppb using EPA method 8260B or 8021B.[43,44] Acid is also generated as a biproduct of CAH dechlorination as shown in **Figure 1.1**. At each step in the dechlorination process, acid is released in a 1:1 molar ratio. Dechlorinating microbes often used in remediation efforts such as *Dehalococcoides mccartyi*, *Dehalobacter*, and *Dehalogenimonas* are sensitive to system pH, and their dechlorination efficiency will decrease as pH varies from their optimal range.[45] In extreme cases, cell death will occur at a pH of 5.0.[46] Previous work utilizing microbial consortia for dechlorination have combat acid generation by directly injecting buffers such as sodium bicarbonate to decreases system pH, but multiple injections were required to keep up with acid accumulation.[47] While shown to be effective, frequent injection of bicarbonates can be costly and time consuming.

Anaerobic reductive dechlorinating microorganisms can also be inhibited by other CAHs.[48,49] CAH concentration induced inhibition can limit the efficiency of dechlorination by limiting where microbes can be injected into the aquifer. If microbes are placed too close to the source plume, they will be inhibited and may die, but if placed too far away, there is a risk that the CAHs will spread or volatilize before the microbes get a chance to degrade them. Therefore, protecting microorganisms from inhibitory factors is vital to more efficient and successful CAH bioremediation efforts.

1.3 Proposed Solution

1.3.1 Microorganism encapsulation

The proposed solution to acid buildup and CAH inhibition in anaerobic reductive dechlorinating systems is to encapsulate microorganisms in a biocompatible hydrogel, creating a “biobead.” The hydrogel will provide a diffusive barrier to shield microorganisms from large concentration changes

which allows microbes to better control their local environment. Environmental conditions such as salinity, temperature, and pH are some of the site-specific factors which should be considered when utilizing this technology since transport through the hydrogel may differ based on these factors. Hydrogels are tunable materials that can be modified to limit or intensify the effects of these factors. Studies completed by Zhou et al.,[13] Wang and Tseng,[50] and Kim et al.[51] have demonstrated the capability of encapsulated microorganisms to degrade CAHs, but do not attempt to optimize the biobead design parameters such as gel material, cell density, or bead diameter. To optimize the design of biobeads, the speed at which each species of interest travels through the hydrogel must be determined to estimate the reactivity of the microorganism and to complete a mass balance. Therefore, the diffusion of hydronium and CAHs through various hydrogel membranes, made by chemical or physical crosslinking, were investigated in deionized water and ionic conditions. Various ionic concentrations were investigated to cover a range of possible conditions found in groundwater systems. Understanding how the diffusion of each species of interest changed with ionic concentration, as well has how the hydrogel was affected, provides important first principle design information needed to optimize biobeads.

1.4 References

(1) Doherty, R. E. History of TCE. In *Trichloroethylene: Toxicity and Health Risks*; Gilbert, K. M., Blossom, S. J., Eds.; Molecular and Integrative Toxicology; Springer: London, 2014; pp 1–14. https://doi.org/10.1007/978-1-4471-6311-4_1.

(2) *A History of the Production and Use of Carbon Tetrachloride, Tetrachloroethylene, Trichloroethylene and 1,1,1-Trichloroethane in the United States: Part 2--Trichloroethylene and 1,1,1-Trichloroethane: Environmental Forensics: Vol 1, No 2*. https://www.tandfonline.com/doi/abs/10.1006/enfo.2000.0011 (accessed 2021-09-25).

(3) ATSDR. Toxicological Profile for Trichloroethylene. **2019**.

(4) US EPA, O. *National Priorities List (NPL) Sites - by State*. https://www.epa.gov/superfund/national-priorities-list-npl-sites-state (accessed 2022-05-10).

(5) *ATSDR's Substance Priority List*. https://www.atsdr.cdc.gov/spl/index.html (accessed 2022-04-11).

(6) Huling, S.; Weaver, J. Ground Water Issue: Dense Nonaqueous Phase Liquids. 21.

(7) Ma, J.; McHugh, T.; Beckley, L.; Lahvis, M.; DeVaull, G.; Jiang, L. Vapor Intrusion Investigations and Decision-Making: A Critical Review. *Environ. Sci. Technol.* **2020**, *54* (12), 7050–7069. https://doi.org/10.1021/acs.est.0c00225.

(8) Dai, C.; Zhou, Y.; Peng, H.; Huang, S.; Qin, P.; Zhang, J.; Yang, Y.; Luo, L.; Zhang, X. Current Progress in Remediation of Chlorinated Volatile Organic Compounds: A Review. *J. Ind. Eng. Chem.* **2018**, *62*, 106–119. https://doi.org/10.1016/j.jiec.2017.12.049.

(9) Dai, Q.; Wang, X.; Lu, G. Low-Temperature Catalytic Combustion of Trichloroethylene over Cerium Oxide and Catalyst Deactivation. *Appl. Catal. B Environ.* **2008**, *81* (3), 192–202. https://doi.org/10.1016/j.apcatb.2007.12.013.

(10) Gerhard, J. I.; Grant, G. P.; Torero, J. L. Chapter 9 - Star: A Uniquely Sustainable in Situ and Ex Situ Remediation Process. In *Sustainable Remediation of Contaminated Soil and Groundwater*;

Hou, D., Ed.; Butterworth-Heinemann, 2020; pp 221–246. https://doi.org/10.1016/B978-0-12-817982-6.00009-4.

(11) Nikam, S.; Mandal, D. Experimental Study of the Effect of Different Parameters on the Adsorption and Desorption of Trichloroethylene Vapor on Activated Carbon Particles. *ACS Omega* **2020**, *5* (43), 28080–28087. https://doi.org/10.1021/acsomega.0c03648.

(12) Shih, Y.; Li, M. Adsorption of Selected Volatile Organic Vapors on Multiwall Carbon Nanotubes. *J. Hazard. Mater.* **2008**, *154* (1), 21–28. https://doi.org/10.1016/j.jhazmat.2007.09.095.

(13) Zhou, Y.-Z.; Yang, J.; Wang, X.-L.; Pan, Y.-Q.; Li, H.; Zhou, D.; Liu, Y.-D.; Wang, P.; Gu, J.-D.; Lu, Q.; Qiu, Y.-F.; Lin, K.-F. Bio-Beads with Immobilized Anaerobic Bacteria, Zero-Valent Iron, and Active Carbon for the Removal of Trichloroethane from Groundwater. *Environ. Sci. Pollut. Res.* **2014**, *21* (19), 11500–11509. https://doi.org/10.1007/s11356-014-3110-6.

(14) Orchard, B. J.; Doucette, W. J.; Chard, J. K.; Bugbee, B. A Novel Laboratory System for Determining Fate of Volatile Organic Compounds in Planted Systems. *Environ. Toxicol. Chem.* **2000**, *19* (4), 888–894. https://doi.org/10.1002/etc.5620190415.

(15) Orchard, B. J.; Doucette, W. J.; Chard, J. K.; Bugbee, B. Uptake of Trichloroethylene by Hybrid Poplar Trees Grown Hydroponically in Flow-through Plant Growth Chambers. *Environ. Toxicol. Chem.* **2000**, *19* (4), 895–903. https://doi.org/10.1002/etc.5620190416.

(16) Shang, T. Q.; Doty, S. L.; Wilson, A. M.; Howald, W. N.; Gordon, M. P. Trichloroethylene Oxidative Metabolism in Plants: The Trichloroethanol Pathway. *Phytochemistry* **2001**, *58* (7), 1055–1065. https://doi.org/10.1016/S0031-9422(01)00369-7.

(17) Doty, S. L.; Shang, T. Q.; Wilson, A. M.; Moore, A. L.; Newman, L. A.; Strand, S. E.; Gordon, M. P. Metabolism of the Soil and Groundwater Contaminants, Ethylene Dibromide and Trichloroethylene, by the Tropical Leguminous Tree, Leuceana Leucocephala. *Water Res.* **2003**, *37* (2), 441–449. https://doi.org/10.1016/S0043-1354(02)00291-9.

(18) Chard, B. K.; Doucette, W. J.; Chard, J. K.; Bugbee, B.; Gorder, K. Trichloroethylene Uptake by Apple and Peach Trees and Transfer to Fruit. *Environ. Sci. Technol.* **2006**, *40* (15), 4788–4793. https://doi.org/10.1021/es060156k.

(19) Doucette, W. J.; Chard, J. K.; Fabrizius, H.; Crouch, C.; Petersen, M. R.; Carlsen, T. E.; Chard, B. K.; Gorder, K. Trichloroethylene Uptake into Fruits and Vegetables: Three-Year Field Monitoring Study. *Environ. Sci. Technol.* **2007**, *41* (7), 2505–2509. https://doi.org/10.1021/es0621804.

(20) Schöftner, P.; Watzinger, A.; Holzknecht, P.; Wimmer, B.; Reichenauer, T. G. Transpiration and Metabolisation of TCE by Willow Plants – a Pot Experiment. *Int. J. Phytoremediation* **2016**, *18* (7), 686–692. https://doi.org/10.1080/15226514.2015.1131228.

(21) Zhang, Y.; Liu, J.; Zhou, Y.; Gong, T.; Wang, J.; Ge, Y. Enhanced Phytoremediation of Mixed Heavy Metal (Mercury)–Organic Pollutants (Trichloroethylene) with Transgenic Alfalfa Co-Expressing Glutathione S-Transferase and Human P450 2E1. *J. Hazard. Mater.* **2013**, *260*, 1100–1107. https://doi.org/10.1016/j.jhazmat.2013.06.065.

(22) Tripathi, S.; Singh, V. K.; Srivastava, P.; Singh, R.; Devi, R. S.; Kumar, A.; Bhadouria, R. Chapter 4 - Phytoremediation of Organic Pollutants: Current Status and Future Directions. In *Abatement of Environmental Pollutants*; Singh, P., Kumar, A., Borthakur, A., Eds.; Elsevier, 2020; pp 81–105. https://doi.org/10.1016/B978-0-12-818095-2.00004-7.

(23) Moccia, E.; Intiso, A.; Cicatelli, A.; Proto, A.; Guarino, F.; Iannece, P.; Castiglione, S.; Rossi, F. Use of Zea Mays L. in Phytoremediation of Trichloroethylene. *Environ. Sci. Pollut. Res.* **2017**, *24* (12), 11053–11060. https://doi.org/10.1007/s11356-016-7570-8.

(24) Yan, Y. E.; Schwartz, F. W. Kinetics and Mechanisms for TCE Oxidation by Permanganate. *Environ. Sci. Technol.* **2000**, *34* (12), 2535–2541. https://doi.org/10.1021/es991279q.

(25) Che, H.; Bae, S.; Lee, W. Degradation of Trichloroethylene by Fenton Reaction in Pyrite Suspension. *J. Hazard. Mater.* **2011**, *185* (2), 1355–1361. https://doi.org/10.1016/j.jhazmat.2010.10.055.

(26) Chang, Y.-C.; Chen, T.-Y.; Tsai, Y.-P.; Chen, K.-F. Remediation of Trichloroethene (TCE)-Contaminated Groundwater by Persulfate Oxidation: A Field-Scale Study. *RSC Adv.* **2018**, *8* (5), 2433–2440. https://doi.org/10.1039/C7RA10860E.

(27) Mao, X.; Ciblak, A.; Amiri, M.; Alshawabkeh, A. N. Redox Control for Electrochemical Dechlorination of Trichloroethylene in Bicarbonate Aqueous Media. *Environ. Sci. Technol.* **2011**, *45* (15), 6517–6523. https://doi.org/10.1021/es200943z.

(28) Deng, J.; Hu, X.-M.; Gao, E.; Wu, F.; Yin, W.; Huang, L.-Z.; Dionysiou, D. D. Electrochemical Reductive Remediation of Trichloroethylene Contaminated Groundwater Using Biomimetic Iron-Nitrogen-Doped Carbon. *J. Hazard. Mater.* **2021**, *419*, 126458. https://doi.org/10.1016/j.jhazmat.2021.126458.

(29) Tratnyek, P. G.; Scherer, M. M.; Johnson, T. L.; Matheson, L. J. Permeable Reactive Barriers of Iron and Other Zero-Valent Metals. In *Chemical Degradation Methods for Wastes and Pollutants*; CRC Press, 2003.

(30) Wang, X.; Xin, J.; Yuan, M.; Zhao, F. Electron Competition and Electron Selectivity in Abiotic, Biotic, and Coupled Systems for Dechlorinating Chlorinated Aliphatic Hydrocarbons in Groundwater: A Review. *Water Res.* **2020**, *183*, 116060. https://doi.org/10.1016/j.watres.2020.116060.

(31) Farrell, J.; Kason, M.; Melitas, N.; Li, T. Investigation of the Long-Term Performance of Zero-Valent Iron for Reductive Dechlorination of Trichloroethylene. *Environ. Sci. Technol.* **2000**, *34* (3), 514–521. https://doi.org/10.1021/es990716y.

(32) Teerakun, M.; Reungsang, A.; Lin, C.-J.; Liao, C.-H. Coupling of Zero Valent Iron and Biobarriers for Remediation of Trichloroethylene in Groundwater. *J. Environ. Sci.* **2011**, *23* (4), 560–567. https://doi.org/10.1016/S1001-0742(10)60448-2.

(33) Cheng, S.-F.; Wu, S.-C. The Enhancement Methods for the Degradation of TCE by Zero-Valent Metals. *Chemosphere* **2000**, *41* (8), 1263–1270. https://doi.org/10.1016/S0045-6535(99)00530-5.

(34) Marshall, T.; Pensini, E. Vitamin B12 and Magnesium: A Healthy Combo for the Degradation of Trichloroethylene. *Water. Air. Soil Pollut.* **2021**, *232* (8), 336. https://doi.org/10.1007/s11270-021-05295-w.

(35) Jang, W.; Aral, M. M. Multiphase Flow Fields in In-Situ Air Sparging and Its Effect on Remediation. *Transp. Porous Media* **2009**, *76* (1), 99–119. https://doi.org/10.1007/s11242-008-9238-4.

(36) Connon, S. A.; Tovanabootr, A.; Dolan, M.; Vergin, K.; Giovannoni, S. J.; Semprini, L. Bacterial Community Composition Determined by Culture-Independent and -Dependent Methods during Propane-Stimulated Bioremediation in Trichloroethene-Contaminated Groundwater. *Environ. Microbiol.* **2005**, *7* (2), 165–178. https://doi.org/10.1111/j.1462-2920.2004.00680.x.

(37) Kuo, Y. C.; Cheng, S. F.; Liu, P. W. G.; Chiou, H. Y.; Kao, C. M. Application of Enhanced Bioremediation for TCE-Contaminated Groundwater: A Pilot-Scale Study. *Desalination Water Treat.* **2012**, *41* (1–3), 364–371. https://doi.org/10.1080/19443994.2012.664742.

(38) Reineke, W.; Kaschabek, S. R. Chlorinated Hydrocarbon Metabolism. In *eLS*; American Cancer Society, 2002. https://doi.org/10.1038/npg.els.0000472.

(39) Xiao, Z.; Jiang, W.; Chen, D.; Xu, Y. Bioremediation of Typical Chlorinated Hydrocarbons by Microbial Reductive Dechlorination and Its Key Players: A Review. *Ecotoxicol. Environ. Saf.* **2020**, *202*, 110925. https://doi.org/10.1016/j.ecoenv.2020.110925.

(40) Dolinová, I.; Štrojsová, M.; Černík, M.; Němeček, J.; Macháčková, J.; Ševců, A. Microbial Degradation of Chloroethenes: A Review. *Environ. Sci. Pollut. Res.* **2017**, *24* (15), 13262–13283. https://doi.org/10.1007/s11356-017-8867-y.

(41) Juwarkar, A. A.; Misra, R. R.; Sharma, J. K. Recent Trends in Bioremediation. In *Geomicrobiology and Biogeochemistry*; Parmar, N., Singh, A., Eds.; Soil Biology; Springer: Berlin, Heidelberg, 2014; pp 81–100. https://doi.org/10.1007/978-3-642-41837-2_5.

(42) *40 CFR Part 141 -- National Primary Drinking Water Regulations*. https://www.ecfr.gov/current/title-40/chapter-I/subchapter-D/part-141 (accessed 2022-05-11).
(43) TARGET DETECTION LIMITS AND DESIGNATED ANALYTICAL METHODS. 20.
(44) ATSDR. Toxicological Profile for Vinyl Chloride, 2006.
(45) Lacroix, E.; Brovelli, A.; Barry, D. A.; Holliger, C. Use of Silicate Minerals for PH Control during Reductive Dechlorination of Chloroethenes in Batch Cultures of Different Microbial Consortia. *Appl. Environ. Microbiol.* **2014**, *80* (13), 3858–3867. https://doi.org/10.1128/AEM.00493-14.
(46) Puentes Jácome, L. A.; Wang, P.-H.; Molenda, O.; Li, Y. X. (Jine-J.; Islam, M. A.; Edwards, E. A. Sustained Dechlorination of Vinyl Chloride to Ethene in Dehalococcoides-Enriched Cultures Grown without Addition of Exogenous Vitamins and at Low PH. *Environ. Sci. Technol.* **2019**, *53* (19), 11364–11374. https://doi.org/10.1021/acs.est.9b02339.
(47) Robinson, C.; Barry, D. A.; McCarty, P. L.; Gerhard, J. I.; Kouznetsova, I. PH Control for Enhanced Reductive Bioremediation of Chlorinated Solvent Source Zones. *Sci. Total Environ.* **2009**, *407* (16), 4560–4573. https://doi.org/10.1016/j.scitotenv.2009.03.029.
(48) Yu, S.; Semprini, L. Kinetics and Modeling of Reductive Dechlorination at High PCE and TCE Concentrations. *Biotechnol. Bioeng.* **2004**, *88* (4), 451–464. https://doi.org/10.1002/bit.20260.
(49) Haest, P. J.; Springael, D.; Smolders, E. Dechlorination Kinetics of TCE at Toxic TCE Concentrations: Assessment of Different Models. *Water Res.* **2010**, *44* (1), 331–339. https://doi.org/10.1016/j.watres.2009.09.033.
(50) Wang, S.-M.; Tseng, S. Dechlorination of Trichloroethylene by Immobilized Autotrophic Hydrogen-Bacteria and Zero-Valent Iron. *J. Biosci. Bioeng.* **2009**, *107* (3), 287–292. https://doi.org/10.1016/j.jbiosc.2008.11.010.
(51) Kim, S.; Bae, W.; Hwang, J.; Park, J. Aerobic TCE Degradation by Encapsulated Toluene-Oxidizing Bacteria, Pseudomonas Putida and Bacillus Spp. *Water Sci. Technol.* **2010**, *62* (9), 1991–1997. https://doi.org/10.2166/wst.2010.471.

Chapter 2: Investigation of Hydronium Diffusion in Poly(vinyl alcohol) Hydrogels: A Critical First Step to Describe Acid Transport for Encapsulated Bioremediation

This chapter is a manuscript currently under review in ACS ES&T Engineering

2.1 Abstract

Bioremediation of chlorinated aliphatic hydrocarbon (CAH) contaminated aquifers can be hindered by high contaminant concentrations and acids generated during remediation. Encapsulating microbes in hydrogels may provide a protective, tunable environment from inhibiting compounds, however, current approaches to formulate successful encapsulated systems rely on trial and error rather than engineering approaches because fundamental information on mass transfer coefficients are lacking. To address this knowledge gap, hydronium ion mass transfer rates through two commonly used hydrogel materials, poly(vinyl alcohol) (PVA) and alginic acid (Alg), under two solidification methods (chemical and cryogenic) were measured. Variations in hydrogel crosslinking conditions, polymer composition, and solvent ionic strength were investigated to understand how each influenced hydronium ion diffusivity. A three-way ANOVA indicated ionic strength, membrane type, and crosslinking method significantly ($p<0.001$) contributed to changes in hydronium ion mass transfer. Hydronium ion diffusion increased with ionic strength, counter to what is observed in aqueous-only (no polymer) solutions. Co-occurring mechanisms correlated to increased hydronium ion diffusion with ionic strength included increased water fraction within hydrogel matrices and hydrogel contraction. Measured diffusion rates determined in this study provide first principal design information to further optimize encapsulating hydrogels for bioremediation.

2.2 Introduction

Remediation of chlorinated aliphatic hydrocarbons (CAHs), such as trichloroethylene (TCE), are primary or co-contaminants in over 50% of superfund sites and brownfields across the United States.[1,2] Bioremediation of CAHs by anaerobic reductive dechlorination is one potential remediation technique being researched at the lab scale[3–6] and in the field.[7–9] Microbial consortia are key players in bioremediation due to their ability to chemotax towards contaminant sources in the environment, act as self-replicating catalysts, degrade contaminants to low regulatory requirements, and provide low cost treatment compared to other methods. However, Robinson *et al.*[10] demonstrated that metabolically generated acids in poorly buffered systems could severally inhibit microbial consortia and stop the degradation process before complete dechlorination was achieved. Yu and Semprini[11] and Haest *et al.*[12] also showed that microbial anaerobic reductive dechlorinators were inhibited by CAHs, which lead to

decreased dechlorination efficiency and incomplete dechlorination in highly contaminated areas. Halting dechlorination prior to complete degradation of vinyl chloride may leave the system in a more toxic state; therefore, processes that protect microorganisms from inhibitory conditions may improve the efficiency of microbial anaerobic reductive dechlorination.

Accumulation of the acids generated during each step of anaerobic reductive dechlorination of CAHs can also inhibit biodegradative processes. Puentes Jácome *et al*. determined that biological rates of reductive dechlorination for *Sporomusa sp.* KB-1 were inhibited at pH 5.5 and ceased at 5 or below.[4] Natural carbonate buffers within groundwater systems can protect organisms for a time, but may be overwhelmed. Once natural buffers within groundwater were depleted, Robinson *et al*[10] found that acid neutralizers were required at 2-13 times the amount of contaminant dechlorination, and without frequent reinjection of neutralizers, remediation would fail. Common acid neutralizers include bicarbonate, carbonate, sodium hydroxide, lime, and silicate.[10,13]

Biofilms, flocs, and multicellular clusters are natural forms of encapsulation used to control transport and are one of the means by which microorganisms have adapted to a wide variety of environmental conditions including extreme pH changes.[14] A potential solution to toxic acid accumulation and high contaminant concentrations is to artificially encapsulate microorganisms in a biocompatible hydrogel, or "biobead."[15,16] Hydrogels, the primary material for biobead encapsulation, are three-dimensional matrices formed by polymer chains crosslinked into a cage like structure separated by water domains.[17] Biobeads provide a microenvironment for better native and localized control of acid by microorganisms and protection from inhibition by environmental toxins, including CAHs. Additionally, biobeads can be modified to include buffers and other passive and active compounds (e.g. zero-valent metals, activated carbon).[18] Studies by Zhou *et al*.,[19] Wang *et al*.,[20] and Kim *et al*.,[21] each used encapsulated microorganisms for the dechlorination of TCE and its biproducts; however, all studies utilized buffering compounds to maintain pH ~7 during dechlorination. To the authors' knowledge, no studies to date have evaluated the ability of encapsulating hydrogels to protect microbes *in vitro* or *in situ* without buffers or where system buffering was overwhelmed.

An additional knowledge gap toward engineering these hydrogel materials for remediation are a lack of published fundamental mass transfer constants (diffusivity) of key metabolites, waste products (acid), and contaminants, which would allow for development of reaction-diffusion type computational models, proper geometry sizing, and materials tuning to match biological degradation rates of contaminants to mass transfer rates. Consumption of TCE and complete breakdown to ethylene or CO_2 requires a balance of both reaction rate (governed by the microorganism growth rate and metabolism of each constituent) and mass transfer (governed by bead size, polymer properties, diffusivity of

constituents) to the microbial self-replicating "catalysts". Optimal conditions balance reaction and mass transfer of CAHs, acid, and nutrients so that CAHs and hydronium mass transfer is kept at a level where inhibition is minimal, and nutrients are supplied in sufficient quantities to maintain growth conditions. Determining CAH and nutrient effective diffusion coefficients is also critical, but hydronium diffusion will be the main focus of this study because, fundamentally, regulation of pH is the most critical priority of microorganisms because it directly impacts all metabolic processes. Microorganisms resist pH change thorough a variety of internal means (e.g., proton efflux or accumulation, reactions to form neutral chemical species and buffering compounds, control of membrane permeability to restrict transport), but at the cost of metabolic energy and optimal growth.

Polymer domains within hydrogels are made up of amorphous and crystalline regions. Crystalline regions are impermeable to solute diffusion and have been shown to hinder solute transport, while amorphous regions are more flexible but act as roadblocks to solute diffusion. Poly(vinyl alcohol) (PVA) hydrogels are commonly used in cryogel and chemically crosslinked hydrogel studies.[22–31] Previous work by Schuszter *et al*.[22] investigated hydronium diffusion in non-PVA hydrogels, and Choudhury *et al*.[23], Ajith *et al*.[24], and Wang *et al*.[32] measured hydronium conductivity in PVA hydrogels but did not quantify hydronium diffusivity, a critical knowledge gap in these materials. NMR analysis of hydronium diffusion in aqueous systems is common, but this technique is infeasible in hydrogel systems because the high water content in the hydrogel would drown out the hydronium signal.[22]

Describing mass transfer of acid (e.g., hydronium ions) in hydrogels, especially under different environmentally or biologically relevant conditions, is a critical first step needed to design first principle models of CAH dechlorination using biobeads and to better understand how physcial changes within a hydrogel may alter mass transfer rates.

Previous mass transfer research has explored three areas of distinct overlap with this study: scaling models of general diffusion in hydrogels,[33] the diffusivity of hydronium ions in electrolytes,[34,35] and structural hydrogel changes in electrolyte solutions.[29,36,37] Generally, for most molecules, Brownian motion describes the mechanism of mass transport in hydrogels influenced by polymer-solute, and/or polymer-solvent-solute interactions. However, hydronium ions possess a unique propagation pathway, the Grotthuss mechanism,[38] or "proton hopping", which greatly enhances hydronium ion diffusion beyond the limitations of Brownian motion.

Solution and hydrogel interaction at interfaces may also influence hydronium diffusion. Roberts[35] found that hydronium diffusion was suppressed in electrolyte solutions, while Roberts and Zundel[39] reported hydronium diffusion was enhanced at quartz surfaces. With the potential for multiple mechanisms to

influence hydronium diffusion in hydrogels, this study seeks to define hydronium effective diffusivities in blends of PVA and alginic acid (Alg) hydrogels under different ionic strength solutions to encompass a wide range of potential groundwater types where these materials may be used. Additional evaluated design factors included the effects of PVA weight per volume fraction and crosslinking method. Experimental results were compared with theoretical predictions of hydronium ion diffusion using scaling law models.[33] This study provides fundamental mass transfer constants critical for first principal design of biobeads.

2.3 Materials and Methods

2.3.1 Reagents:

Alg, 98.0-98.8% hydrolyzed PVA (MW: 31-50k, 85-124k, and 146-186k Da) powders, 99% potassium chloride, and calcium chloride were obtained from Sigma Aldrich. Food-grade sucrose was obtained from a local grocery store. Trace metal grade hydrochloric acid from Fisher Scientific, was diluted with house distilled and deionized water to pH 2.35. Technical grade boric acid was obtained from ChemProducts. All chemicals were used without further purification. NIST traceable pH standards (Fisher) were used to calibrate pH probes before each diffusion run.

2.3.2 Polymer Crosslinking:

10% poly(vinyl alcohol) - 2% alginate (10% PVA / 2% Alg) polymers were prepared as follows: 10.0 g of PVA (MW: 146,000-186,000 Da) was added to 100 mL of deionized water and heated to 80ºC with vigorous stirring. Once PVA was dissolved, 2.0 g of Alg polymer was added to the mixture and held at 80ºC while the solution reached a homogenous consistency. Hydrogel blended polymer solutions were transferred to disc-shaped casting molds, frozen at -20°C, and crosslinked by sequential freeze/thaw cycles as done previously by Holloway et al.[40] These hydrogels which are also known as ‘cryogels’ were used as a comparative control. A cycle consisted of thawing a frozen hydrogel for one hour at room temperature, then refreezing at -20°C for one hour. After five repeated cycles of freezing and thawing, the hydrogel formed dense crystallized domains which prevented polymer dissolution in water.[40] No crosslinking agents were added to these cryogels. PVA hydrogels from 7-15% were prepared with 146-186 kDa PVA, while 20% cryogels were from 85-124 kDa PVA, and 30% hydrogels were from 31-50 kDa PVA due to aqueous solubility limits.

Alternatively, after initially freezing the casted gel for at least 1 hour, the hydrogel was submerged in an ionic crosslinking solution at 4°C for 4-8 hours, and repeatedly rinsed with deionized water to remove excess crosslinking agents, similar to the preparation of biobeads by Wu *et al*.[41] Unless otherwise stated, blends of PVA / Alg hydrogels were crosslinked using an aqueous saturated boric acid solution with 2% (w/v) calcium chloride. Non-blended PVA hydrogels were crosslinked using

only saturated boric acid. Prior to measuring diffusion, all hydrogels were pre-equilibrated in deionized water, 0.1 M sucrose, or 0.001-1 M KCl, solution for at least 2 hours, in accordance with the solute/solvent used in the experiment.

2.3.3 Variation of Solvent Ionic Strength:

Diffusive measurements were conducted in solutions with ionic strengths ranging from 0 to 1 M, using KCl as the ionic species in water. Sucrose was used as a non-ionic alternative to KCl.

2.3.4 Apparatus for Diffusion Measurements:

The diaphragm cell method was used to quantify effective diffusivity of hydronium through hydrogels. This method separates a "source" solution containing the solute of interest from a "sink" chamber by a thin diaphragm or hydrogel membrane. Detailed diagrams of the apparatus can be found in the **Appendix A.1** (**Figure A.1 and A.2**). Constant stirring of both the sink and source chambers minimize mass transfer limitations and boundary layer effects. Concentration of solute in the sink was monitored over time and related to effective diffusivity by Fick's first law and the definition of flux. The mathematical derivation using the diaphragm cell is shown in more detail by Northrup and Anson[42] and provided in **Appendix A.5** (**Equation A-1 – A-2**).

Concentration in the sink chamber was measured by pH probes (Oakton). To enable simultaneous triplicate pH measurements, a diaphragm cell was constructed of PVC pipe with three sinks connected to a single larger source. Final source pH was measured using a commercial benchtop pH meter (Hach H170) and pH probe (Accumet). Final sink pH values were recorded and used to correct instrument drift (see **Appendix A.3**). Both source and sink were unbuffered to provide a maximum concentration driving force and avoid interference of counter diffusing species once protonated. Source pH remained nearly constant (<0.5% concentration difference) over the course of the entire experimental measurement.

2.3.5 Theoretical Hydronium Diffusion:

To estimate hydronium diffusion through PVA membranes, the scaling law developed by Lustig and Peppas was employed to normalize the diffusion coefficient.[33] Calculations were only completed for 10% PVA hydrogels due to equation limitations for single component hydrogels. Swelling experiments, requisite for estimating parameters for the model, were performed to determine the swelling behavior of the hydrogels after crosslinking. Membranes were cast and crosslinked as described above. The volume of each hydrogel was calculated using the known cross-sectional area of each casting mold and measuring the average equilibrated thickness of the membranes from five spatial points after swelling. The polymers were dried in a vacuum oven at 40 ºC until no weight change was observed. Physical

parameters were calculated using **Equation A-4 – A-7** as described by Meadows and Peppas[43] and Peppas and Merrill.[44] The mesh size of the swelled polymer gel was calculated using **Equation 2-1**[45], where Q is the degree of swelling (**Equation A-5**), C_n is the Flory characteristic ratio (8.3 for PVA), N is the number of links between repeating units per poly chain (**Equation A-7**), and *l* is the (C – C) bond length across the polymer chains (1.54 Å for PVA).[45]

$$\xi = Q^{1/3}(C_n \times N)^{1/2} l$$

Equation 2-1

The normalized diffusion coefficient was determined using the scaling law as defined by Lustig and Peppas,[33] where subscripts α, β, and γ denote water, polymer, and solute respectively:

$$\widehat{D} = \frac{D_{\gamma,\alpha\beta}}{D_{\gamma,\alpha}} \cong \left[1 - \frac{r}{\xi}\right] e^{\left[-\frac{Y}{(Q-1)}\right]}$$

Equation 2-2

$\widehat{D}$ is the normalized diffusion coefficient, $D_{\gamma,\alpha\beta}$ is the diffusion coefficient of the solute through the hydrogel, $D_{\gamma,\alpha}$ is the diffusion coefficient of the solute through water, r is the Stokes hydrodynamic radius of the solute (2.82 Å H_3O^+,[46] 3.58 Å Na^+,[46] 1.30 Å H_2O [47]), and Y is a structural parameter (assumed to equal 1 as an approximation).[33]

Hydrogel water content was calculated as done previously by Ajith *et al*.[24] and is shown in **Equation 2-3**, where w_w and w_p are the weight of water in the hydrogel after swelling and the hydrogel dry weight respectively. ρ_w and ρ_p are the densities of the hydrogel equilibration solution and of the initial polymer (i.e. PVA or a weighted average of PVA and Alg). The density of electrolyte solutions were calculated using linear interpolation of experimental data reported by Zhang and Han.[48]

$$WC = \frac{\frac{\rho_p}{\rho_w}\frac{w_w}{w_p}}{1 + \frac{\rho_p}{\rho_w}\frac{w_w}{w_p}}$$

Equation 2-3

Previous work by Wraight[49] used sodium as a surrogate for hydronium. The size and charge of a sodium ion is comparable to hydronium, allowing for the estimation of diffusive properties of hydronium through a hydrogel without the enhanced transport provided by the Grotthuss mechanism. For comparison, diffusion coefficients used as parameters in **Equation 2-2** were hydronium ($D_{\gamma,\alpha} = D_{e_{(H_3O^+,aq)}}$= 9.3x10^{-5} cm^2/s)[49] , sodium ($D_{\gamma,\alpha} = D_{e_{(Na^+,aq)}}$= 1.33x10^{-5} cm^2/s)[49], and water

($D_{\gamma,\alpha} = D_{e_{(H_2O)}}$= 1.73x10^{-5} cm^2/s)[47]. Additional models relevant to solute diffusion in hydrogels have been reported by Masaro and Zhu.[50]

A sensitivity analysis of parameters used in the Lustig and Peppas model was also performed for solution conditions of 0, 0.1, and 1 M KCl in both chemically crosslinked and cryogel forms from at least triplicate hydrogel samples (included as **Appendix A.17**). Adjusted parameters for sensitivity analysis included polymer structural parameter, Flory characteristic ratio, Flory interaction parameter, specific volume of polymer repeating unit, and Stokes hydrodynamic radius of the diffusing species.

2.3.6 NMR Analysis:

1H and 11B NMR analyses were completed using a Bruker AVANCE III 500 spectrometer equipped with a Prodigy cold probe. The frequency used for 1H NMR was 500.13 MHz and 160.47 MHz for 11B NMR. All spectra were collected at +30 °C. 11B NMR spectra were collected in Quartz NMR tubes, but due to the presence of borosilicate glass on the instrument probe further corrections were required. To remove the broad borosilicate glass peak, a blank D_2O spectra was subtracted from each sample spectra. All NMR and Raman experiments were completed using 2,4-pentanediol as a substitute for PVA as done previously by Itou *et al*.[25] to avoid polymerization. Samples were prepared by dissolving 2,4-pentanediol, boric acid, and potassium chloride in D_2O. Sodium hydroxide was used to adjust pH. Samples varying ionic strength were 10% 2,4-pentanediol in saturated boric acid and 0, 0.001, 0.5, and 1 M KCl. Samples studying the effects of changing pH were composed of 0.23 M 2,4-pentanediol and 0.02 M boric acid. Sodium hydroxide was added until a pH of 9 was achieved, similar to a preparation done by Sinton.[51]

2.3.7 Raman Spectroscopy:

Raman spectroscopy was completed using a WITec alpha300 Raman microscope with a UHTS-300 spectrometer and 1600 x 200 pixel CCD array detector. A 532.53 nm laser source was used with a nominal 100-mW (max) power manually adjusted for appropriate signal-to-noise (baseline) quality below 15-mW incident through a 20x objective (Nikon). Reported spectra represent the control software-averages of 10 spectral accumulations each acquired at 0.5-second integration times. Data was analyzed using WITec Control FOUR software v4.1. Equimolar liquid samples were prepared with combinations of 2,4-pentanediol, boric acid, and potassium chloride in DI water.

2.3.8 FTIR Spectroscopy:

FTIR analysis was done using a Nicolet 6700 FTIR spectrometer (Thermo Scientific) with a circle liquid analyzer (0005-105, Spectra-Tech Inc.) attachment. Spectra were collected between 650-4000

cm^{-1} with a resolution of 4 cm^{-1} by averaging 32 scans and analyzed using OMNIC software v8.3. Liquid samples were prepared as described in the Raman spectroscopy section.

2.3.9 XRD:

X-ray diffraction analysis was done using a Bruker D8 XRD equipped with a 2-D detector and a copper x-ray tube (1.54056 Å). A collimated x-ray beam of 500 microns was used to collect data. Spectra were collected in four separate frames at 300 seconds per frame for a total scan range of 6-95˚. Samples were prepared as mentioned in the polymer crosslinking section above then dried at room temperature before analysis, the samples did not undergo any further modification.

2.3.10 Data Analysis:

Diffusion experiments were performed in triplicate at a minimum. Reported hydronium diffusion in hydrogel values were the compiled average of these measurements, with error bars representing a 95% confidence interval. Comparisons between values were conducted using a 2-sample t-test in Origin Lab 2018b (OriginLab Corporation, MA) and adjusted using Holm's correction in R (v4.1.1).[52] R packages car,[53] multcomp,[54] phia,[55] afex,[56] and emmeans[57] were used for data analysis. Group comparisons were done using type II analysis of variance (ANOVA) in R with all results considered statistically significant at the 95% confidence level ($p<0.05$).

2.4 Results and discussion

Diffusion of solutes through hydrogels are influenced primarily by physical obstruction from the polymer, electrostatic effects, and polymer-solute chemical interactions such as hydrogen bonding.[58–60] In order to separate some of these effects and gain insights into mass transfer mechanisms, diffusion measurements were performed in single component gels (e.g. 10% PVA), multicomponent gels (e.g., 10% PVA / 2% Alg), different solidification methods (e.g., cryogels vs. chemical cross-linking), and at different ionic strengths. Each treatment set is addressed individually below.

2.4.1 Influence of Crosslinking Method on Hydronium Diffusion – Cryogels:

Aqueous hydronium ion diffusivity as reported by Agmon[38] and Wraight[49] was 81.1% faster than the measured diffusivity in 10% PVA cryogels, 1.76 x 10^{-5} cm^2/s. Schuszter *et al.*[22] calculated hydronium ion diffusivity in agarose hydrogels at the same order of magnitude. A reduction in hydronium effective diffusivity relative to pure water may be explained by physical obstruction by polymer domains within the hydrogel including impermeable crystalline regions.[30,61] Polymer chains, which make up the hydrogel structure, act as roadblocks to diffusing species as they move between water domains. Two physical parameters which may exacerbate obstruction within the hydrogel are polymer mass fraction and crystallinity.

Increasing the polymer mass fraction increases the density of polymer chains within a membrane which decreases the free volume of the hydrogel and presents a higher possibility for obstruction to diffusion. To examine whether polymer mass fraction influenced hydronium transport, several different PVA blended cryogels were evaluated. Several PVA molecular weights were used to accommodate solubility limits (see methods section), but the effects of PVA molecular weight on hydronium diffusivity were not investigated.

Figure 2.1 depicts the effective diffusivity of hydronium through several PVA hydrogel blends. Statistical analysis of **Figure 2.1** was completed using the Tukey method to compare individual means. 15% PVA was the only polymer composition that had significantly different hydronium diffusivity when compared to any of the other PVA compositions. Hydronium diffusion through 15% PVA was statistically significant when compared to 7% ($p=0.002$), 10% ($p=0.002$), and 30% PVA ($p=0.008$), all other combinations were insignificant. Molecular weight likely influenced hydronium diffusivity in the hydrogels tested due to variations in chain length and mobility corresponding to the PVA used in each hydrogel blend. Chain mobility can make crystallization more favorable due to chain movement during crystallite formation. Hydronium diffusivity in 20 and 30% PVA cryogels was likely only

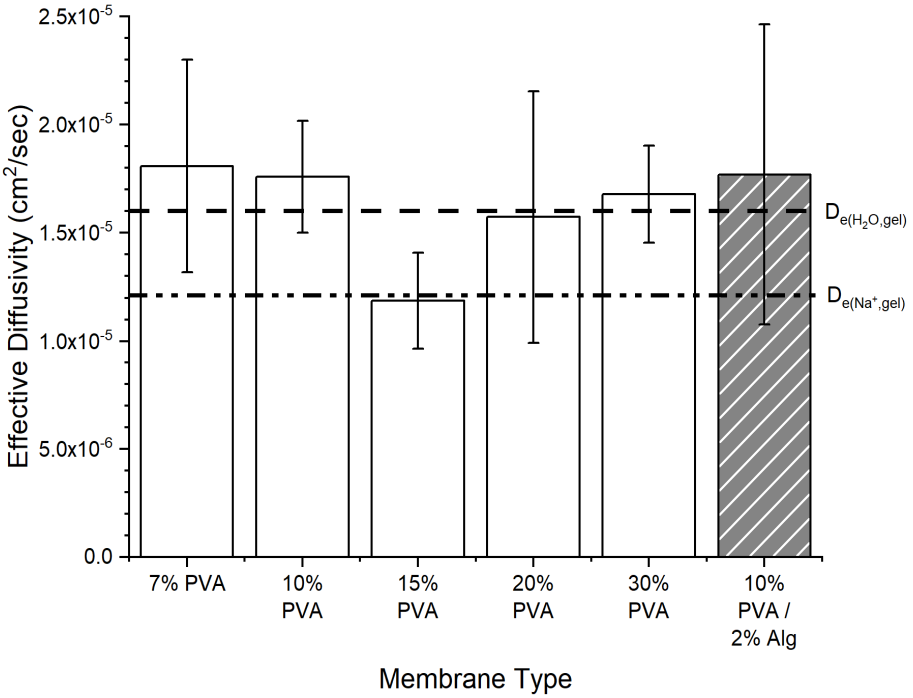

Figure 2.1: *Effective diffusivity of hydronium through cryogels of various polymer compositions. Statistical analysis showed that 15% PVA was the only significantly different membrane composition when compared with 7%, 10%, and 30% PVA. The horizontal lines represent calculated self-diffusion of the given species in a 10% PVA cryogel. Error bars represent a 95% confidence interval.*

similar to 10% PVA cryogels due to the decrease in PVA molecular weight. Additional low molecular weight PVA added to the hydrogel mixture to make 20% and 30% PVA, likely made the polymer density close enough to 10% PVA to make the diffusivity behavior similar.

Considering the impact of crystallinity on changes in diffusivity, increases in polymer mass fraction, regardless of molecular weight, may lead to an increase in crystallinity due to the increasingly close proximity of polymer chains as more polymer is added to the hydrogel blend. With more polymer chains present, the chains are simply more likely to be pushed together during crystal formation, making the development of crystalline regions more favorable. The formation of crystalline regions increases obstruction to diffusion in a hydrogel because crystalline regions are impermeable to solute diffusion[30,62] in comparison to amorphous regions where solute molecules can simply navigate around polymer chains within the hydrogel. In a study done by Holloway *et al*.[40], using a PVA molecular weight similar to the 20% PVA cryogels in this study, researchers found that the crystallinity of 30% PVA cryogels was ten times that of 10% PVA.

While fully assessing gel crystallinity was beyond the scope of this study, we note that polymer molecular weight can also affect the formation of crystalline domains within the hydrogel due to chain length. For the same mass fraction, a higher molecular weight polymer will provide fewer but longer chains, while a lower molecular weight polymer will be made up of more shorter chains. Shorter polymer chains will be expected to have significantly more mobility to adopt a crystalline conformation in comparison to highly entangled, long polymer chains. This is the hypothesized reason for the drop in diffusivity when PVA polymer composition was increased to 15% PVA using the high molecular weight PVA, a mass fraction which was approaching the solubility limit. Hydronium diffusivity decreases from 10-15% PVA indicating obstruction may be caused by chain entanglement and a larger proportion of amorphous polymer gel. A similar trend would be expected when using lower molecular weight PVA at polymer mass fractions approaching the solubility limit. Clearly, additional studies into the effects of PVA molecular weight on crystallinity and hydronium diffusion, with a complete assessment of the fraction of crystallinity using the methods of Ricciardi et al.[63] would be beneficial to better understanding these mechanisms.

Interestingly, when testing whether the number of freeze / thaw cycles would have an effect on hydronium diffusivity, no significant difference was found between 10% PVA cryogels crosslinked with between two to five freeze/thaw cycles ($p=0.3857$, **Figure A.5**). Holloway *et al*.[40] calculated the relative crystallinity of PVA cryogels (10%, 20%, 30%, 35% PVA) prepared by similar procedures, with a lower molecular weight PVA, and found that the relative crystallinity of 10% PVA cryogels increased by less than 0.5% after over five freeze / thaw cycles with a max relative crystallinity of about

0.2%. However, the relative crystallinity of 30% PVA cryogels increased by about 2% after the same number of cycles with a max of about 3.5% which, along with the experimental results previously discussed, indicates PVA volume fraction, and therefore hydrogel polymer density, had a greater effect on hydrogel crystallinity and hydronium diffusivity than the number of freeze / thaw cycles.

2.4.2 Influence of Crosslinking Method on Hydronium Diffusion - Chemically Crosslinked Hydrogels

To examine the combined effects of polymer and crosslinking chemical constituents on hydronium diffusivity, chemically crosslinked PVA and PVA/Alg hydrogels were studied. Cryogels were used as control groups for comparison purposes to elucidate the effects of introducing additional chemical constituents into the hydrogel as done previously by Patachia *et al*.[64] Significant differences in hydronium effective diffusivities were observed between hydrogels crosslinked by chemical reagents (**Figure 2.2.a-e**) and freeze/thaw cycles (**Figure 2.2.f** and **2.2.g**). Boric acid crosslinked 10% PVA hydrogels (**Figure 2.2.a**) had an effective diffusivity that was 58% higher than 10% PVA cryogels (*p=0.002,* **Figure 2.2.f**). Crosslinking 10% PVA / 2% Alg hydrogels with calcium chloride and boric acid for 4.5 hours (**Figure 2.2.b**) decreased hydronium diffusivity by 47% (*p=0.03*) when compared to the equivalent cryogel (**Figure 2.2.g**). Calcium ions integrated into the polymer network may have electrostatically repelled hydronium ions, decreasing hydronium's effective diffusivity by inhibiting transport efficiency. Longer crosslinking times (4.5 versus 6.5 and 8 hours) for 10% PVA / 2% Alg hydrogels increased the measured effective diffusion rates (*p= 0.004*) as shown in **Figure 2.2.b-d** potentially due to increased boric acid crosslinking. After chemically crosslinking for at least 6.5 hours, 10% PVA / 2% Alg hydrogels had an effective diffusivity similar (~0.003% difference, *p=1*) to the equivalent cryogel. Alternatively, when crosslinked for 4.5 hours with only boric acid (**Figure 2.2.e**), 10% PVA / 2% Alg hydrogels performed identically (~0.009% difference, *p = 1*) to 10% PVA treated in a similar fashion (**Figure 2.2.a**). This suggests that in the absence of the calcium crosslinker, Alg acts as a passive component in the hydrogel blend with no additional crosslinking behavior.

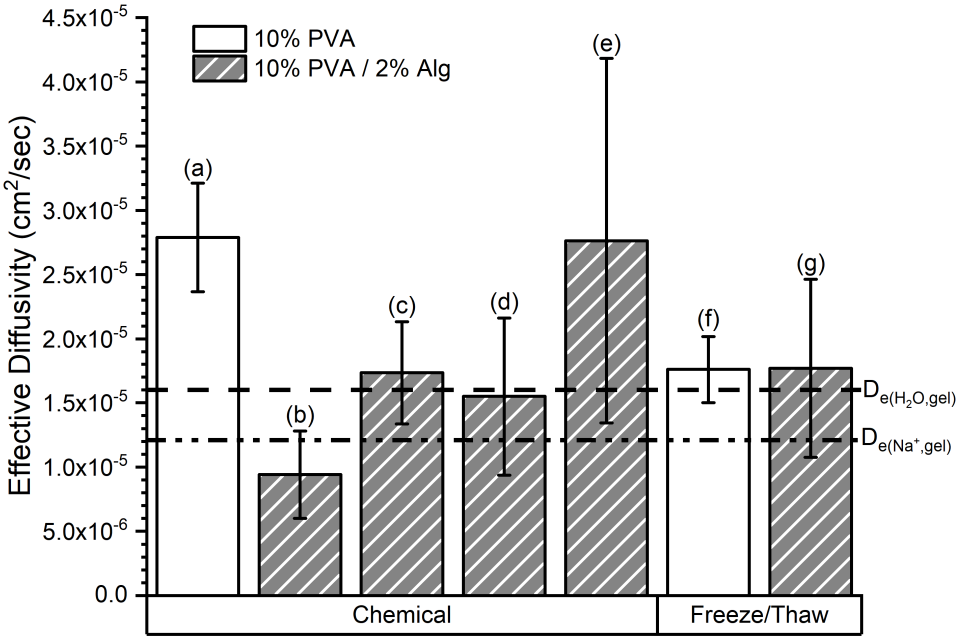

Figure 2.2: *Effective diffusivity of hydronium in chemically crosslinked 10% PVA and 10% PVA / 2% Alg hydrogels, crosslinked by different methods. Letters indicate different crosslinking methods:* ***a)*** *10% PVA crosslinked for 4.5 hrs. in saturated boric acid,* ***b)*** *10% PVA / 2% Alg crosslinked for 4.5 hrs. in 2% $CaCl_2$ and saturated boric acid,* ***c)*** *10% PVA / 2% Alg crosslinked for 6.5 hrs. in 2% $CaCl_2$ and saturated boric acid,* ***d)*** *10% PVA / 2% Alg crosslinked for 8 hrs. in 2% $CaCl_2$ and saturated boric acid,* ***e)*** *10% PVA / 2% Alg crosslinked for 4.5 hrs. only in saturated boric acid,* ***f)*** *10% PVA cryogel, and* ***g)*** *10% PVA / 2% Alg cryogel. The horizontal lines represent calculated self-diffusion of the given species in a 10% PVA cryogel. Error bars represent a 95% confidence interval. Average diffusivity and error values for each data point can be found in* ***Table A.5****.*

The differences observed between effective diffusivities in **Figure 2.2** may be due to these co-occurring factors: 1) chemically crosslinking PVA with boric acid prevented formation of crystalline PVA-PVA structures allowing the membrane to expand water domains and increase hydronium diffusivity (**Figure 2.2.a** and **2.2.f** & **Figure 2.2.e** and **2.2.g**), 2) the formation of PVA-borate complexes increased the acidity of the hydrogel environment and improved the ability of the hydrogel to transport protons, and 3) electrostatic repulsion by calcium ions bonded to Alg (**Figure A.7**) decreased hydronium diffusivity (**Figure 2.2.b** and **2.2.g**). The first factor is supported by Huang *et al*,[65] who states that boric acid crosslinking decreases hydrogel crystallinity allowing for additional water uptake and water domain expansion. Crystallinity hinders water uptake by binding polymer chains together with hydrogen bonds therefore restricting hydrogel expansion. When boric acid crosslinks PVA chains, the resulting complex prevents hydrogen bonding by separating polymer chains with a rigid structure. Even though the PVA-borate complex is rigid, the polymer chains are amorphous after crosslinking so unlike crystalline regions, are far more flexible and present no additional obstruction to solute transport. Water content

experiments (shown in **Table 2.1**) further support factor 1 and the results described by Huang *et al*.[65] as water content significantly increased from 94.1 to 95.8% in 10% PVA hydrogels (*p=0.003*) when chemically crosslinked. Water domain expansion is expressed by an increase in water content since more water occupies the hydrogel volume. As water domains expand, the hydrogel swells and the relative space occupied by polymer chains decreases making it easier for solute molecules to traverse the hydrogel and avoid obstruction from polymer domains. Similar results were reported by Gayet and Fortier[66] who determined that an increase in water content led to more efficient mass transport due to less obstruction from polymer domains.

The second factor is supported by Rietjens and Steenbergen[67] who demonstrated that complexed borate, like the complex shown in **Figure 2.3.d**, is strongly acidic due to ring strain (C-O-B-O-C-C). The second factor can also be supported by aqueous conductivity measurements which can be correlated to diffusivity.[68] If, in aqueous systems, conductivity is increased, it stands to follow that within a hydrogel, those complexes would have the same effect and increase proton (i.e. hydronium) transport efficiency. Frahn showed that the conductivity of aqueous solutions increased after hydroxy-boric acid complexes were formed, therefore the increase in hydronium diffusivity observed when comparing **Figure 2.2.a** and **2.2.f** may be in part due to the increased acidic nature of the PVA-borate complex.[69]

The third factor was supported by Cassone *et al*[34] who states that hydrated calcium ions repelled hydronium ions in aqueous solution and hindered transport efficiency. Unlike with 10% PVA, 10% PVA / 2% Alg hydrogels did not show a significant change in water content (*p=0.051*) after chemical crosslinking, indicating that crosslinking alginate with calcium hindered hydrogel expansion due the strength and rigidity of the calcium-alginate bond. Cassone *et al*.[34] also found that calcium ions act as "structure makers" in aqueous systems e.g., hydrated calcium ions reinforce water lattice structures which restricts water rotation, hindering the Grotthuss mechanism. While Cassone *et al*.[34] completed measurements in aqueous systems, the same principles likely apply to hydrogels due to high water content and water domain dominant transport. No significant differences in hydronium diffusion were observed between 10% PVA and 10% PVA / 2% Alg cryogels, so the significant decrease in hydronium diffusivity observed after chemical crosslinking Alg with calcium indicates interactions between hydronium and calcium are likely the cause. Although, longer crosslinking times do change these results as discussed previously. Significant differences in diffusivity were observed in 10% PVA / 2% Alg hydrogels with longer crosslinking times (*p=0.0043*, **Figure 2.2.b-d).** Differences can be explained by an interplay between slow kinetics to incorporate boric acid crosslinks (which increase diffusivity) and calcium (which decreases diffusivity). The use of saturated boric acid during crosslinking eliminates crosslinker concentration limitations to complex formation which has been noted by

Miyazaki *et al*.[70], Nickerson[71], and Rietjens and Steenbergen[67] and instead makes time, or diffusion, the limiting factor since boric acid must diffuse through the crosslinked hydrogel to encounter unreacted PVA. Therefore, longer crosslinking times lead to additional PVA-borate complex formation which in turn causes additional expansion of the water domains within the hydrogel and improves hydronium transport efficiency.

Table 2.1: *Water content and percentage of swelling for each membrane type crosslinked both chemically and physically.*

Membrane	WC (DI)	% Swell† (DI)	WC (0.1 M)	% Swell† (0.1 M)	WC (1 M)	% Swell† (1 M)
10% PVA Freeze / Thaw	94.1±0.33%	-5±8%	93.6±0.30%	-3±6%	87.8±0.06%	-18±2%
10% PVA / 2% Alg Freeze / Thaw	94.8±0.40%	7±4%	93.3±0.33%	-2±19%	88.1±1.11%	-5±6%
10% PVA Chemical	95.8±0.73%	30±23%	95.1±1.30%	28±41%	87.5±0.81%	-4±10%
10% PVA / 2% Alg Chemical	94.3±0.13%	19±4%	93.6±0.55%	17±9%	87.4±0.57%	1±3%
†Negative percent swelling means contraction. Error is based on a 95% confidence interval.						

PVA crosslinked in boric acid has been examined in recent years by Itou *et al*,[25] Tsai *et al*,[26] and Wang *et al*,[31] to determine the possible PVA-borate complexes formed under acidic and basic conditions.[25,26,31] The synthesized PVA-borate complex is pH dependent with the formation of a 3-coordinate complex in acidic conditions and a 4-coordinate complex in basic conditions.[26,31] The crosslinking structures shown in **Figure 2.3** are the most probable complexes formed when PVA is crosslinked with boric acid under acidic conditions.[25,26,31] Itou *et al*.[25] found that **Figure 2.3.b** and **2.3.d** were the most probable complexes based on Raman analysis of 2,4-pentanediol reacted with boric acid. Tsai *et al*.[26] found that **Figure 2.3.a** and **2.3.d** were the most probable complexes formed based on Raman and NMR analysis. Wang *et al*.[31] found that **Figure 2.3.d** was the most likely structure based on Raman and NMR analysis. In summary, **Figure 2.3.b** and **2.3.d** seem to be the most probable complexes formed by PVA and boric acid crosslinking under the conditions used in this study, although the authors were unable confirm this configuration using FTIR, Ramen, or NMR (see **Appendix A.11 – A.13**).

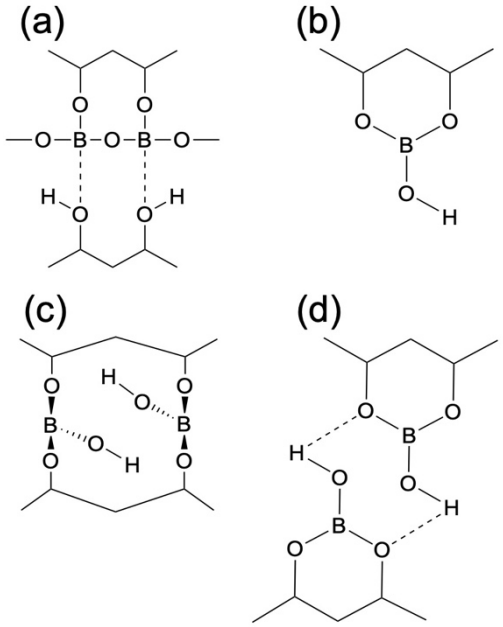

Figure 2.3: *Possible co-existing PVA-borate complexes formed when PVA is crosslinked with saturated boric acid under acidic conditions. (a) 3-coordinate PVA-borate complex. (b) 3-coordinate PVA-borate group. (c) 3-coordinate O-B-O complex. (d) 3-coordinate PVA borate complex.*

2.4.3 Influence of Solvent Ionic Strength on Hydronium Diffusion

The effect of ionic strength on hydronium ion diffusion in 10% PVA and 10% PVA / 2% Alg hydrogels are shown in **Figure 2.4**. Hydronium diffusion was measured in ionic solutions from 0.001 – 1 M KCl to represent surface water and many natural aquifer systems (0.001 – 0.01 M) and saline or contaminated aquifers (>0.1 M).[72] Increases in ionic strength produced an increase in effective diffusivity in 10% PVA cryogels up to 0.01 M KCl before leveling off between 0.01-0.5 M KCl and decreasing from 0.5-1 M KCl. Ionic strength had a significant effect on hydronium diffusivity in 10% PVA cryogels ($p=4.08x10^{-6}$). Hydronium diffusion through 10% PVA / 2% Alg cryogels at low ionic strength was similar to diffusion in DI water. An increase in hydronium ion diffusion in 10% PVA / 2% Alg hydrogels was seen when ionic strength was increased from 0.001 – 0.1 M, began to level off at 0.1 – 0.5 M, and decreased slightly at 1 M KCl. Ionic strength also had a significant effect on hydronium diffusivity in 10% PVA / 2% Alg cryogels ($p=2.71x10^{-5}$).

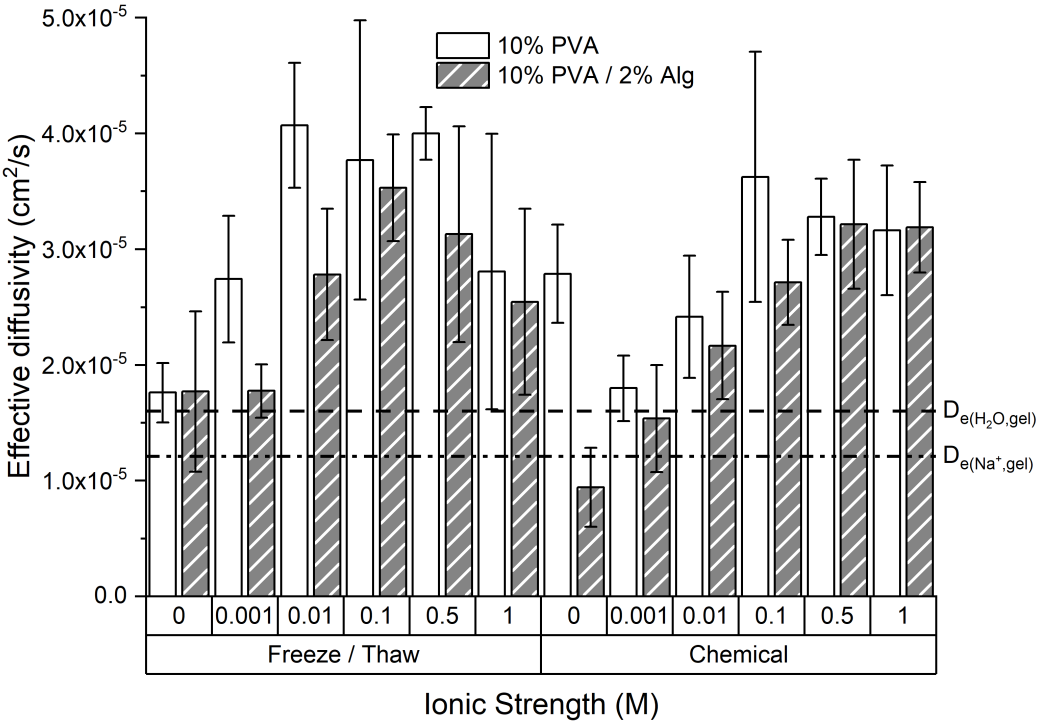

Figure 2.4: *Hydronium effective diffusivity in 10% PVA and 10% PVA / 2% Alg hydrogels with different ionic strength solutions and different crosslinking methods. The horizontal lines represent calculated self-diffusion of the given species in a 10% PVA cryogel. Error bars represent a 95% confidence interval. Average diffusivity and error values for each data point can be found in* ***Table A.6****.*

Chemically crosslinked 10% PVA hydrogels showed an immediate decrease in hydronium diffusivity at low ionic strength (0.001 M KCl compared to DI water), bringing the effective diffusivity to similar levels as the equivalent cryogel in DI water. Diffusivity increased from 0.001 - 0.1 M and leveled off between 0.1 – 1 M KCl. Ionic strength had a statistically significant effect on hydronium diffusivity in chemically crosslinked 10% PVA hydrogels (p=9.30x10-6). Alternatively, chemically crosslinked 10% PVA / 2% Alg hydrogels showed a steady increase in diffusivity from 0 – 0.5 M before plateauing between 0.5 - 1 M KCl. Ionic strength also had a statistically significant effect on hydronium diffusivity in chemically crosslinked 10% PVA / 2% Alg hydrogels (p=9.29x10-10). When sucrose was substituted for KCl at 0.1 M, hydronium effective diffusivity through 10% PVA cryogels was similar to that of hydronium in DI water (p=0.896, **Figure A.8**). This similarity indicated that diffusivity increased as ionic strength increased due to the presence of potassium or chloride ions. NMR, Raman, and FTIR results showed no indication of an interaction between the PVA-borate complex and potassium chloride (**Figure A.10 - A.13**), indicating that the change in diffusivity observed with increasing ionic strength was driven by potassium/chloride ion-solvent and not potassium/chloride ion-polymer interactions. A diffusion mechanism is proposed and discussed further in the following sections.

A type-II, three-way ANOVA (**Table A.8**) was completed for further statistical analysis on the data presented in **Figure 2.4**. The ANOVA table showed that each individual factor (membrane type, crosslinking method, and ionic strength) had a significant effect ($p<0.001$) on hydronium diffusivity. Additionally, when comparing the interactions between each factor, all two-way interactions except the membrane type and crosslinking method ($p=0.660$), and the three-way interaction were statistically significant. Interaction plots were generated to determine which factor influenced the three-way interaction the most by comparing each factor in a two-way interaction while varying the third factor. All generated interaction plots are available in **Appendix A.14** (**Figure A.13-A.15**). The results of each interaction plot agree that ionic strength has the most significant effect on hydronium diffusivity at low (0 – 0.001 M KCl) and high (0.1 – 1 M KCl) ionic strength and that this effect drove the three-way interaction observed between membrane type, crosslinking method, and ionic strength. Bioremediation applications would likely require these materials to be placed in groundwater where the elevated ionic strength would enhance hydronium diffusivity.

2.4.4 Hydronium Diffusive Theory vs Experimental

A model developed by Lustig and Peppas[33] was used to evaluate the theoretical diffusion coefficient of hydronium through PVA hydrogels. The model has been shown to predict solute diffusion in various hydrogels accurately; however, this model excludes solute-solvent and solute-solute interactions which are important factors in hydronium mass transfer.[33,38,73]

Measured diffusion in cryogels were 80% less than the theoretical predictions (see **Table 2.2**). Likewise, measured diffusion in boric acid crosslinked 10% PVA hydrogels was 70% less than the theoretical predictions. Since the measured hydronium aqueous diffusivity did not agree with modeled hydronium diffusivity in hydrogels, sodium was used for comparison to predict how a molecule of similar size and charge would diffuse through a 10% PVA hydrogel without the influence of the Grotthuss mechanism as done previously by Wraight.[49] Using sodium as a surrogate for hydronium diffusion, an effective diffusivity of $1.21\text{x}10^{-5}\pm2.54\text{x}10^{-8}$ cm^2/s in 10% PVA cryogels was predicted. Experimental hydronium diffusivity was 45% more than calculated sodium diffusivity in 10% PVA cryogels ($p=1.16\text{x}10^{-4}$). For cryogels, diffusion coefficients of sodium more closely match that of measured hydronium diffusivity, which suggests that both Brownian motion and Grotthuss mechanisms continue to play a role in diffusion. Although, one or both mechanisms are likely hindered within hydrogels since diffusivity in all the hydrogels tested exhibited a slower effective diffusivity than aqueous hydronium diffusion. Roberts[35] found that electrostatic interactions could hinder hydronium transport in aqueous systems leaving Brownian motion to be the dominant mechanism for diffusion. This result is possible in hydrogel systems too due to the competing interactions from polymer-solvent

and solvent-solute interactions and may explain how the Grotthuss mechanism is hindered. In chemically crosslinked 10% PVA, $1.25x10^{-5}\pm9.65x10^{-8}$ cm^2/s was calculated as the "Brownian only" hydronium diffusivity in hydrogels using sodium as a surrogate. Experimental hydronium diffusivity was 120% greater than that of the calculated sodium diffusivity ($p=1.59x10^{-5}$). The increase in diffusivity seen when comparing cryogels to boric acid crosslinked hydrogels may be due to an increase in water content. Water content of a hydrogel can increase when the hydrogel is less constrained, in the case of 10% PVA chemically crosslinked hydrogels, the major crosslinker is boric acid which forms non-crystalline PVA-borate complexes. Even though one freeze / thaw cycle is still performed before chemically crosslinking is started, the presence of fewer crystalline domains allows the hydrogel to expand more freely.

Table 2.2: *Measured and theoretical hydronium diffusivities of hydronium and sodium in 10% PVA hydrogels at 0 M KCl.*

Value Type	Membrane	Solute	Crosslinking Type	Crosslinker	Average $\widehat{D}$	Effective Diffusivity (cm^2/s)	+/- Error
Calculated	10% PVA	H_3O^+	Freeze / Thaw	-	0.914	$8.50x10^{-5}$	$1.69x10^{-7}$
Calculated	10% PVA	H_3O^+	Chemical - 4.5 hrs.	Sat. Boric Acid	0.939	$8.73x10^{-5}$	$6.42x10^{-7}$
Calculated	10% PVA	Na^+	Freeze / Thaw	-	0.910	$1.21x10^{-5}$	$2.54x10^{-8}$
Calculated	10% PVA	Na^+	Chemical - 4.5 hrs.	Sat. Boric Acid	0.888	$1.25x10^{-5}$	$9.65x10^{-8}$
Measured	10% PVA	H_3O^+	Freeze / Thaw	-	0.189	$1.76x10^{-5}$	$2.58x10^{-6}$
Measured	10% PVA	H_3O^+	Chemical - 4.5 hrs.	Sat. Boric Acid	0.300	$2.79x10^{-5}$	$4.23x10^{-6}$

A sensitivity analysis of parameters was performed for the model and the complete analysis is included in **Appendix A.17**. The influence of solute hydrodynamic radius on hydronium diffusion was examined since hydronium ion complexes can be present in solution in several forms including Zundel and Eigen cations.[74] Additionally the presence of charge balancing chloride ion as a counterion for hydronium may be a potential factor influencing mass transfer.[68] With the hydrodynamic radius of the solute varied from 0.1 to 8 Å at 0 M KCl, hydronium diffusivity ranged between 8.65 – 7.56 x 10^{-5} cm^2/s for cryogels and 8.85 – 8.19 x 10^{-5} cm^2/s for chemically crosslinked hydrogels. At 1M KCl, hydronium diffusivity ranged between 8.16 – 5.54 x 10^{-5} cm^2/s for cryogels and 8.12 – 5.71 x 10^{-5} cm^2/s for chemically crosslinked hydrogels. A larger hydrodynamic radius was predicted to decrease hydronium diffusion, as expected, however, the model was not able to predict trends observed with increased ionic strength.

Mesh size was altered indirectly over a wide range of mesh sizes by changing each of the following variables: Flory characteristic ratio (C_N), Flory interaction parameter ($\chi_{\alpha\beta}$), and specific volume of the polymer repeat unit ($\bar{v}$). Sensitivity analysis for mesh size showed that the theoretical model at 0 M KCl from mesh sizes 46 to 565 Å for cryogels and from 71 to 1807 Å for chemically crosslinked hydrogels only altered diffusivity in a range of 8.15 - 8.62 x 10^{-5} cm^2/s and 8.50 – 8.83 x 10^{-5} cm^2/s for cryogels and chemically crosslinked hydrogels, respectively. For 1 M KCl, mesh sizes for the same variable ranges were smaller, from 20 to 565 Å in cryogels and 34 to 1807 Å in chemically crosslinked hydrogels, resulting in a lower predicted range of diffusivities with increased ionic strength of 7.19 - 8.00 x 10^{-5} cm^2/s for cryogels and 7.24 - 7.97 x $10^{-5}cm^2/s$. Increased ionic strength was predicted to decrease mesh size and hydronium diffusion, however, this is counter to what was observed.

2.4.5 Theoretical Hydronium Diffusion Mechanism Within Polymer Domain - Microscale

In polymer systems, hydronium transport may behave differently than in strictly aqueous systems due to competing interactions between hydronium, bulk water, and the polymer backbone. Diffusion within, or around, the polymer domain acts as the diffusion limiting step due to physical obstruction, although, the relatively small size of the hydronium ion (~2.82 Å) in comparison to the mesh size of the hydrogel (~70 – 340 Å, **Equation 2-1**) indicates that polymer obstruction should not be a significant factor in hydronium diffusion in the hydrogels tested. Solvent-polymer (water-OH hydrogen bonding) and solvent-solute (water-KCl) interactions are postulated to alter the efficiency of diffusion through hydrogel water domains by similar mechanisms to aqueous diffusion as discussed by Huang *et al*.[65] and Patachia *et al*.[64] since diffusion predominately occurs in the water domains of the hydrogel.

In aqueous systems, hydronium ion transport is dependent on the rotation and alignment of water molecules to facilitate Grotthuss transport according to Hassanali *et al*.[73] and Agmon.[38] Bound water, as described by Horne[75], either in a solvation shell, or bound to a hydroxyl group[63], is inhibited from participating in the Grotthuss mechanism due to its inability to rotate and align with other water molecules. Horne and Axelrod[76] stated that water molecules in the same solvent lattice as the molecules bonded to PVA could be considered bound since their movement was hindered making the effects of water-hydroxyl hydrogen bonding restricting to hydronium transport. If complexed water molecules are bonded to PVA hydroxyl groups, fewer free water molecules would be available for Grotthuss transport, decreasing the overall efficiency of hydronium diffusion through the hydrogel. When PVA is chemically crosslinked with boric acid, hydrogel expansion due to fewer crystalline regions allows for more water molecules to enter the system and provide additional free water molecules to participate in the Grotthuss mechanism, assuming PVA hydroxyl groups are already hydrated. Additionally,

expanding water domains and the presence of fewer crystalline domains will decrease the probability of polymer obstruction and therefore increase hydronium diffusivity.

According to Patachia *et al*.[64] and Tretinnikov *et al*.,[29] the potassium ion acts as a "structure breaker," the opposite of calcium as a "structure maker." Therefore, when potassium chloride is added to the system, potassium ions will shield PVA hydroxyl groups from water molecules and break water-water hydrogen bonding.[35,64] Roberts[35] states that water can more freely rotate when structure breakers like potassium are present in solution and lattice structures are broken which in aqueous solutions has been shown to decrease hydronium diffusivity. Although, in the case of this study, an increase in diffusivity was observed which can potentially be explained by potassium ions interacting more favorably with PVA hydroxyl groups over water. When sodium alginate was added to the polymer blend as a cryogel, carboxylate groups on the alginate chain may have chelated free potassium ions in solution, decreasing interactions between potassium ions and hydroxyl groups on PVA. At low concentrations (≤ 0.1 M) the effects of potassium on the polymer structure were negligible (**Table 2.1**), so electrostatic interactions are likely to dominate hydronium diffusion behavior. At high ionic strength, macromolecular changes to the polymer domain became more dominant as the hydrogel physically collapsed. Macromolecular changes to the polymer domain and its effect on hydronium diffusivity will be discussed in the next section.

2.4.6 Theoretical Hydronium Diffusion Mechanism Within Polymer Domain - Macroscale:

Figure 2.5 presents a conceptual model of mass transfer of hydronium within these polymer hydrogels. Hydronium ions transit the hydrogel through regions of water and polymer domains with the latter thought to be the rate controlling mass transfer barrier. Lozinsky *et al*.[37] postulates that potassium ions added to increase ionic strength, may form weak coordination bonds with hydroxyl groups on PVA, resulting in contraction of the polymer domain, decreasing space between water domains and increasing hydronium effective diffusivity. Tretinnikov *et al*. further postulates that contraction of the polymer domains may lead to the formation of additional crystalline regions once water near these regions was expelled. The contraction process in this case is similar to the formation of crystalline regions during the freeze/thaw process in which ice crystals push PVA chains in close proximity providing an opportunity for hydrogen bonding. Similar to proteins as described by Lozinsky *et al*.[37] and Hua *et al*.[36], a polymer "salting out" effect may also explain the observed diffusivity behavior through polymer aggregation and physical contraction, decreasing the volume that hydronium ions must transit between water domains. Hydrogels shrunk by up to 18% after equilibrating in 1 M KCl at room temperature (**Table 2.1**). 10% PVA cryogels shrunk by 18% and 10% PVA / 2% Alg chemically crosslinked hydrogels maintained volume or swelled by up to 2%. When 30% PVA cryogels were equilibrated in

0.5 M KCl, hydronium diffusivity decreased when compared to a 10% PVA cryogel in similar conditions (see **Figure A.20**). The observed decrease in diffusivity was likely due to polymer obstruction caused by contraction of the polymer domain, which may have a greater effect on 30% PVA cryogels due to chain mobility of lower molecular weight PVA, with respect to 10% PVA, and aggregation of crystalline domains (see **Figure 2.5**). This result further supported the hypothesis that polymer obstruction was the main factor affecting hydronium diffusivity at high ionic strength. If more crystalline regions are present, the amorphous region will likely push crystalline regions closer together at lower ionic strength in comparison to 10% PVA cryogels as shown by Tretinnikov *et al*.,[29] leading to a decrease in diffusivity as the crystalline regions block direct diffusion pathways. 10% PVA / 2% Alg cryogels behaved similarly to 10% PVA cryogels in ionic strength solutions greater than 0.001 M KCl, once alginate groups were chelated.

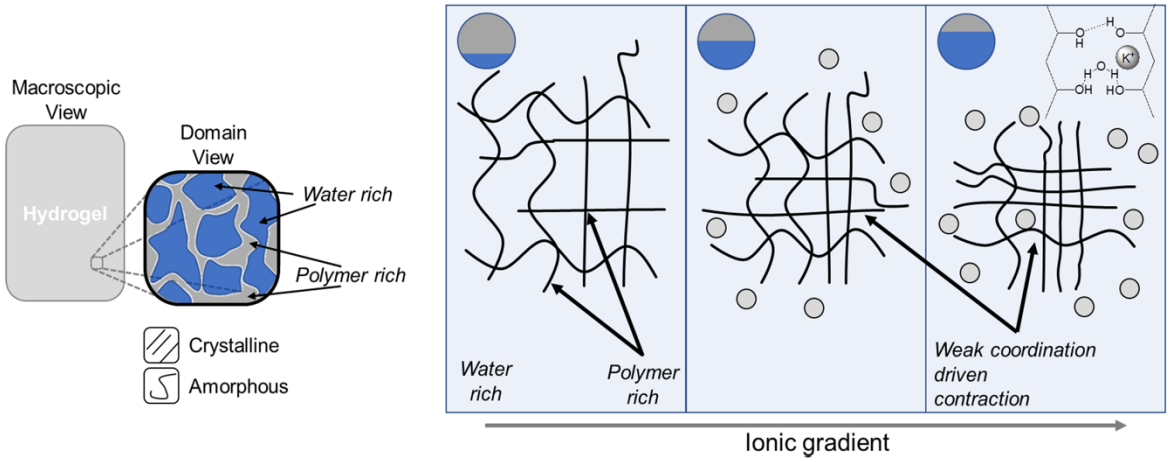

Figure 2.5: *Polymer rich domain contraction due to coordination between potassium ions (light grey circles) and PVA hydroxyl groups. Ionic strength is shown to increase from left to right with the upper left-hand circle showing water (blue) and polymer (grey) volume fraction. Crystalline and amorphous regions in the polymer rich domain are shown and not drawn to scale.*[37]

Chemically crosslinked PVA exhibits a similar response to increases in ionic strength as PVA cryogels except for at low ionic strength, 0.001 M KCl, when a decrease in diffusivity was observed (**Figure 2.4**). The cause of this decrease in diffusivity from 0 - 0.001 M KCl is unknown and requires further investigation. Additional increases in ionic strength from 0.001 – 0.1 M KCl resulted in increases in diffusivity followed by a plateau from 0.1 – 1 M KCl where the effects of polymer contraction were limited. Unlike cryogels which were potentially further crosslinked by the formation of additional crystalline domains as the hydrogel contracted, chemically crosslinked PVA was covalently crosslinked by a rigid PVA-borate complex (**Figure 2.3**), so when contraction occurred, the formation of crystalline

domains was likely hindered by the rigid spacing between PVA chains caused by the presence of PVA-borate complexes as discussed by Miyazaki *et al*.[70] When sodium alginate was crosslinked with calcium chloride, calcium ions bound carboxylate groups together, so the effects of chelation were not observed at any ionic strength. The steady increase in diffusivity from 0 – 0.5 M KCl and the plateau observed from 0.5 – 1 M KCl for 10% PVA / 2% Alg chemically crosslinked hydrogels was caused by polymer contraction, similar to 10% PVA chemically crosslinked hydrogels.

In natural encapsulated systems (e.g., biofilms), sustainable cell densities of up to approximately 10^{11} cells/mL[77] occupy 5.5% of the total system volume. The contribution of cells to hindering mass transfer by creating an impermeable fraction of the hydrogel volume is within the error of the current measurements. Alteration of the hydrogel system from actively metabolizing cells, which generate hydronium ions would be condition dependent (cell metabolic status, availability of nutrients, cell type, and hydrogel dimension/geometry) as discussed by Westrin and Axelsson.[78] According to Riley *et al*.,[79] quantifying the diffusivity of the solutes of interest in pure hydrogel are necessary to first predict how to solute diffusivity changes based on cell concentration. Hydrogel physical parameters can modify mesh size as has been discussed here which will affect the diffusivity of not only the solute but of the encapsulate microorganisms (e.g., cell leakage from/to hydrogel).

2.5 Conclusions

Co-occurring factors of polymer contraction, solvent-polymer, and solvent-solute interactions were hypothesized to increase hydronium ion diffusivity in hydrogels. When ionic species were added to the solvent, unknown interactions with the PVA-borate complex in 10% PVA hydrogels slowed diffusivity at low ionic strength, but further additions increased diffusivity. Changes in hydronium ion effective diffusivity resulting from crosslinking type, ionic strength, and polymer formulation can be used to optimize biobead design parameters. Specifically, sizing characteristic length and geometry to minimize acid accumulation within a hydrogel bead when microorganisms are actively generating acid during anaerobic reductive dechlorination. Mass transfer in hydrogels is influenced by polymer composition, solution pH, and concentration and charge of the solute and solvent, allowing for application specific tunability.[45,59,80–82] Results from this study could also aid in interpretation of and predicting pH gradients within other hydrogel and biological systems including tissue scaffolds,[83] drug release platforms,[84] environmental remediation,[85] encapsulated whole cell and enzymatic bioprocesses.[86]

2.6 References

(1) Nikam, S.; Mandal, D. Experimental Study of the Effect of Different Parameters on the Adsorption and Desorption of Trichloroethylene Vapor on Activated Carbon Particles. *ACS Omega* **2020**, *5* (43), 28080–28087. https://doi.org/10.1021/acsomega.0c03648.

(2) Toxicological Profile for Trichloroethylene. 511.

(3) Mendoza-Sanchez, I.; Autenrieth, R. L.; McDonald, T. J.; Cunningham, J. A. Biological Limitations of Dechlorination of Cis-Dichloroethene during Transport in Porous Media. *Environ. Sci. Technol.* **2018**, *52* (2), 684–691. https://doi.org/10.1021/acs.est.7b04426.

(4) Puentes Jácome, L. A.; Wang, P.-H.; Molenda, O.; Li, Y. X. (Jine-J.; Islam, M. A.; Edwards, E. A. Sustained Dechlorination of Vinyl Chloride to Ethene in Dehalococcoides-Enriched Cultures Grown without Addition of Exogenous Vitamins and at Low PH. *Environ. Sci. Technol.* **2019**, *53* (19), 11364–11374. https://doi.org/10.1021/acs.est.9b02339.

(5) Mao, X.; Oremland, R. S.; Liu, T.; Gushgari, S.; Landers, A. A.; Baesman, S. M.; Alvarez-Cohen, L. Acetylene Fuels TCE Reductive Dechlorination by Defined Dehalococcoides/Pelobacter Consortia. *Environ. Sci. Technol.* **2017**, *51* (4), 2366–2372. https://doi.org/10.1021/acs.est.6b05770.

(6) Xiao, Z.; Jiang, W.; Chen, D.; Xu, Y. Bioremediation of Typical Chlorinated Hydrocarbons by Microbial Reductive Dechlorination and Its Key Players: A Review. *Ecotoxicol. Environ. Saf.* **2020**, *202*, 110925. https://doi.org/10.1016/j.ecoenv.2020.110925.

(7) Ellis, D. E.; Lutz, E. J.; Odom, J. M.; Buchanan, R. J.; Bartlett, C. L.; Lee, M. D.; Harkness, M. R.; DeWeerd, K. A. Bioaugmentation for Accelerated In Situ Anaerobic Bioremediation. *Environ. Sci. Technol.* **2000**, *34* (11), 2254–2260. https://doi.org/10.1021/es990638e.

(8) Liu, M.-H.; Hsiao, C.-M.; Lin, C.-E.; Leu, J. Application of Combined In Situ Chemical Reduction and Enhanced Bioremediation to Accelerate TCE Treatment in Groundwater. *Appl. Sci.* **2021**, *11* (18), 8374. https://doi.org/10.3390/app11188374.

(9) Liu, P.-W. G.; Wu, Y.-J.; Whang, L.-M.; Lin, T.-F.; Hung, W.-N.; Cho, K.-C. Molecular Tools with Statistical Analysis on Trichloroethylene Remediation Effectiveness. *Int. Biodeterior. Biodegrad.* **2020**, *154*, 105050. https://doi.org/10.1016/j.ibiod.2020.105050.

(10) Robinson, C.; Barry, D. A.; McCarty, P. L.; Gerhard, J. I.; Kouznetsova, I. PH Control for Enhanced Reductive Bioremediation of Chlorinated Solvent Source Zones. *Sci. Total Environ.* **2009**, *407* (16), 4560–4573. https://doi.org/10.1016/j.scitotenv.2009.03.029.

(11) Yu, S.; Semprini, L. Kinetics and Modeling of Reductive Dechlorination at High PCE and TCE Concentrations. *Biotechnol. Bioeng.* **2004**, *88* (4), 451–464. https://doi.org/10.1002/bit.20260.

(12) Haest, P. J.; Springael, D.; Smolders, E. Dechlorination Kinetics of TCE at Toxic TCE Concentrations: Assessment of Different Models. *Water Res.* **2010**, *44* (1), 331–339. https://doi.org/10.1016/j.watres.2009.09.033.

(13) Lacroix, E.; Brovelli, A.; Barry, D. A.; Holliger, C. Use of Silicate Minerals for PH Control during Reductive Dechlorination of Chloroethenes in Batch Cultures of Different Microbial Consortia. *Appl. Environ. Microbiol.* **2014**, *80* (13), 3858–3867. https://doi.org/10.1128/AEM.00493-14.

(14) Charles, C. J.; Rout, S. P.; Patel, K. A.; Akbar, S.; Laws, A. P.; Jackson, B. R.; Boxall, S. A.; Humphreys, P. N. Floc Formation Reduces the PH Stress Experienced by Microorganisms Living in Alkaline Environments. *Appl. Environ. Microbiol.* **2017**, *83* (6), e02985-16. https://doi.org/10.1128/AEM.02985-16.

(15) Yang, Y.-C.; Huang, W.-S.; Hu, S.-M.; Huang, C.-W.; Chiu, C.-H.; Chen, H.-Y. Synergistic and Regulatable Bioremediation Capsules Fabrication Based on Vapor-Phased Encapsulation of Bacillus Bacteria and Its Regulator by Poly-p-Xylylene. *Polymers* **2020**, *13* (1), 41. https://doi.org/10.3390/polym13010041.

(16) Valdivia-Rivera, S.; Ayora-Talavera, T.; Lizardi-Jiménez, M. A.; García-Cruz, U.; Cuevas-Bernardino, J. C.; Pacheco, N. Encapsulation of Microorganisms for Bioremediation: Techniques

and Carriers. *Rev. Environ. Sci. Biotechnol.* **2021**, *20* (3), 815–838. https://doi.org/10.1007/s11157-021-09577-x.

(17) Jen, A. C.; Wake, M. C.; Mikos, A. G. Review: Hydrogels for Cell Immobilization. *Biotechnol. Bioeng.* **1996**, *50* (4), 357–364. https://doi.org/10.1002/(SICI)1097-0290(19960520)50:4<357::AID-BIT2>3.0.CO;2-K.

(18) Zhou, Y.-Z.; Yang, J.; Wang, X.-L.; Pan, Y.-Q.; Li, H.; Zhou, D.; Liu, Y.-D.; Wang, P.; Gu, J.-D.; Lu, Q.; Qiu, Y.-F.; Lin, K.-F. Bio-Beads with Immobilized Anaerobic Bacteria, Zero-Valent Iron, and Active Carbon for the Removal of Trichloroethane from Groundwater. *Environ. Sci. Pollut. Res.* **2014**, *21* (19), 11500–11509. https://doi.org/10.1007/s11356-014-3110-6.

(19) Zhou, Y.-Z.; Yang, J.; Wang, X.-L.; Pan, Y.-Q.; Li, H.; Zhou, D.; Liu, Y.-D.; Wang, P.; Gu, J.-D.; Lu, Q.; Qiu, Y.-F.; Lin, K.-F. Bio-Beads with Immobilized Anaerobic Bacteria, Zero-Valent Iron, and Active Carbon for the Removal of Trichloroethane from Groundwater. *Environ. Sci. Pollut. Res.* **2014**, *21* (19), 11500–11509. https://doi.org/10.1007/s11356-014-3110-6.

(20) Wang, S.-M.; Tseng, S. Dechlorination of Trichloroethylene by Immobilized Autotrophic Hydrogen-Bacteria and Zero-Valent Iron. *J. Biosci. Bioeng.* **2009**, *107* (3), 287–292. https://doi.org/10.1016/j.jbiosc.2008.11.010.

(21) Kim, S.; Bae, W.; Hwang, J.; Park, J. Aerobic TCE Degradation by Encapsulated Toluene-Oxidizing Bacteria, Pseudomonas Putida and Bacillus Spp. *Water Sci. Technol.* **2010**, *62* (9), 1991–1997. https://doi.org/10.2166/wst.2010.471.

(22) Schuszter, G.; Gehér-Herczegh, T.; Szűcs, Á.; Tóth, Á.; Horváth, D. Determination of the Diffusion Coefficient of Hydrogen Ion in Hydrogels. *Phys. Chem. Chem. Phys.* **2017**, *19* (19), 12136–12143. https://doi.org/10.1039/C7CP00986K.

(23) Choudhury, R. R.; Gohil, J. M.; Dutta, K. Poly(Vinyl Alcohol)-Based Membranes for Fuel Cell and Water Treatment Applications: A Review on Recent Advancements. *Polym. Adv. Technol. n/a* (n/a). https://doi.org/10.1002/pat.5431.

(24) Ajith, C.; Deshpande, A. P.; Varughese, S. Proton Conductivity in Crosslinked Hydrophilic Ionic Polymer System: Competitive Hydration, Crosslink Heterogeneity, and Ineffective Domains. *J. Polym. Sci. Part B Polym. Phys.* **2016**, *54* (11), 1087–1101. https://doi.org/10.1002/polb.24012.

(25) Itou, T.; Kitai, H.; Shimazu, A.; Miyazaki, T.; Tashiro, K. Clarification of Cross-Linkage Structure in Boric Acid Doped Poly(Vinyl Alcohol) and Its Model Compound As Studied by an Organized Combination of X-Ray Single-Crystal Structure Analysis, Raman Spectroscopy, and Density Functional Theoretical Calculation. *J. Phys. Chem. B* **2014**, *118* (22), 6032–6037. https://doi.org/10.1021/jp5026569.

(26) Tsai, C.-J.; Chang, Y.-R.; Lee, D.-J. Shape Stable Poly(Vinyl Alcohol) and Alginate Cross-Linked Hydrogel under Drying-Rewetting Cycles: Boron Substitution. *Ind. Eng. Chem. Res.* **2018**, *57* (42), 14213–14222. https://doi.org/10.1021/acs.iecr.8b03420.

(27) Chang, C.-C.; Tseng, S.-K. Immobilization of Alcaligenes Eutrophus Using PVA Crosslinked with Sodium Nitrate. *Biotechnol. Tech.* **1998**, *12* (12), 865–868. https://doi.org/10.1023/A:1008895525476.

(28) Chang, C.; Lue, A.; Zhang, L. Effects of Crosslinking Methods on Structure and Properties of Cellulose/PVA Hydrogels. *Macromol. Chem. Phys.* **2008**, *209* (12), 1266–1273. https://doi.org/10.1002/macp.200800161.

(29) Tretinnikov, O. N.; Sushko, N. I.; Zagorskaya, S. A. Effect of Salt Concentration on the Structure of Poly(Vinyl Alcohol) Cryogels Obtained from Aqueous Salt Solutions. *J. Appl. Spectrosc.* **2015**, *82* (1), 40–45. https://doi.org/10.1007/s10812-015-0061-8.

(30) Harland, R. S.; Peppas, N. A. Solute Diffusion in Swollen Membranes VII. Diffusion in Semicrystalline Networks. *Colloid Polym. Sci.* **1989**, *267* (3), 218–225. https://doi.org/10.1007/BF01410578.

(31) Wang, P.-H.; Chang, Y.-R.; Lee, D.-J. Structure for Shape Stable Poly(Vinyl Alcohol) Hydrogel under PH Shock. *J. Taiwan Inst. Chem. Eng.* **2019**, *104*, 341–350. https://doi.org/10.1016/j.jtice.2019.09.011.

(32) Wang, X.; You, J.; Wu, Y. In Situ Gelation of Aqueous Sulfuric Acid Solution for Fuel Cells. *RSC Adv.* **2021**, *11* (36), 22461–22466. https://doi.org/10.1039/D1RA02629A.
(33) Lustig, S. R.; Peppas, N. A. Solute Diffusion in Swollen Membranes. IX. Scaling Laws for Solute Diffusion in Gels. *J. Appl. Polym. Sci.* **1988**, *36* (4), 735–747. https://doi.org/10.1002/app.1988.070360401.
(34) Cassone, G.; Creazzo, F.; Saija, F. Ionic Diffusion and Proton Transfer of MgCl2 and CaCl2 Aqueous Solutions: An Ab Initio Study under Electric Field. *Mol. Simul.* **2019**, *45* (4–5), 373–380. https://doi.org/10.1080/08927022.2018.1513650.
(35) Roberts, N. K. Proton Diffusion and Activity in the Presence of Electrolytes. *J. Phys. Chem.* **1976**, *80* (10), 1117–1120. https://doi.org/10.1021/j100551a018.
(36) Hua, M.; Wu, S.; Ma, Y.; Zhao, Y.; Chen, Z.; Frenkel, I.; Strzalka, J.; Zhou, H.; Zhu, X.; He, X. Strong Tough Hydrogels via the Synergy of Freeze-Casting and Salting Out. *Nature* **2021**, *590* (7847), 594–599. https://doi.org/10.1038/s41586-021-03212-z.
(37) Lozinsky, V. I.; Sakhno, N. G.; Damshkaln, L. G.; Bakeeva, I. V.; Zubov, V. P.; Kurochkin, I. N.; Kurochkin, I. I. Study of Cryostructuring of Polymer Systems: 31. Effect of Additives of Alkali Metal Chlorides on Physicochemical Properties and Morphology of Poly(Vinyl Alcohol) Cryogels. *Colloid J.* **2011**, *73* (2), 234. https://doi.org/10.1134/S1061933X11020086.
(38) Agmon, N. The Grotthuss Mechanism. *Chem. Phys. Lett.* **1995**, *244* (5–6), 456–462. https://doi.org/10.1016/0009-2614(95)00905-J.
(39) Roberts, N. K.; Zundel, G. *IR studies of long-range surface effects—excess proton mobility in water in quartz pores | Nature*. https://www.nature.com/articles/278726a0 (accessed 2022-03-31).
(40) Holloway, J. L.; Lowman, A. M.; Palmese, G. R. The Role of Crystallization and Phase Separation in the Formation of Physically Cross-Linked PVA Hydrogels. *Soft Matter* **2013**, *9* (3), 826–833. https://doi.org/10.1039/C2SM26763B.
(41) Wu, K.-Y. A.; Wisecarver, K. D. Cell Immobilization Using PVA Crosslinked with Boric Acid. *Biotechnol. Bioeng.* **1992**, *39* (4), 447–449. https://doi.org/10.1002/bit.260390411.
(42) Northrop, J. H.; Anson, M. L. A Method for the Determination of Diffusion Constants and the Calculation of the Radius and Weight of the Hemoglobin Molecule. *J. Gen. Physiol.* **1929**, *12* (4), 543–554. https://doi.org/10.1085/jgp.12.4.543.
(43) Meadows, D. L.; Peppas, N. A. Solute Diffusion in Swollen Membranes Iii. Non-Equilibrium Thermodynamic Aspects of Solute Diffusion in Polymer Network Membranes. *Chem. Eng. Commun.* **1984**, *31* (1–6), 101–119. https://doi.org/10.1080/00986448408911144.
(44) Peppas, N. A.; Merrill, E. W. Poly(Vinyl Alcohol) Hydrogels: Reinforcement of Radiation-Crosslinked Networks by Crystallization. *J. Polym. Sci. Polym. Chem. Ed.* **1976**, *14* (2), 441–457. https://doi.org/10.1002/pol.1976.170140215.
(45) Gudeman, L. F.; Peppas, N. A. Preparation and Characterization of PH-Sensitive, Interpenetrating Networks of Poly(Vinyl Alcohol) and Poly(Acrylic Acid). *J. Appl. Polym. Sci.* **1995**, *55* (6), 919–928. https://doi.org/10.1002/app.1995.070550610.
(46) Nightingale, E. R. Phenomenological Theory of Ion Solvation. Effective Radii of Hydrated Ions. *J. Phys. Chem.* **1959**, *63* (9), 1381–1387. https://doi.org/10.1021/j150579a011.
(47) Masaro, L.; Ousalem, M.; Baille, W. E.; Lessard, D.; Zhu, X. X. Self-Diffusion Studies of Water and Poly(Ethylene Glycol) in Solutions and Gels of Selected Hydrophilic Polymers. *Macromolecules* **1999**, *32* (13), 4375–4382. https://doi.org/10.1021/ma990211s.
(48) Zhang; Han. Viscosity and Density of Water + Sodium Chloride + Potassium Chloride Solutions at 298.15 K. *J. Chem. Eng. Data* **1996**, *41* (3), 516–520. https://doi.org/10.1021/je9501402.
(49) Wraight, C. A. Chance and Design—Proton Transfer in Water, Channels and Bioenergetic Proteins. *Biochim. Biophys. Acta BBA - Bioenerg.* **2006**, *1757* (8), 886–912. https://doi.org/10.1016/j.bbabio.2006.06.017.
(50) Masaro, L.; Zhu, X. X. Physical Models of Diffusion for Polymer Solutions, Gels and Solids. *Prog. Polym. Sci.* **1999**, *24* (5), 731–775. https://doi.org/10.1016/S0079-6700(99)00016-7.

(51) Sinton, S. W. Complexation Chemistry of Sodium Borate with Poly(Vinyl Alcohol) and Small Diols: A Boron-11 NMR Study. *Macromolecules* **1987**, *20* (10), 2430–2441. https://doi.org/10.1021/ma00176a018.
(52) R Core Team. *R: A Language and Environment for Statistical Computing*; R Foundation for Statistical Computing: Vienna, Austria, 2021.
(53) Fox, J.; Weisberg, S. *An R Companion to Applied Regression*; Sage: Thousand Oaks CA, 2019.
(54) Hothorn, T.; Bretz, F.; Westfall, P. Simultaneous Inference in General Parametric Models. *Biom. J.* **2008**, *50* (3), 346–363.
(55) De Rosario-Martinez, H. *Phia: Post-Hoc Interaction Analysis*; 2015.
(56) Singmann, H.; Bolker, B.; Westfall, J.; Aust, F.; Ben-Shachar, M. S. *Afex: Analysis of Factorial Experiments*; 2021.
(57) Lenth, R. V. *Emmeans: Estimated Marginal Means, Aka Least-Squares Means*; 2021.
(58) Hoare, T. R.; Kohane, D. S. Hydrogels in Drug Delivery: Progress and Challenges. *Polymer* **2008**, *49* (8), 1993–2007. https://doi.org/10.1016/j.polymer.2008.01.027.
(59) Fatin-Rouge, N.; Milon, A.; Buffle, J.; Goulet, R. R.; Tessier, A. Diffusion and Partitioning of Solutes in Agarose Hydrogels: The Relative Influence of Electrostatic and Specific Interactions. *J. Phys. Chem. B* **2003**, *107* (44), 12126–12137. https://doi.org/10.1021/jp0303164.
(60) Kapellos, G. E.; Alexiou, T. S.; Payatakes, A. C. A Multiscale Theoretical Model for Diffusive Mass Transfer in Cellular Biological Media. *Math. Biosci.* **2007**, *210* (1), 177–237. https://doi.org/10.1016/j.mbs.2007.04.008.
(61) Harland, R. S.; Peppas, N. A. Solute Diffusion in Swollen Membranes. *Polym. Bull.* **1987**, *18* (6), 553–556. https://doi.org/10.1007/BF00255341.
(62) Peterlin, A. Dependence of Diffusive Transport on Morphology of Crystalline Polymers. *J. Macromol. Sci. Part B* **1975**, *11* (1), 57–87. https://doi.org/10.1080/00222347508217855.
(63) Ricciardi, R.; Auriemma, F.; De Rosa, C.; Lauprêtre, F. X-Ray Diffraction Analysis of Poly(Vinyl Alcohol) Hydrogels, Obtained by Freezing and Thawing Techniques. *Macromolecules* **2004**, *37* (5), 1921–1927. https://doi.org/10.1021/ma035663q.
(64) Patachia, S.; Valente, A. J. M.; Baciu, C. Effect of Non-Associated Electrolyte Solutions on the Behaviour of Poly(Vinyl Alcohol)-Based Hydrogels. *Eur. Polym. J.* **2007**, *43* (2), 460–467. https://doi.org/10.1016/j.eurpolymj.2006.11.009.
(65) Huang, Y.; Zhang, M.; Ruan, W. High-Water-Content Graphene Oxide/Polyvinyl Alcohol Hydrogel with Excellent Mechanical Properties. *J. Mater. Chem. A* **2014**, *2* (27), 10508–10515. https://doi.org/10.1039/C4TA01464B.
(66) Gayet, J.-C.; Fortier, G. High Water Content BSA-PEG Hydrogel for Controlled Release Device: Evaluation of the Drug Release Properties. *J. Controlled Release* **1996**, *38* (2), 177–184. https://doi.org/10.1016/0168-3659(95)00118-2.
(67) Rietjens, M.; Steenbergen, P. A. Crosslinking Mechanism of Boric Acid with Diols Revisited. *Eur. J. Inorg. Chem.* **2005**, *2005* (6), 1162–1174. https://doi.org/10.1002/ejic.200400674.
(68) Kamcev, J.; Paul, D. R.; Manning, G. S.; Freeman, B. D. Ion Diffusion Coefficients in Ion Exchange Membranes: Significance of Counterion Condensation. *Macromolecules* **2018**, *51* (15), 5519–5529. https://doi.org/10.1021/acs.macromol.8b00645.
(69) Frahn, J. L. Paper Electrophoresis of Hydroxycarboxylic Acids as Their Borate Complexes with Special Reference to Viridifloric, Trachelanthic, Lasiocarpic and Heliotric Acids: The Importance of the "Gem- Dialkyl" Effect in Complex Formation. *J. Chromatogr. A* **1984**, *314*, 167–181. https://doi.org/10.1016/S0021-9673(01)97731-3.
(70) Miyazaki, T.; Takeda, Y.; Akane, S.; Itou, T.; Hoshiko, A.; En, K. Role of Boric Acid for a Poly (Vinyl Alcohol) Film as a Cross-Linking Agent: Melting Behaviors of the Films with Boric Acid. *Polymer* **2010**, *51* (23), 5539–5549. https://doi.org/10.1016/j.polymer.2010.09.048.
(71) Nickerson, R. F. Thickening of Poly(Vinyl Alcohol) by Borate. *J. Appl. Polym. Sci.* **1971**, *15* (1), 111–116. https://doi.org/10.1002/app.1971.070150110.

(72) Polemio, M.; Bufo, S.; Paoletti, S. Evaluation of Ionic Strength and Salinity of Groundwaters: Effect of the Ionic Composition. *Geochim. Cosmochim. Acta* **1980**, *44* (6), 809–814. https://doi.org/10.1016/0016-7037(80)90262-8.
(73) Hassanali, A.; Giberti, F.; Cuny, J.; Kühne, T. D.; Parrinello, M. Proton Transfer through the Water Gossamer. *Proc. Natl. Acad. Sci.* **2013**, *110* (34), 13723–13728. https://doi.org/10.1073/pnas.1306642110.
(74) Kornyshev, A. A.; Kuznetsov, A. M.; Spohr, E.; Ulstrup, J. Kinetics of Proton Transport in Water. *J. Phys. Chem. B* **2003**, *107* (15), 3351–3366. https://doi.org/10.1021/jp020857d.
(75) Horne, R. A. Electrical Conductance in Acidic, Aqueous Solutions. *J. Electrochem. Soc.* **1965**, *112* (8), 857. https://doi.org/10.1149/1.2423711.
(76) Horne, R. A.; Axelrod, E. H. Proton Mobility and Electron Exchange in Aqueous Media. *J. Chem. Phys.* **1964**, *40* (6), 1518–1522. https://doi.org/10.1063/1.1725356.
(77) Hou, J.; Wang, C.; Rozenbaum, R. T.; Gusnaniar, N.; de Jong, E. D.; Woudstra, W.; Geertsema-Doornbusch, G. I.; Atema-Smit, J.; Sjollema, J.; Ren, Y.; Busscher, H. J.; van der Mei, H. C. Bacterial Density and Biofilm Structure Determined by Optical Coherence Tomography. *Sci. Rep.* **2019**, *9* (1), 9794. https://doi.org/10.1038/s41598-019-46196-7.
(78) Westrin, B. A.; Axelsson, A. Diffusion in Gels Containing Immobilized Cells: A Critical Review. *Biotechnol. Bioeng.* **1991**, *38* (5), 439–446. https://doi.org/10.1002/bit.260380502.
(79) Riley, M. R.; Muzzio, F. J.; Buettner, H. M.; Reyes, S. C. A Simple Correlation for Predicting Effective Diffusivities in Immobilized Cell Systems. *Biotechnol. Bioeng.* **1996**, *49* (2), 223–227. https://doi.org/10.1002/bit.260490202.
(80) Hagel, V.; Haraszti, T.; Boehm, H. Diffusion and Interaction in PEG-DA Hydrogels. *Biointerphases* **2013**, *8* (1), 36. https://doi.org/10.1186/1559-4106-8-36.
(81) Risbud, M. V.; Hardikar, A. A.; Bhat, S. V.; Bhonde, R. R. PH-Sensitive Freeze-Dried Chitosan–Polyvinyl Pyrrolidone Hydrogels as Controlled Release System for Antibiotic Delivery. *J. Controlled Release* **2000**, *68* (1), 23–30. https://doi.org/10.1016/S0168-3659(00)00208-X.
(82) Cha, R.; He, Z.; Ni, Y. Preparation and Characterization of Thermal/PH-Sensitive Hydrogel from Carboxylated Nanocrystalline Cellulose. *Carbohydr. Polym.* **2012**, *88* (2), 713–718. https://doi.org/10.1016/j.carbpol.2012.01.026.
(83) Bharadwaz, A.; Jayasuriya, A. C. Recent Trends in the Application of Widely Used Natural and Synthetic Polymer Nanocomposites in Bone Tissue Regeneration. *Mater. Sci. Eng. C* **2020**, *110*, 110698. https://doi.org/10.1016/j.msec.2020.110698.
(84) Zhu, Y.-J.; Chen, F. PH-Responsive Drug-Delivery Systems. *Chem. – Asian J.* **2015**, *10* (2), 284–305. https://doi.org/10.1002/asia.201402715.
(85) Robinson, C.; Barry, D. A. Design Tool for Estimation of Buffer Requirement for Enhanced Reductive Dechlorination of Chlorinated Solvents in Groundwater. *Environ. Model. Softw.* **2009**, *24* (11), 1332–1338. https://doi.org/10.1016/j.envsoft.2009.03.012.
(86) Pierre, A. C. The Sol-Gel Encapsulation of Enzymes. *Biocatal. Biotransformation* **2004**, *22* (3), 145–170. https://doi.org/10.1080/10242420412331283314.

Chapter 3: Modeling of Anaerobic Reductive Dechlorination of Chlorinated Aliphatic Hydrocarbons in Hydrogel Beads

3.1 Abstract

Bioremediation of chlorinated aliphatic hydrocarbons (CAHs) is a common technique used in groundwater cleanup efforts due to its reliability in degrading trichloroethylene (TCE) and other CAHs. Although, dechlorinating microorganisms are often inhibited before decontamination is complete due to buildup of acid and high CAH concentrations. Protecting microbes from inhibitory factors by encapsulation is a potential solution, although key mass transfer coefficients needed to optimize the encapsulated system geometry, size, and cell density are lacking. To address this knowledge gap, effective diffusion coefficients of TCE, 1,2-*cis*-dichloroethylene (cDCE), and vinyl chloride (VC) were measured in 10% poly(vinyl alcohol) / 2% alginate hydrogels in a range of ionic solutions. A reaction-diffusion model was implemented using similar diffusion coefficients to predict optimal parameters for complete dechlorination in a single hydrogel bead inoculated with anaerobic dechlorinating microorganisms. The max predicted ratio of ethylene generated to TCE degraded was 0.0005. By combining measured diffusivities with a computational model, it was found that biobeads were capable of complete TCE degradation, but without additional pH control, the hydrogel would be unable to protect microorganisms at high cell concentrations. This study provides key information needed to optimize this promising technology.

3.2 Introduction

Chlorinated aliphatic hydrocarbons (CAHs), such as trichloroethylene (TCE) and vinyl chloride (VC), are persistent groundwater pollutants found in over 1000 superfund sites across the United States.[1] One promising method for CAH degradation is bioremediation, which has been identified as an effective low-cost remediation strategy relative to typical chemical separation techniques.[2] TCE is biologically degraded by anaerobic reductive dechlorination as shown in **Figure 3.1**. During biological reductive dechlorination of CAHs, build-up of metabolic end products (H^+) and biproducts, cis-1,2-dichloroethylene (cDCE) and VC, may lead to microbial inhibition and the release of highly toxic VC, potentially leaving the system in a more hazardous state. To limit the inhibitory effects of CAHs on dechlorinating microorganisms, the microbes must be placed further downstream from the contaminant plume at a location with lower concentrations, but by doing so the contaminant plume is left to spread and volatilize, increasing the risk of exposure to the general public or additional contamination of nearby water sources. To combat the effects of pH inhibition, dechlorinating microorganisms already

utilize natural buffering compounds as well as other naturally occurring microorganisms, but these natural buffering systems can be overwhelmed due to constant acid generation.[3] Additional buffers can be injected, but in some cases, may be depleted too, requiring frequent reinjection which can be time intensive and expensive. Therefore, protecting microorganisms from these inhibitory factors is desirable for efficient and effective dechlorination of CAHs.

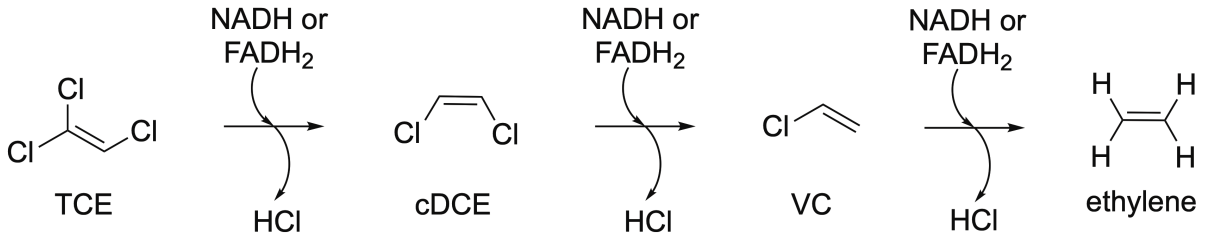

Figure 3.1: *Anaerobic reductive dechlorination mechanism of TCE to ethylene.*

Synthetic biofilms using encapsulating media may hold substantial promise in addressing H^+ and CAH concentration challenges in anaerobic reductive dechlorination. Encapsulating microorganisms in hydrogels provides a diffusion barrier between contaminants and the microbes shielding them in high concentration areas such as directly in contaminant plumes. Likewise, acid generated by microorganisms is present in a smaller more controllable environment that may be amiable to localized microbe or anthropogenic adjustment or acids may diffuse away, assuming the bulk pH around the bead is higher than within the bead. **Figure 3.2** depicts three different scenarios where a biobead may operate. We call these schemes the Goldilocks scenarios, based on the popular fairy tale *Goldilocks and the Three Bears* where Goldilocks tries three soups, one "too hot," one "too cold," and another "just right." NASA uses a similar distinction to determine how habitable a planet might be based on its temperature, or distance from its sun.[4] Planets are said to be in a Goldilocks zone when they are in a position far enough away from their sun that the water on the planet doesn't boil off and evaporate because the planet is too hot, and simultaneously not too far away from the sun that all the water freezes because the planet is too cold. A planet is in the Goldilocks zone when water is bioavailable, and life is sustainable, and the temperature is "just right." A similar principle can be applied to biobeads where favorable conditions for microbial life are defined by the encapsulated microorganisms' reactivity at steady state. Microbial inhibition by concentrated acid and CAHs make conditions unfavorable for anaerobic reductive dechlorination by reducing microbial reactivity with CAHs. Therefore, if at steady state the system pH is below inhibitory levels, CAHs are likely consumed quickly, creating

uninhabitable conditions for microorganism due to generation of acid (**Figure 3.2.A**). This scenario will be denoted as "too hot" since microbial reactivity is much faster than acid diffusion out of the biobead. If, at steady state the system pH is near 7, microbial reactivity is low, likely due to low cell concentrations, in comparison to CAH diffusivity into the biobead (**Figure 3.2.B**). This scenario can be denoted as "too cold" since CAH concentrations inhibited microorganisms before they could degrade a significant amount of the CAHs. A balanced reaction-diffusion biobead allows for microorganisms to degrade CAHs as they diffuse through the biobead while simultaneously allowing acid to diffuse out quickly so that pH does not decrease to inhibitory levels (**Figure 3.2.C**). This scenario can be denoted as "just right."

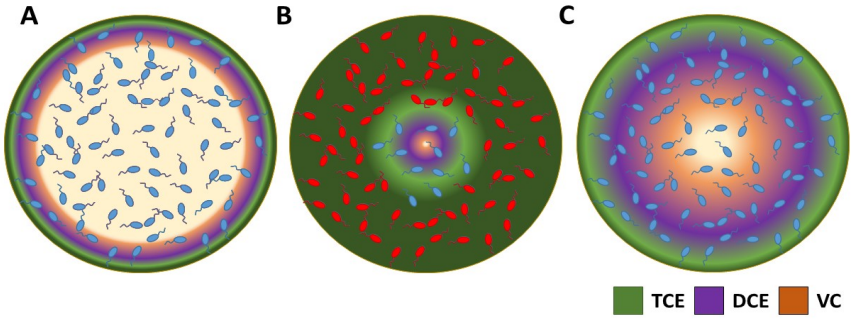

Figure 3.2: *Biobead goldilocks scenarios. (A) Diffusion limited, (B) Reaction limited, (C) Balanced reaction and diffusion.*

Polymers used as synthetic biofilms may be readily tuned to system requirements (e.g., ionic strength, initial pH) to ensure a balanced biobead (**Figure 3.2.C**) which make them uniquely adaptable to various groundwater conditions. The use of encapsulated microorganisms made of different polymer matrices have been successful in many applications including degradation of various CAHs,[5–7] co-metabolic or reductive degradation of TCE,[8,9] and hybrid organic/inorganic framework of zero-valent iron[5,6,10,11] and activated carbon[5,12] for reductive dechlorination of CAHs. However, data for CAH mass transfer is lacking and needed to optimize these engineered materials.

To address this knowledge gap, the effective diffusivities of TCE and its biodegradation products, cDCE and VC were determined through 10% poly(vinyl alcohol) / 2% alginate (10% PVA / 2% Alg) blended hydrogels using the diaphragm cell method and are presented herein. Measured diffusivities were applied in a numerical model simulating CAH diffusion and degradation simultaneously at steady state in a single spherical bead. The percentage of TCE fully degraded to ethylene was assessed in a

Monte Carlo simulation to determine how dechlorination efficiency varied with bead radius and cell concentration.

3.3 Materials and Methods

3.3.1 Reagents:

98.0-98.8% hydrolyzed PVA (MW: 146-186k Da, Acros), Alginic acid (Alg) sodium salt, potassium chloride, TCE, cDCE (97%), and VC (2000 μg/mL in methanol) were obtained from Sigma Aldrich. All chemicals were used without further purification.

3.3.2 Polymer Crosslinking:

10% PVA / 2% Alg hydrogels were prepared and cast as outline previously in Chapter 2. PVA and Alg were added to water and heated to 80 ˚C until all components were dissolved. The solution was cooled to 45 ˚C and the stirring rate was slowed for about 1 hour before casting to allow for the solution to degas. After casting, the polymer solutions were transferred to a -20 ˚C freezer and subjected to five freeze-thaw cycles before being placed in the appropriate solution (0 M, 0.001 M, or 0.01 M KCl), in accordance with desired solute concentration. Gels were allowed to equilibrate and swell in the solute solution for 2-8 days before use. The gels and solute solution were placed in a refrigerator to limit gel contraction from the walls of the steel casting mold for at least the first 2 days of equilibration.

3.3.3 Apparatus for Diffusion Measurements:

316 stainless steel (SS) pipe, tubing, caps, luer-lok fittings, and rods were obtained from McMaster. Glass stir bars were obtained from Cole-Parmer. Torr Seal was obtained from Agilent. A diaphragm diffusion cell made from 316 SS was used to determine effective diffusion coefficients of CAHs in 10% PVA / 2% Alg hydrogels. A membrane cast and crosslinked in a stainless-steel mold was placed in a steel pipe to separate a source (high concentration CAH) and sink (No CAH at t=0). Stainless steel was used to limit the necessity for Teflon and other plastic seals which absorb TCE.[13] Membrane molds were manufactured in house with the addition of two Viton O-rings to prevent leaking between the sink and source chambers. CAH concentrations in the sink side of the diffusion cell were monitored using an Evolution 60S UV-visible spectrometer (Thermo Scientific). A flow through cuvette was used to allow for continuous measurements. The cuvette was retrofitted with 1/16” stainless steel tubing down the inlet and outlet ports and sealed with torr seal to stop leaks or CAH evaporation.

3.3.4 Diffusion-Reaction Model:

The finite difference method was used to model and track the transport, accumulation, and degradation of CAHs through a single spherical hydrogel bead (see **Equation 3-1– 3-3** and **Figure 3.3**).

$$\frac{\partial C}{\partial t} = \frac{C_{i,j,k+1} - C_{i,j,k}}{\Delta t}$$

Equation 3-1

$$\frac{\partial C}{\partial r} = \frac{C_{i,j+1,k} - C_{i,j-1,k}}{2\Delta r}$$

Equation 3-2

$$\frac{\partial^2 C}{\partial r^2} = \frac{C_{i,j+1,k} - 2C_{i,j,k} + C_{i,j-1,k}}{\Delta r^2}$$

Equation 3-3

Where $C_{i,j,k}$ is the concentration of species i at spatial point j and time step k, Δt is the time step size, and Δr is the spatial, i.e., radial, step size. A partial differential equation was solved at each spatial point assuming one dimensional diffusion for all time steps (**Equation 3-4**).

$$\frac{\partial C_{CAH}}{\partial t} + D_{e,CAH}\left(\frac{2}{r}\frac{\partial C_{CAH}}{\partial r} + \frac{\partial^2 C_{CAH}}{\partial r^2}\right) - r_{CAH} = 0$$

Equation 3-4

Reaction rates (r_{CAH}) were calculated using equations developed by Haest et al.[14] who experimentally determined reaction coefficients using EC_{50} kinetics and planktonic KB-1 cell cultures for each CAH of interest. A pH inhibition model developed by Lacroix et al.[15] (**Equation 3-5**) was added (**Equation 3-6**) to the rate equations developed by Haest et al. to simulate dechlorination in the absence of buffers or other pH moderating compounds. pH_{opt} was the optimal pH for each CAH (TCE: 6.99, cDCE: 6.60, VC: 6.50)[15], pH was the observed pH, n and σ were empirical parameters, and $r_{i,max}$ was the maximum rate possible without pH inhibition. The parameters taken from Lacroix et al. were determined by fitting a model to experimental data using a consortium of *Dehalococcoides* spp. and *Sulfurospirillum* spp.[15]

$$f(pH) = \exp\left(-\frac{\left|pH_{opt} - pH\right|^n}{\sigma^2}\right)$$

Equation 3-5

$$r_i = r_{i,max} \times f(pH)$$

Equation 3-6

These kinetic parameters may[16] or may not[17] match encapsulated cell growth kinetics, but provide an order of magnitude approximation for coupling reaction and diffusion in hydrogel systems.

Bulk fluid around the bead was assumed to have a constant pH of 7.0 and TCE concentration of 1500 ppb.[9] A constant cell density within the bead was assumed to reflect a steady state cell concentration. Boundary conditions were set up in three sections: (1) At t = 0 for 0 < r < R concentration is uniform. (2) At r = 0 for t > 0, at the center of the bead, $\frac{dC}{dr} = 0$ with symmetry. (3) At the bulk-gel interface (r = R), the TCE concentration is constant at 0.011 mM, and cDCE and VC at the interface are defined by balanced flux. The bulk fluid outside the hydrogel was assumed to be an infinite sink where C_{TCE} = 1500 ppb and $C_{cDCE} = C_{VC} = 0$ ppb.

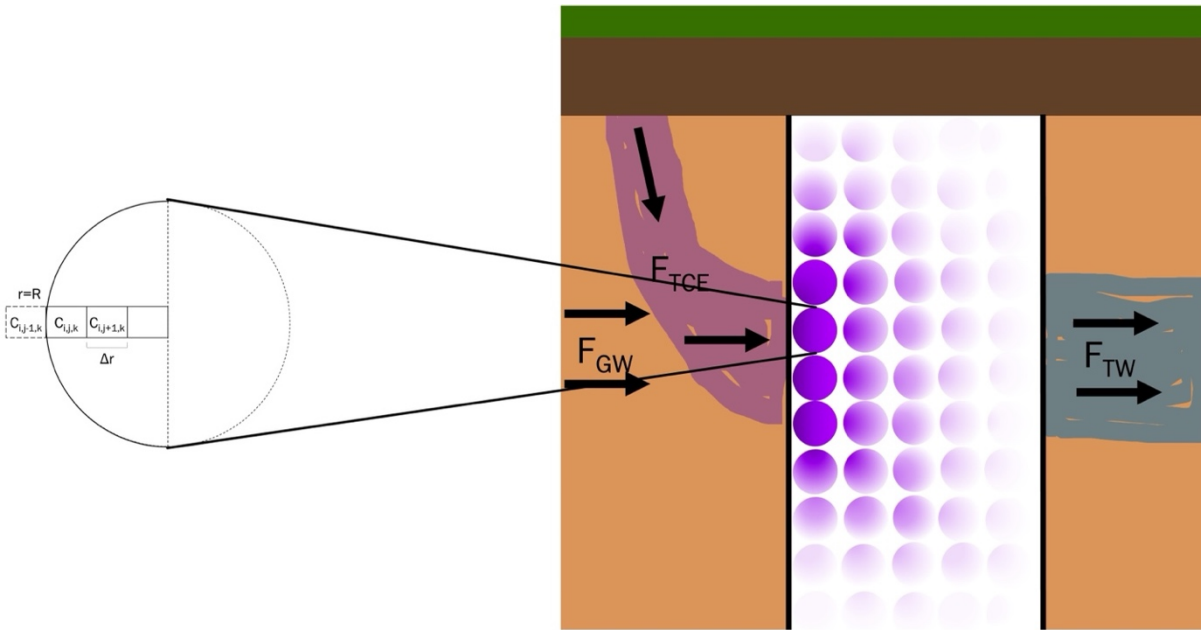

Figure 3.3: *Schematic of the model used for a single pass bead and a theoretical representation of a permeable reactive barrier where C is the concentration of species i in the bead at spacial point j, at time point k. F_{GW} is groundwater flow, F_{TCE} is TCE contaminant flow, and F_{TW} is the treated water flow.*

The model described above was made in MATLAB (R2021a, v9.10) and compiled using Matlab Compiler (v8.2) to be used outside the MATLAB software in a cluster computing system. Slurm Workload Manager was used as a scheduler on the University of Idaho Research Computing and Data Services computational cluster where the compiled MATLAB app was run in parallel with multiple random biobead radii and cell concentration inputs as part of a Monte Carlo simulation. Origin 2018b (OriginLab Corporation, MA) was used to visualize graphic results. The R package multcomp[18] was used for statistical analysis in R studio[19] (v4.1.1).

3.3.5 Data Analysis:

Diffusion of TCE was measured at 238 nm, cDCE at 220 nm, and VC at 202 nm. Approximate source concentrations for each CAH were 800 ppm (TCE), 150 ppm (cDCE), and 80 ppm (VC). Measurements were taken every 5 minutes to ensure adequate mixing and run for 20-48 hrs. A calibration curve was initially made for each CAH between 190 – 250 nm to determine the best wavelength to measure concentration. The best wavelength was determined based on linearity and replicate variability. Diffusion experiments were replicated at least three times. Error bars represent a 95% confidence interval. The diffusion coefficient was calculated using an equation derived by Northrop and Anson,[20] using the assumption that the sink concentration was insignificant compared to the source as shown in **Equation 3-7**. $\frac{dC_{CAH}}{dt}$ was the change in CAH concentration over time at pseudo steady state, V_{sink} was the sink chamber volume, A_m was the membrane cross-sectional area, and L_m was the membrane thickness.

$$D_e = \left(\frac{L_m V_{sink}}{A_m C_{CAH,source}}\right)\frac{dC_{CAH}}{dt}$$

Equation 3-7

3.4 Results and Discussion

3.4.1 Diffusion Measurement:

Figure 3.4 shows a side-by-side comparison of the diffusivities of TCE, cDCE, and VC through 10% PVA / 2% Alg cryogels in DI water (0 M), 0.001 M, and 0.01 M KCl. To the authors knowledge, these are the first recorded measurements of CAH diffusivity through hydrogel materials. In DI water, an increase in diffusivity was expected from TCE to cDCE to VC due to sequentially decreasing molar volumes from molecule to molecule (**Figure 3.1**). A significant increase in diffusivity was observed when comparing TCE and cDCE ($p=0.029$), but not when comparing cDCE and VC ($p=1.00$) in DI water. Due to error in the experiment, no discernable differences can be observed between cDCE and VC. Size based obstruction was unlikely to hinder diffusivity in the hydrogels tested due to the relatively small size of the diffusing solute (~6.7 Å for a molecule of TCE, based on the largest distance between atoms)[21] in comparison to the pore size which for 10% PVA hydrogels was >100 nm after 5 or more freeze-thaw cycles as stated by Millon et al.[22] and Yokoyama et al.[23] There were likely no significant electrostatic effects that could hinder or promote diffusion of VC or cDCE in the hydrogels tested.

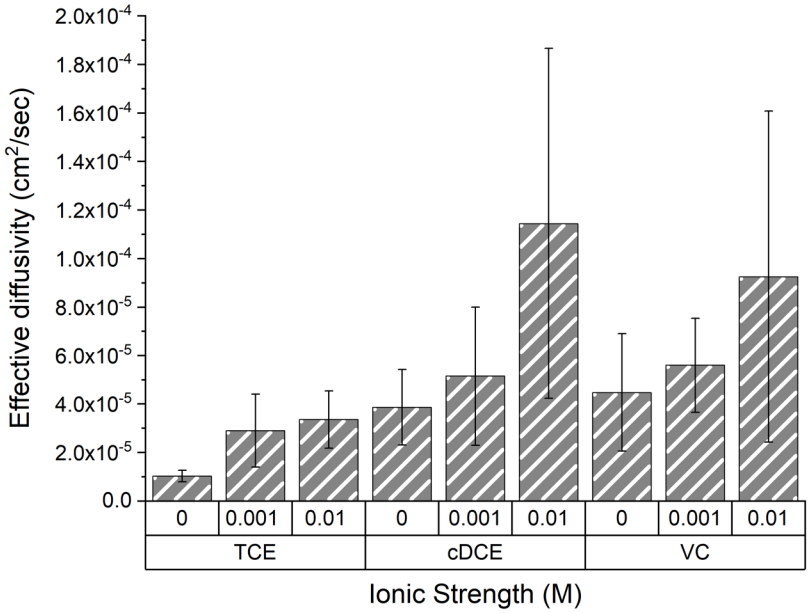

Figure 3.4: *Experimental effective diffusion coefficients for multiple CAH species at various ionic strengths. Error bars represent a 95% confidence interval. Numerical data is presented in* ***Table B.1****, with additional statistical analysis in* ***Table B.2****.*

When ionic strength was increased from 0 to 0.01 M KCl, diffusivity of TCE, cDCE, and VC through 10% PVA / 2% Alg cryogels more than doubled. The increase in diffusivity for TCE (*p=0.009*) and cDCE (*p=0.029*) from 0 to 0.01 M KCl was significant, while the increase for VC from 0 to 0.01 M KCl was not (*p=0.124*). The increase in diffusivity with ionic strength for TCE and cDCE could likely be in part due to hydrogel contraction as described previously in chapter 2. As the hydrogel contracts, the volume fraction of the hydrogel occupied by water increases, allowing for more efficient solute transport through the hydrogel. As in DI water, VC diffusivity seemed to be similar to cDCE at both 0.001 M KCl (*p=1.00*) and 0.01 M KCl (*p=1.00*). Overall statistical analysis showed that CAH species, ionic strength, and the interaction of the two factors had a statistically significant effect on diffusivity in 10% PVA / 2% Alg hydrogels under the conditions tested (**Table B.2**).

3.4.2 Diffusion-Reaction Model

The diffusion-reaction model discussed here and outlined above, was originally created by Counts[24] using a CAH degradation model developed by Haest et al.[14] and later modified by Dr. James Moberly and Dr. Dave MacPherson. The model was further modified for this work to improve speed by adding a logic loop to determine when the system reached steady state, cutting computational time in half in

some scenarios. A pH inhibition function was also added to rate law calculations to make the system more realistic. A total of 1445 iterations were run to complete the data sets presented here.

Modeling results were compiled in parallel with diffusion experiments and used previous diffusion measurements reported by Counts[24] in DI water for all calculations for comparison purposes. **Table 3.1** shows a comparison of the diffusion measurements of CAHs through 10% PVA / 2% Alg hydrogels in DI water reported by Counts[24] and those reported in this work. The diffusion coefficients reported by Counts were used in the model to directly compare results to the previous model generated without pH inhibition (**Figure 3.5**). Future model iterations will incorporate the diffusivity of each CAH in DI water and ionic solutions as presented in the section above.

Table 3.1: *Diffusivity comparisons of all CAHs in DI water from work completed by Counts[24] and for this thesis. Error represents the 95% confidence interval.*

CAH	Diffusivity (cm^2/s) × 10^6	
	Counts (10% PVA / 2% Alg chemically crosslinked)	**This Work (10% PVA / 2% Alg physically crosslinked)**
TCE	11.0 ± 6.27	10.3 ± 2.36
cDCE	6.90 ± 2.91	38.6 ± 15.5
VC	4.04 ± 5.48	44.7 ± 24.2

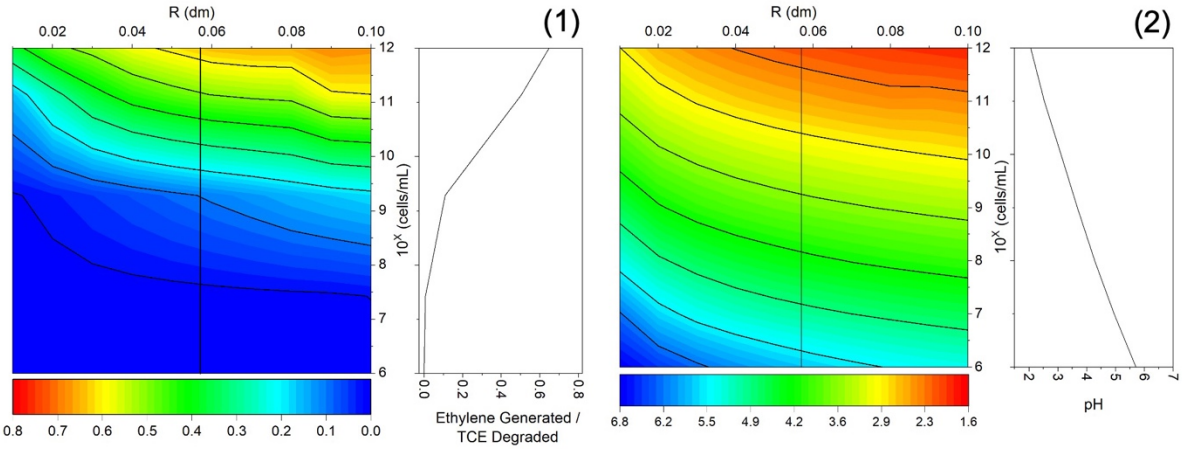

Figure 3.5: *Contour plot of reaction-diffusion model results not incorporating pH inhibition.* ***(1)*** *Molar ratio of ethylene generated to TCE degraded at steady state as a function of biobead radius and cell concentration.* ***(2)*** *pH of the biobead at steady state as a function of bead radius and cell concentration.[24]*

Figure 3.5 depicts the model results reported by Counts[24] which did not incorporate pH inhibition. **Figure 3.5.1** shows that without pH inhibition, simply increasing the cell concentration within the biobead would increase the amount of dechlorination possible, which is not feasible due to acid

generation during each dechlorination step (**Figure 3.5.2**). A max ratio of ~0.7 moles ethylene generated per moles TCE degraded was achieved with cell concentrations up to 10^{12} cells/mL, resulting in an unrealistic pH of ~1.6. Puentes Jácome et al.[25] found that dechlorinating microorganisms would be severely inhibited below a pH of 5.5, indicating that inhibition would affect dechlorination at nearly all the scenarios tested above a cell concentration of $10^{6.5}$ cells/mL.

Figure 3.6 depicts the results from the model when pH inhibition was accounted for. The model showed biobeads would stabilize within a narrow window of operability at steady state with around 10^{6} cells/mL and that pH was a major limiting factor to dechlorination in biobeads. The Goldilocks scenarios described previously in **Figure 3.2** can be clearly observed by comparing **Figure 3.6.1 – 3.6.4** which depicts molar ratios of each reaction product of interest (ethylene, cDCE, and VC) in comparison to the moles of TCE degraded at steady state and the pH at the edge of the biobead at steady state. **Figure 3.6.1** depicts the molar ratio of ethylene generated to TCE consumed and represents the main result of interest because ethylene is the final nontoxic product of anaerobic reductive dechlorination of TCE. **Figure 3.6.2** depicts the pH at the outer edge of the biobead at steady state, and **Figure 3.6.3 and 3.6.4** depict the molar ratios of cDCE and VC fluxed out of the biobead to TCE degraded at steady state.

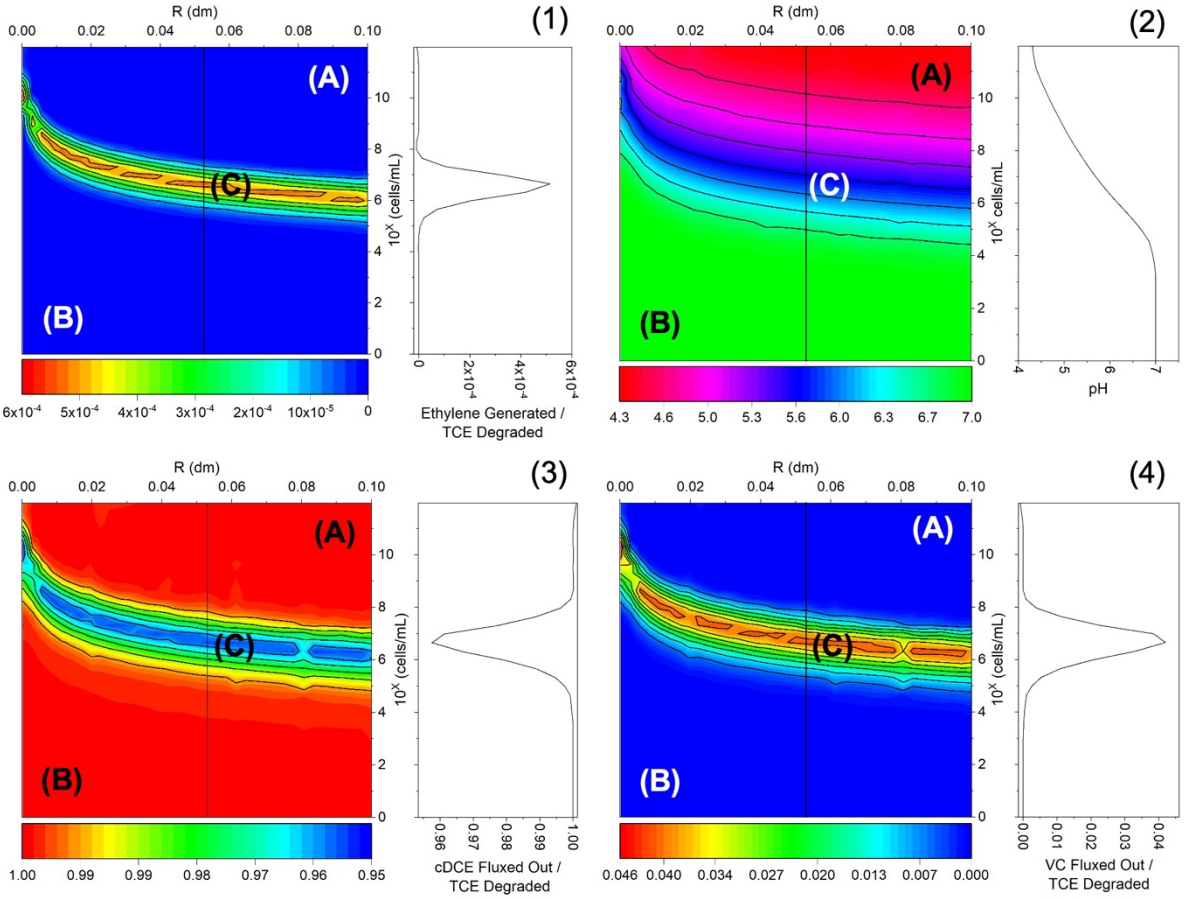

Figure 3.6: *Contour plots of reaction-diffusion model results incorporating pH inhibition.* ***(1)*** *Molar ratio of ethylene generated to TCE degraded at steady state as a function of biobead radius and cell concentration.* ***(2)*** *pH of the biobead at steady state as a function of biobead radius and cell concentration.* ***(3)*** *Molar ratio of cDCE fluxed out of the biobead to TCE degraded at steady state as a function of biobead radius and cell concentration.* ***(4)*** *Molar ratio of VC fluxed out of the biobead to TCE degraded at steady state as a function of biobead radius and cell concentration.*

Figure 3.6.A, the region above the optimal range (**Figure 3.6.C**), is an excellent illustration of the "too hot" scenario depicted in **Figure 3.2.A**, where a large concentration of cells quickly degrades CAHs, but the generation and accumulation of acid, due to relatively low acid diffusivity, inhibits the microbes, stopping dechlorination before TCE can be completely dechlorinated to ethylene. **Figure 3.6.2.A** illustrates this conclusion well since a drop in pH at or below 5 can be observed when above the optimal range for dechlorination in **Figure 3.6.1.C**. Additionally, in **Figure 3.6.3.A**, a ratio of 1 is observed indicating that all the cDCE generated by degrading TCE is fluxed out of the bead and therefore no VC is generated (**Figure 3.6.4.A**). Likewise, below the optimal range, a reaction limited, or "too cold," system is observed in **Figure 3.6.1.B – 3.6.4.B**. In **Figure 3.6.1.B**, little to no TCE is converted

completely to ethylene, and in **Figure 3.6.2.B**, a pH near 7 indicates that acid was able to diffuse out of the system nearly at the same rate as it was being generated due to the low concentration of cells. A similar conclusion can be drawn from **Figure 3.6.3.B and 3.6.4.B** which show that all the cDCE generated was fluxed out of the biobead and no VC was generated at steady state. At the optimal, "just right," conditions of **Figure 3.6.1.C – 3.6.4.C**, the max molar ratio of ethylene generated to TCE consumed was 0.0005 with a pH of around 5.6. **Figure 3.6.3.C** shows that even at these "optimal" conditions, 0.95 moles of cDCE were fluxed out of the biobead per mole of TCE consumed, indicating that only a small fraction of cDCE was ever converted to VC. Likewise, in **Figure 3.6.4.C**, it can be reasoned when comparing to **Figure 3.6.1.C**, that the majority of VC that was generated was fluxed out of the biobead since 0.046 moles of VC were fluxed out of the biobead per mole of TCE degraded compared to only 0.0005 moles of VC that was reacted to form ethylene per mole of TCE degraded.

From **Figure 3.6.1 – 3.6.4** it was predicted that with too low a cell concentration, CAHs would diffuse out of the biobead before the cells present were able to fully degrade them, and with a high cell concentration, the rapid production of acid would inhibit or kill the microorganisms before any ethylene was formed, releasing cDCE and VC (**Figure 3.6.2-3.6.3**). These results were drastically different from the model predictions reported previously by Counts (**Figure 3.5**) which showed that without pH inhibition, the optimum dechlorination efficiency was achieved by increasing the cell density within the biobead. We can now see that this method would be counterproductive since the constant generation of acid in the system would eventually overwhelm the microorganisms leading to inhibition or cell death. At the optimal conditions found in **Figure 3.6.C** a pH near 5.6 was predicted, which was in agreement with the physical constraints of dechlorinating microorganisms as reported by Puentes Jácome et al.,[25] who states that dechlorinating microorganisms would be severely inhibited below a pH of 5.5. Although, the rate of dechlorination would likely increase if the pH was mediated to between 6 and 7 as has been shown in previous studies using nonencapsulated dechlorinating cultures by Puentes Jácome et al.[25] Previous work done by Counts (**Figure 3.5**) also indirectly illustrates that if pH inhibition is controlled, high conversion of TCE to ethylene can be achieved, although selectively controlling pH may be necessary to keep the pH within the optimal ranges for each degradation reaction to maximize efficiency.

Microbial encapsulation in a hydrogel is not a new concept and has been shown to work for anaerobic reductive dechlorination in the past by Zhou et al.,[5] Wang and Tseng,[6] and Kim et al.,[7] but only in buffered systems. In a wastewater treatment study done by Zhu et al.,[26] encapsulation actually improved degradation efficiency, although this type of study has not been done with anaerobic reductive dechlorinators. The results depicted here will help inform future research efforts by predicting how

dechlorination efficiency changes with variations in cell density and hydrogel bead size. As shown in **Figure 3.6**, the dechlorination efficiency of a biobead can change drastically based on bead size and cell concentrations. Previous studies have not investigated how these fundamental parameters affect dechlorination. These models were carried out with the assumption that no buffers were present in the system, so the effects of pH on dechlorination would be readily apparent.

3.5 Conclusions

Effective diffusivity of each CAH more than doubled when ionic strength was increased from 0 to 0.01 M KCl, leading to a max molar ratio of ethylene generated to TCE degraded of 0.0005 at steady state based on a reaction-diffusion model. This model exemplifies the utility of mass transfer coefficients and illustrates the limitations of pH on anaerobic reductive dechlorination even in a protective hydrogel environment. The predicted max molar ratio of ethylene generated to TCE degraded decreased by 100% when pH inhibition was accounted for. Further research on the kinetics of TCE dechlorination in encapsulated systems are needed to validate this model and to determine the attritional effects of encapsulation on the microbes' metabolism. The addition of pH regulating compounds into the hydrogel should also be studied as a long-term solution to acid generation during CAH dechlorination.

3.6 References

(1) *ATSDR - ToxFAQs™: Trichloroethylene (TCE)*. https://www.atsdr.cdc.gov/toxfaqs/tf.asp?id=172&tid=30 (accessed 2020-10-08).

(2) Juwarkar, A. A.; Misra, R. R.; Sharma, J. K. Recent Trends in Bioremediation. In *Geomicrobiology and Biogeochemistry*; Parmar, N., Singh, A., Eds.; Soil Biology; Springer: Berlin, Heidelberg, 2014; pp 81–100. https://doi.org/10.1007/978-3-642-41837-2_5.

(3) Robinson, C.; Barry, D. A.; McCarty, P. L.; Gerhard, J. I.; Kouznetsova, I. PH Control for Enhanced Reductive Bioremediation of Chlorinated Solvent Source Zones. *Sci. Total Environ.* **2009**, *407* (16), 4560–4573. https://doi.org/10.1016/j.scitotenv.2009.03.029.

(4) *Goldilocks Zone*. Exoplanet Exploration: Planets Beyond our Solar System. https://exoplanets.nasa.gov/resources/323/goldilocks-zone (accessed 2022-07-18).

(5) Zhou, Y.-Z.; Yang, J.; Wang, X.-L.; Pan, Y.-Q.; Li, H.; Zhou, D.; Liu, Y.-D.; Wang, P.; Gu, J.-D.; Lu, Q.; Qiu, Y.-F.; Lin, K.-F. Bio-Beads with Immobilized Anaerobic Bacteria, Zero-Valent Iron, and Active Carbon for the Removal of Trichloroethane from Groundwater. *Environ. Sci. Pollut. Res.* **2014**, *21* (19), 11500–11509. https://doi.org/10.1007/s11356-014-3110-6.

(6) Wang, S.-M.; Tseng, S. Dechlorination of Trichloroethylene by Immobilized Autotrophic Hydrogen-Bacteria and Zero-Valent Iron. *J. Biosci. Bioeng.* **2009**, *107* (3), 287–292. https://doi.org/10.1016/j.jbiosc.2008.11.010.

(7) Kim, S.; Bae, W.; Hwang, J.; Park, J. Aerobic TCE Degradation by Encapsulated Toluene-Oxidizing Bacteria, Pseudomonas Putida and Bacillus Spp. *Water Sci. Technol.* **2010**, *62* (9), 1991–1997. https://doi.org/10.2166/wst.2010.471.

(8) Azizian, M. F.; Semprini, L. Aerobic Cometabolism of Chlorinated Solvents and 1,4-Dioxane in Continuous-Flow Columns Packed with Gellan-Gum Hydrogels Coencapsulated with ATCC Strain 21198 and TBOS or T2BOS as Slow-Release Compounds. *ACS EST Eng.* **2022**. https://doi.org/10.1021/acsestengg.2c00023.

(9) McCarty, P. L.; Goltz, M. N.; Hopkins, G. D.; Dolan, M. E.; Allan, J. P.; Kawakami, B. T.; Carrothers, T. J. Full-Scale Evaluation of In Situ Cometabolic Degradation of Trichloroethylene in Groundwater through Toluene Injection. *Environ. Sci. Technol.* **1998**, *32* (1), 88–100. https://doi.org/10.1021/es970322b.
(10) Teerakun, M.; Reungsang, A.; Lin, C.-J.; Liao, C.-H. Coupling of Zero Valent Iron and Biobarriers for Remediation of Trichloroethylene in Groundwater. *J. Environ. Sci.* **2011**, *23* (4), 560–567. https://doi.org/10.1016/S1001-0742(10)60448-2.
(11) Zabetakis, K. M.; Niño de Guzmán, G. T.; Torrents, A.; Yarwood, S. Toxicity of Zero-Valent Iron Nanoparticles to a Trichloroethylene-Degrading Groundwater Microbial Community. *J. Environ. Sci. Health Part A* **2015**, *50* (8), 794–805. https://doi.org/10.1080/10934529.2015.1019796.
(12) Krasnova, T. A.; Belyaeva, O. V.; Gorelkina, A. K.; Timoshchuk, I. V.; Gora, N. V.; Golubeva, N. S. Trichloroethylene Adsorption from Aqueous Solutions by Activated Carbons. *Carbon Lett.* **2020**, *30* (3), 281–287. https://doi.org/10.1007/s42823-019-00096-y.
(13) Regan, F.; MacCraith, B. D.; Walsh, J. E.; O'Dwyer, K.; Vos, J. G.; Meaney, M. Novel Teflon-Coated Optical Fibres for TCE Determination Using FTIR Spectroscopy. *Vib. Spectrosc.* **1997**, *14* (2), 239–246. https://doi.org/10.1016/S0924-2031(96)00073-2.
(14) Haest, P. J.; Springael, D.; Smolders, E. Dechlorination Kinetics of TCE at Toxic TCE Concentrations: Assessment of Different Models. *Water Res.* **2010**, *44* (1), 331–339. https://doi.org/10.1016/j.watres.2009.09.033.
(15) Lacroix, E.; Brovelli, A.; Barry, D. A.; Holliger, C. Use of Silicate Minerals for PH Control during Reductive Dechlorination of Chloroethenes in Batch Cultures of Different Microbial Consortia. *Appl. Environ. Microbiol.* **2014**, *80* (13), 3858–3867. https://doi.org/10.1128/AEM.00493-14.
(16) Mirpuri, R.; Jones, W.; Bryers, J. D. Toluene Degradation Kinetics for Planktonic and Biofilm-Grown Cells of Pseudomonas Putida 54G. *Biotechnol. Bioeng.* **1997**, *53* (6), 535–546. https://doi.org/10.1002/(SICI)1097-0290(19970320)53:6<535::AID-BIT1>3.0.CO;2-N.
(17) Heffernan, B.; Murphy, C. D.; Casey, E. Comparison of Planktonic and Biofilm Cultures of Pseudomonas Fluorescens DSM 8341 Cells Grown on Fluoroacetate. *Appl. Environ. Microbiol.* **2009**, *75* (9), 2899–2907. https://doi.org/10.1128/AEM.01530-08.
(18) Hothorn, T.; Bretz, F.; Westfall, P. Simultaneous Inference in General Parametric Models. *Biom. J.* **2008**, *50* (3), 346–363.
(19) R Core Team. R: A Language and Environment for Statistical Computing, 2021.
(20) Northrop, J. H.; Anson, M. L. A Method for the Determination of Diffusion Constants and the Calculation of the Radius and Weight of the Hemoglobin Molecule. *J. Gen. Physiol.* **1929**, *12* (4), 543–554. https://doi.org/10.1085/jgp.12.4.543.
(21) National Institute of Standards and Technology. Experimental Data for CHClCCl2 (Trichloroethylene), 2022. https://doi.org/10.18434/T4D303.
(22) Millon, L. E.; Nieh, M.-P.; Hutter, J. L.; Wan, W. SANS Characterization of an Anisotropic Poly(Vinyl Alcohol) Hydrogel with Vascular Applications. *Macromolecules* **2007**, *40* (10), 3655–3662. https://doi.org/10.1021/ma062781f.
(23) Yokoyama, F.; Masada, I.; Shimamura, K.; Ikawa, T.; Monobe, K. Morphology and Structure of Highly Elastic Poly(Vinyl Alcohol) Hydrogel Prepared by Repeated Freezing-and-Melting. *Colloid Polym. Sci.* **1986**, *264* (7), 595–601. https://doi.org/10.1007/BF01412597.
(24) Counts, J. Diffusion Mechanisms, Measurements, and Models with Applications in Bioremediation of Trichloroethylene and Breakdown Products, University of Idaho, 2020.
(25) Puentes Jácome, L. A.; Wang, P.-H.; Molenda, O.; Li, Y. X. (Jine-J.; Islam, M. A.; Edwards, E. A. Sustained Dechlorination of Vinyl Chloride to Ethene in Dehalococcoides-Enriched Cultures Grown without Addition of Exogenous Vitamins and at Low PH. *Environ. Sci. Technol.* **2019**, *53* (19), 11364–11374. https://doi.org/10.1021/acs.est.9b02339.

(26) Zhu, K.; Davis, C. W.; Novak, P. J.; Arnold, W. A. Effects of Encapsulation on the Chemical Inhibition of Anaerobic Hydrogen- and Methane-Producing Microbial Cells. *Bioresour. Technol. Rep.* **2020**, *11*, 100451. https://doi.org/10.1016/j.biteb.2020.100451.

Chapter 4: Conclusions and Future Work

4.1 Overall conclusions

Diffusion coefficients of hydronium, TCE, cDCE, and VC were experimentally determined in DI water, and in various ionic strength conditions, and then utilized in a reaction-diffusion model which accounted for pH inhibition and found that the max molar ratio of ethylene generated to TCE degraded was 0.0005. The positive effects of ionic strength on the diffusion of each species, except vinyl chloride, through a hydrogel was found to be significant ($p < 0.05$). It was postulated that the positive and negative effects of ionic strength on diffusion of each species was due mainly to contraction of the hydrogel, and in the case of hydronium, additional electrostatic forces (e.g., repulsion between hydronium and calcium ions, and potassium chelation to alginate). Solvent-polymer (hydroxyl group-water hydrogen bonding) and solvent-solute (potassium ions breaking water-water hydrogen bonding) interactions were also suggested to influence hydronium diffusion. Diffusivity increased significantly from TCE to cDCE in 0 and 0.01 M KCl, and in contrast, the change in diffusivity from cDCE to VC was insignificant at all ionic strengths tested. Large error in the experiment made diffusivities between cDCE and VC indistinguishable. Previous model work found a max molar ratio of ethylene generated to TCE degraded of 0.7 by simply increasing the density of microorganisms encapsulated in the hydrogel. This result was unrealistic due to the constant generation of acid and the limited diffusion capabilities within the biobead which would lead to pH inhibition or cell death before a conversion ratio of 0.7 was achieved in a real system. The model presented in this work yields more realistic results while the past work highlights the capabilities of the system if pH inhibition could be controlled. In conclusion, even with encapsulation, it was found that acid generation during dechlorination would likely inhibit anaerobic reductive dechlorination at high cell concentrations. Additional research into pH regulation within the biobead is needed to increase dechlorination efficiency.

4.2 Future Work

4.2.1 Proton consuming species in a hydrogel

Silicotungstic acid (STA) has been shown to react with acid in its reduced form to generate hydrogen.[1] STA can be photochemically reduced by a 300 – 400 nm light,[2] and can be reoxidized. Unlike buffers, which have to be reinjected once used up, a compound like STA can be continuously used and reoxidized, making it a model compound for application in biobeads.[3] Along with removing acid from the system, the generation of molecular hydrogen during this reaction is also of interest, although its effects on the physical stability of the hydrogel are unknown. Many anaerobic reductive dechlorinating microorganisms utilize hydrogen as an electron donor, so the generation of hydrogen in the system would provide an electron donor and limit the need for injection of additional substrates for

microorganism in the hydrogel.[4] Yang and McCarty,[5] Luijten et al.,[6] Heimann et al.,[7] and Lu et al.[8] showed that hydrogen concentrations affected the selectivity of anaerobic reducers, i.e., other reductive degradation processes like methanogenesis could be more favorable than dechlorination depending on the aqueous hydrogen concentration. Yang and McCarty[5] found that low concentrations of hydrogen (2 – 11 nM H_2) allowed for the most dechlorination by hindering other reducing reactions. The speed and amount of hydrogen produced can be tuned to control the concentration of bioavailable hydrogen based on the chosen substrate. For example, fermentation of lactate generates hydrogen quickly, increasing aqueous hydrogen concentrations and leading to a lower selectivity for dechlorinating microbes.[4] If propionate is used as a substrate instead, hydrogen production is slow, making dechlorination a more favorable reaction pathway.[4] A similar result may be achieved using STA by tuning light intensity and duration of light exposure which has been shown to alter the rate of STA reduction, and therefore the rate of hydrogen production, by Rustamov et al.[3] and Muradov and T-Raissi.[2] Although, to the authors knowledge this reaction mechanism has not been tested in a hydrogel material and the effects of STA reduction and hydrogen generation on a PVA hydrogel's physical stability is unknown.

4.2.2 Further exploring other polyoxometalates (POMs)

Previous work by our group looked at the effects of sodium decavanadate and alumina clusters on hydronium diffusivity and found that no statistically significant difference was found when compared to 10% PVA cryogels, although, large amounts of each species would leach out of the hydrogel during equilibration in water which may have influenced the overall results. Future work studying the effects of POM species on hydronium diffusivity should investigate hydrogel preparation methods that keep POMs entrapped within a hydrogel matrix so leeching does not occur.

4.2.3 Model improvement

The model can also be further improved by implementing an acid reactivity component to simulate STA's reaction with acid in the hydrogel, and to show how removing acid would improve dechlorination efficiency in the hydrogel. The effects of hydrogen generation can also be modeled based on the work compiled in a review by Wang et al.[4] which was discussed in detail above.

4.2.4 Kinetics and pilot testing:

Once we have determined a quantifiable method for determining cell concentrations in a hydrogel, kinetics experiments could be run to determine the rate law constants for anaerobic reductive dechlorination. The current reaction-diffusion model (code shown in **Appendix C**) uses kinetic data determined from non-encapsulated microorganisms[9] and would likely better represent the current system if kinetic parameters were determined using encapsulated microorganism. Some studies have

shown that microbial encapsulation improved the reactivity of reductive microorganisms,[10] but none to date have demonstrated this for dechlorinating microbial consortia (e.g., KB-1) made up of *Dehalococcoides, Dehalobacter,* and other anaerobic microorganisms.

Additional work may also be done to run pilot tests using packed columns, or bioreactors, filled with encapsulated KB-1 consortia, to determine the effectiveness of biobeads in an applicable treatment system.

References

(1) Savinov, E. N.; Saidkhanov, S. S.; Parmon, V. N.; Zamaraev, K. I. Evolution of Hydrogen from Aqueous Solutions of 12-Silicon-Tungsten Heteropolyacid. *React. Kinet. Catal. Lett.* **1981**, *17* (3), 407–411. https://doi.org/10.1007/BF02065856.

(2) Muradov, N.; T-Raissi, A. Solar Production of Hydrogen Using "Self-Assembled" Polyoxometalate Photocatalysts. *J. Sol. Energy Eng.* **2006**, *128* (3), 326–330. https://doi.org/10.1115/1.2212442.

(3) Rustamov, M. I.; Muradov, N. Z.; Guseinova, A. D.; Bazhutin, Yu. V. Photocatalytic Hydrogen Generation from Water—Organic Solutions Using Polytungstates. *Int. J. Hydrog. Energy* **1988**, *13* (9), 533–538. https://doi.org/10.1016/0360-3199(88)90132-2.

(4) Wang, X.; Xin, J.; Yuan, M.; Zhao, F. Electron Competition and Electron Selectivity in Abiotic, Biotic, and Coupled Systems for Dechlorinating Chlorinated Aliphatic Hydrocarbons in Groundwater: A Review. *Water Res.* **2020**, *183*, 116060. https://doi.org/10.1016/j.watres.2020.116060.

(5) Yang, Y.; McCarty, P. L. Competition for Hydrogen within a Chlorinated Solvent Dehalogenating Anaerobic Mixed Culture. *Environ. Sci. Technol.* **1998**, *32* (22), 3591–3597. https://doi.org/10.1021/es980363n.

(6) Luijten, M. L. G. C.; Roelofsen, W.; Langenhoff, A. A. M.; Schraa, G.; Stams, A. J. M. Hydrogen Threshold Concentrations in Pure Cultures of Halorespiring Bacteria and at a Site Polluted with Chlorinated Ethenes. *Environ. Microbiol.* **2004**, *6* (6), 646–650. https://doi.org/10.1111/j.1462-2920.2004.00608.x.

(7) Heimann, A. C.; Friis, A. K.; Jakobsen, R. Effects of Sulfate on Anaerobic Chloroethene Degradation by an Enriched Culture under Transient and Steady-State Hydrogen Supply. *Water Res.* **2005**, *39* (15), 3579–3586. https://doi.org/10.1016/j.watres.2005.06.029.

(8) Lu, X.-X.; Tao, S.; Bosma, T.; Gerritse, J. Characteristic Hydrogen Concentrations for Various Redox Processes in Batch Study. *J. Environ. Sci. Health Part A* **2001**, *36* (9), 1725–1734. https://doi.org/10.1081/ESE-100106254.

(9) Haest, P. J.; Springael, D.; Smolders, E. Dechlorination Kinetics of TCE at Toxic TCE Concentrations: Assessment of Different Models. *Water Res.* **2010**, *44* (1), 331–339. https://doi.org/10.1016/j.watres.2009.09.033.

(10) Kim, S.; Bae, W.; Hwang, J.; Park, J. Aerobic TCE Degradation by Encapsulated Toluene-Oxidizing Bacteria, Pseudomonas Putida and Bacillus Spp. *Water Sci. Technol.* **2010**, *62* (9), 1991–1997. https://doi.org/10.2166/wst.2010.471.

Appendix A - Chapter 2 Supplemental Information

A.1 Diaphragm Cell

A diaphragm cell uses a diaphragm or membrane to divide a compartment of high solute concentration (source) from a (sink) compartment of zero initial concentration. In a custom "GelipHish" diffusion cell, three sinks (92.0 mL each) were connected to a single source (~650 mL) and triplicate data were collected using three individual membranes. A basic diaphragm cell with single chamber is shown in **Figure A.1**. Oakton pH probes were used to measure sink pH over time, and source pH was measured at the beginning and end of each experiment using a Hach H170 pH meter and Accumet probe (Fisher Scientific). Membranes used in a GelipHish were approximately 1 cm thick with a cross sectional area of 7.816 cm^2. Both sink and source were well mixed using stir bars at 90 rpm.

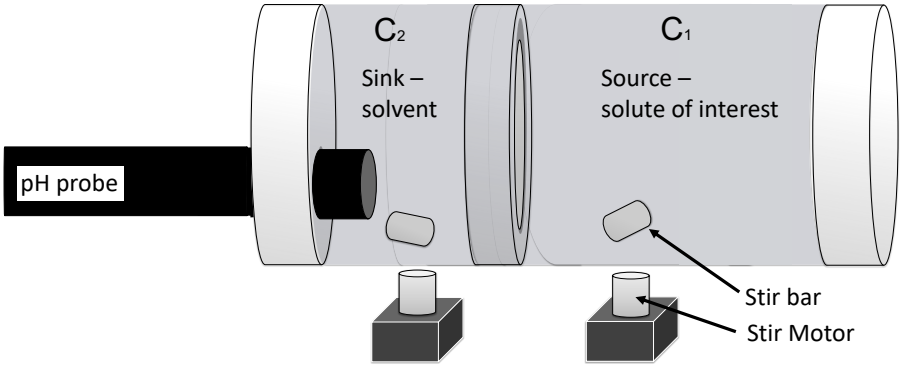

Figure A.1: *A single diaphragm cell. The "GelipHish" custom diffusion cell used in this study has one large source with three sinks connected in parallel. This enables replication under the same operational conditions in a single run.*

A.2 pH Measurement Software

A Raspberry Pi. Model 3B+ ADC HAT was connected to a breadboard which integrated four Oakton pH probes via 6-pin BNC connectors (DIYMore). Solution conductivity was measured in mV, and the value was passed as an analog signal to the breadboard. After passing through a 10 kΩ resistor, the signal was sent to the analog to digital converter, which translated the signal to a digital value. An additional 10 kΩ resistor connected the signal output to ground. The digital value was collected for each probe at 32.0 sesond intervals and stored in a .csv file. A system diagram is shown in **Figure A.2**.

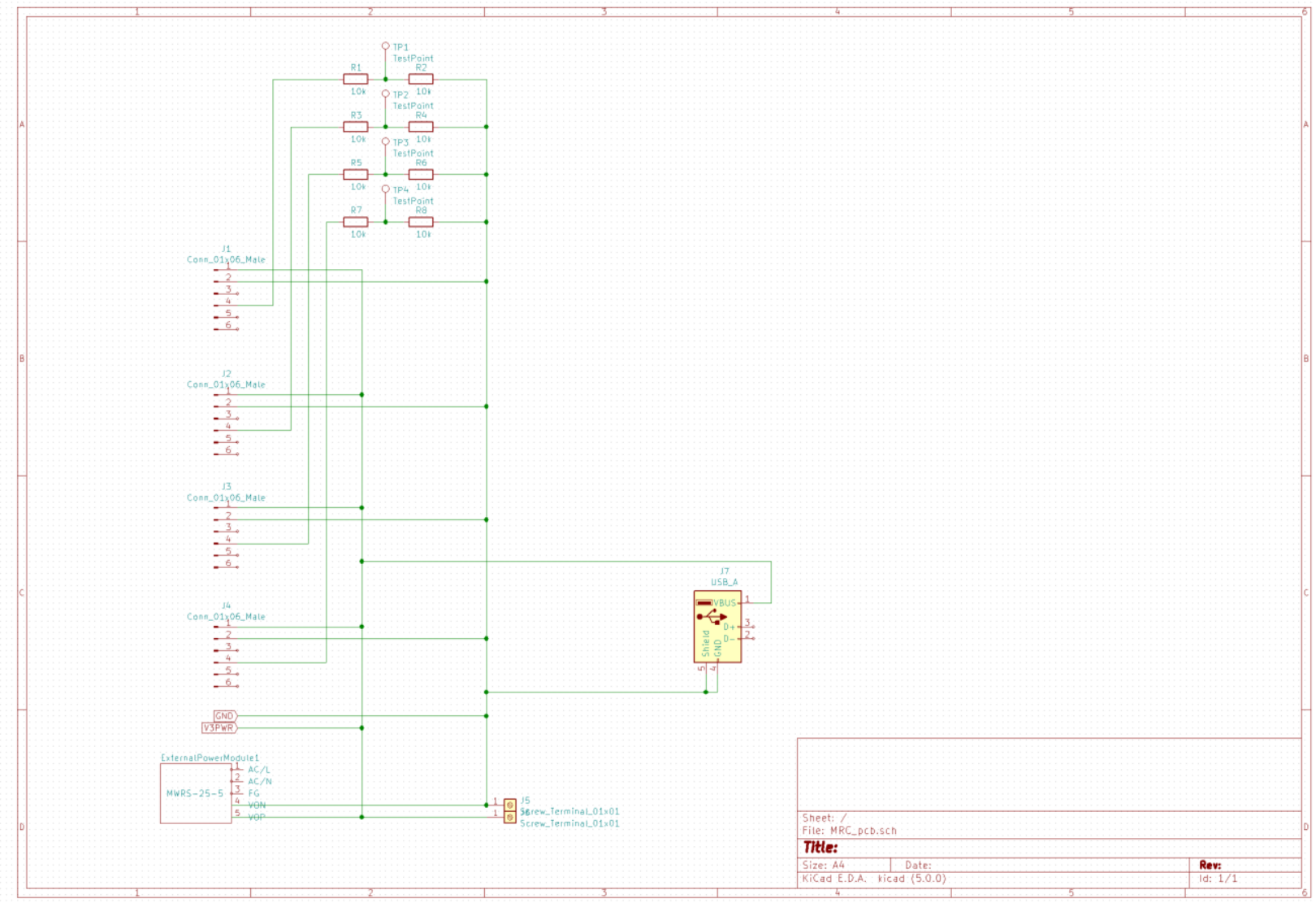

Figure A.2: *Diagram of GelipHish circuitry. Test Point is the analog signal sent to the analog to digital converter.*

A.3 pH Probe Calibration and Correction

Diffusion tests were preceded by system calibration. Each probe was placed in an individual container filled with 10 mL of pH 4.01 buffer. After equilibrating for 45 minutes, the probes were rinsed and immersed in pH 7.0 buffer for an additional 45 minutes. Equilibrated values for solution conductivity (mV) were used to relate pH to conductivity using a linear relationship ($y = m*x + b$). Three-point calibrations using pH 10.0 buffer were in excellent agreement with this method. Instrument drift was a common occurrence due to the length of each diffusion experiment (~12-24 hrs.). Samples of each sink and the source were taken at the end of the experiment and their pH was measured again by a freshly calibrated Hach H170 meter to determine instrument drift. The pH measurement read by the Hach H170 meter and the final pH value recorded during the experiment were compared and the difference was added to the calibration intercept term to account for instrument drift.

A.4 Theoretical Model Comparison

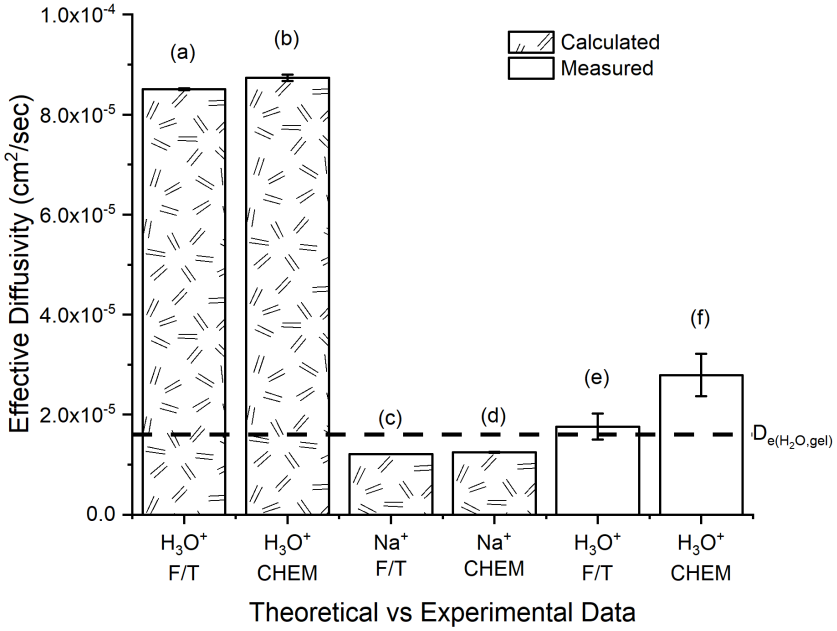

Figure A.3: *Theoretical hydronium effective diffusivity through 10% PVA hydrogels using free volume theory, as developed by Lustig and Peppas, compared with experimentally determined hydronium effective diffusivity. (a - b) Calculated from* ***Equation 2-2****, using the diffusion coefficient of hydronium through water. (c-d) Calculated from* ***Equation 2-2****, using the diffusion coefficient of sodium through water. (e-f) Experimentally determined hydronium diffusion coefficients. The horizontal line represents the calculated self-diffusion coefficient of water in a 10% PVA cryogel. Error bars represent a 95% confidence interval. Average diffusivity and error values for each data point can be found in* ***Table 2.2****.*

A.5 Effective Diffusion Coefficient Calculations

The hydronium diffusion coefficient can be derived from Fick's first law:

$$J = -D_{e_{(H_3O^+,\,gel)}}\left(\frac{dC}{dz}\right)$$

Equation A-1

Under the assumption that the sink concentration is negligible compared to the source concentration, the diffusion coefficient can be determined:

$$D_{e_{(H_3O^+,\,gel)}} = -\frac{J}{\frac{dC}{dz}} = -\frac{\left(\frac{dC}{dt}\right)\left(\frac{V_{sink}}{A}\right)}{\frac{-C_{source}+C_{sink}}{z}} = \left(\frac{dC}{dt}\right)\frac{(z)(V_{sink})}{(C_{source})(A)}$$

Equation A-2

Where z is the thickness of the membrane in cm, V_{sink} is the volume of the sink in mL, $\frac{dC}{dt}$ is the hydronium concentration gradient over time in M/sec, A is the cross-sectional area of the membrane in cm^2, and C_{source} is the hydronium concentration of the source chamber in M. The concentration gradient was determined as the slope from the concentration versus time data as shown in **Figure A.4.** The thickness of each membrane was measured using calipers and was recorded before and after each experiment to confirm a constant thickness throughout. The concentration of the source was determined and corrected as described above.

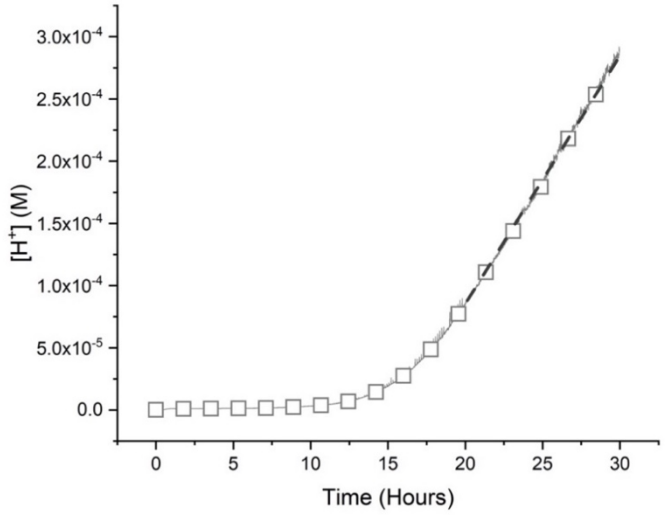

Figure A.4: *An example concentration versus time graph. The black dashed line indicates the slope used to calculate the diffusion coefficient for this data set.*

A.6 $D_{e,H+,gel}$ Relationship to Number of Freeze/Thaw Cycles and Polymer Composition

The number of freeze/thaw cycles used to crosslink PVA membranes are known to change the properties of the hydrogel, including relative porosity, relative crystallinity, and compressive modulus. Diffusion coefficients for hydronium were measured using the GelipHish diffusion cell. No statistically significant difference in $D_{e_{(H_3O^+,\,gel)}}$ was observed between 10% PVA membranes when freeze/thawed 2, 3, 4 or 5 times as shown in **Figure A.5**.

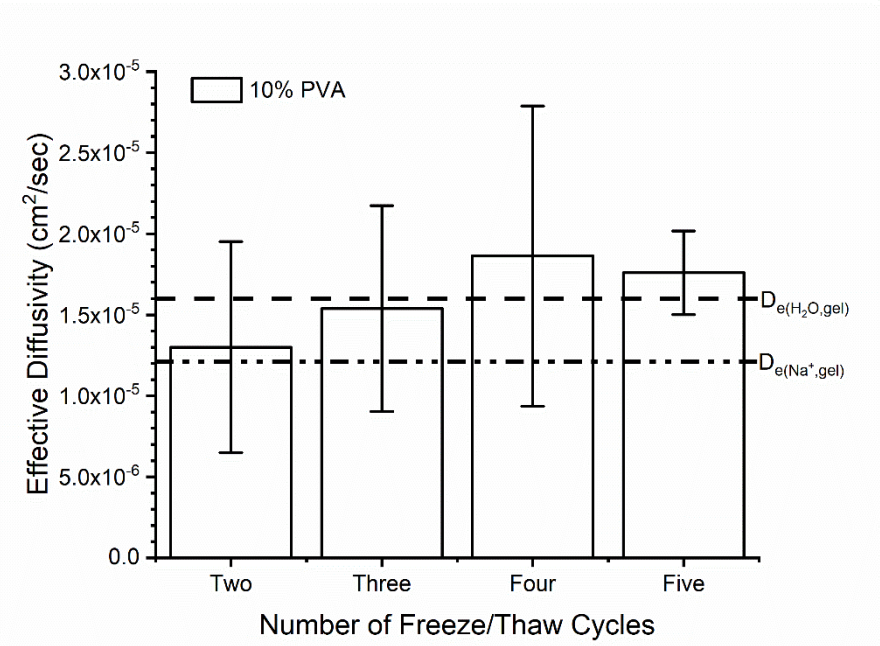

Figure A.5: *Changes in effective diffusivity of hydronium through 10% PVA based on the number of freeze/thaw cycles. No significant differences were observed between the number of freeze/thaw cycles and the effective diffusivity of hydronium. Error bars represent a 95% confidence interval.*

Table A.1: *Hydronium effective diffusivities in 10% PVA cryogels as depicted in* ***Figure A.5****.*

Membrane	Number of Freeze / Thaw Cycles	Effective Diffusivity (cm^2/s)	+/- Error	Number of Replicates
10% PVA	2	1.10×10^{-5}	6.51×10^{-6}	5
10% PVA	3	1.54×10^{-5}	6.35×10^{-6}	4
10% PVA	4	1.86×10^{-5}	9.26×10^{-6}	5
10% PVA	5	1.76×10^{-5}	2.58×10^{-6}	4

A.7 Hydrogel Chemical Structures

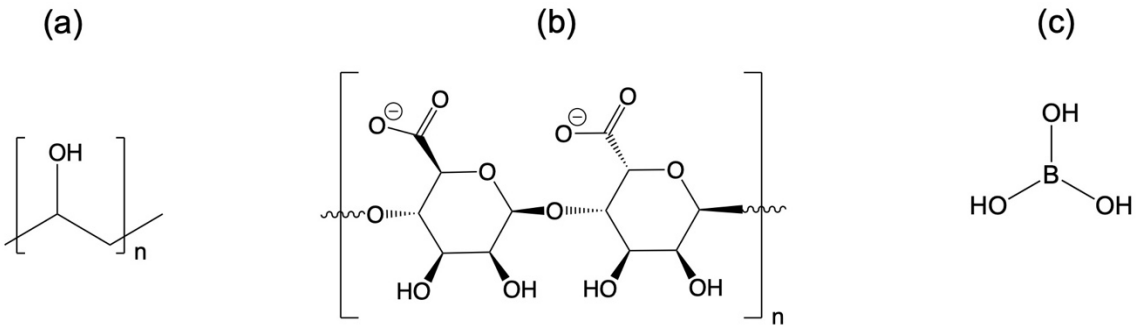

Figure A.6: Chemical Structure of key chemical components. (a) PVA repeat unit, (b) sodium alginate repeat unit, (c) boric acid.

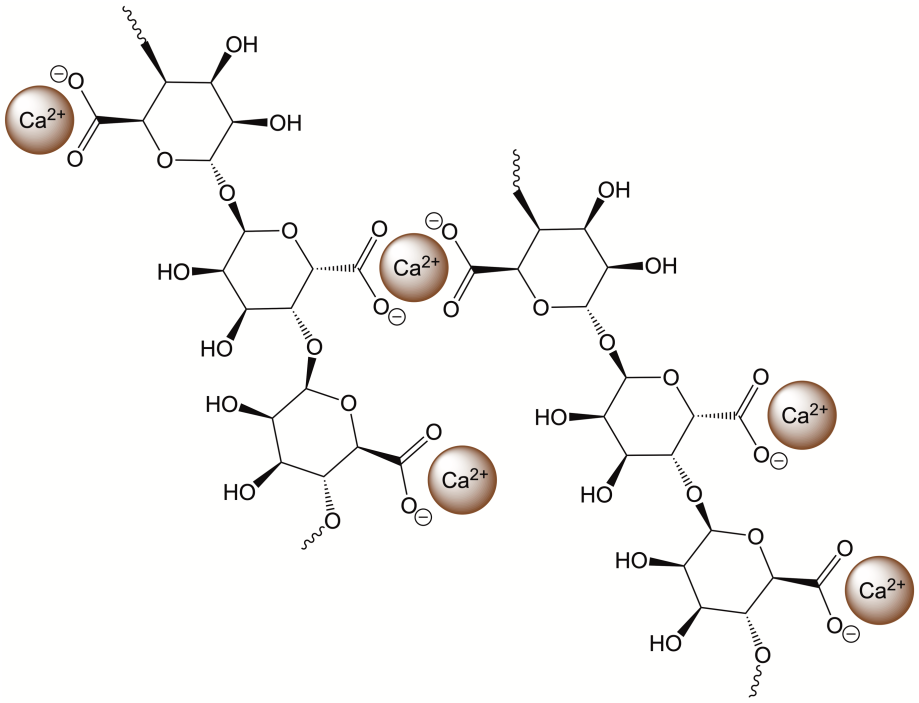

Figure A.7: Structure of crosslinked alginate when chemically crosslinked with calcium chloride.

A.8 $D_{e,H+,gel}$ Relationship to Non-Ionic Solvent

Hydronium diffusion in the presence of sucrose was similar to diffusion in deionized water as shown in **Figure A.8**. Comparing hydronium diffusion in sucrose and potassium chloride solutions under equivalent solvent molarity showed a significant difference with ionic solutions nearly double the effective diffusivity of non-ionic solutions (sucrose).

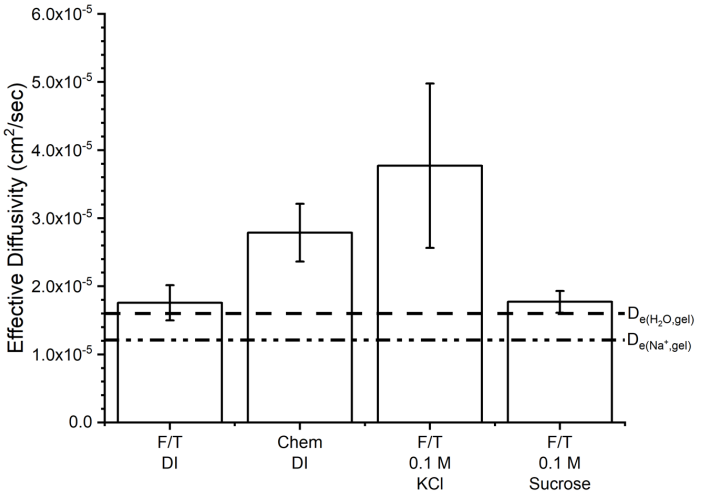

Figure A.8: *Comparison of effective diffusivity between deionized water, 0.1 M KCl, and 0.1 M sucrose for 10% PVA cryogels. Solidification by chemical crosslinking with boric acid or five freeze/thaw cycles are also compared. Error bars represent a 95% confidence interval.*

Table A.2: *Hydronium effective diffusivities of hydrogels depicted in* ***Figure A.8****.*

Membrane	Crosslinking Type	Crosslinker	Additional Species	Concentration of Additional Species (M)	Effective Diffusivity (cm^2/s)	+/- Error	Number of Replicates
10% PVA	Freeze / Thaw	-	-	0	$1.76x10^{-5}$	$2.58x\ 10^{-6}$	4
10% PVA	Chemical	Sat. Boric Acid	-	0	$2.79x10^{-5}$	$4.23x\ 10^{-6}$	3
10% PVA	Freeze / Thaw	-	KCl	0.1	$3.77x10^{-5}$	$1.21x\ 10^{-5}$	5
10% PVA	Freeze / Thaw	-	Sucrose	0.1	$1.77x10^{-5}$	$1.60x\ 10^{-6}$	3

A.9 Hydronium Effective Diffusivities by Figure

Table A.3: *Hydronium effective diffusivities in blends of PVA and PVA / Alg as depicted in* ***Figure 2.1****.*

Membrane	Crosslinking Type	Effective Diffusivity (cm^2/s)	+/- Error	Number of Replicates
7% PVA	Freeze / Thaw	$1.81x10^{-5}$	$4.90x10^{-6}$	3
10% PVA	Freeze / Thaw	$1.76x10^{-5}$	$2.58x10^{-6}$	4
15% PVA	Freeze / Thaw	$1.19x10^{-5}$	$2.22x10^{-6}$	5
20% PVA	Freeze / Thaw	$1.57x10^{-5}$	$5.81x10^{-6}$	3
30% PVA	Freeze / Thaw	$1.68x10^{-5}$	$2.24x10^{-6}$	4
10% PVA / 2% Alg	Freeze / Thaw	$1.77x10^{-5}$	$6.94x10^{-6}$	4

Table A.4: *Measured and theoretical hydronium diffusivities. This table provides additional information on the number of replicates associate with each reported value.*

Value Type	Membrane	Solute	Crosslinking Type	Crosslinker	Effective Diffusivity (cm^2/s)	+/- Error	Number of Replicates
Calculated	10% PVA	H_3O^+	Freeze / Thaw	-	$8.50x10^{-5}$	$1.69x10^{-7}$	5
Calculated	10% PVA	H_3O^+	Chemical - 4.5 hrs.	Sat. Boric Acid	$8.73x10^{-5}$	$6.42x10^{-7}$	4
Calculated	10% PVA	Na^+	Freeze / Thaw	-	$1.21x10^{-5}$	$2.54x10^{-8}$	5
Calculated	10% PVA	Na^+	Chemical - 4.5 hrs.	Sat. Boric Acid	$1.25x10^{-5}$	$9.65x10^{-8}$	4
Measured	10% PVA	H_3O^+	Freeze / Thaw	-	$1.76x10^{-5}$	$2.58x10^{-6}$	4
Measured	10% PVA	H_3O^+	Chemical - 4.5 hrs.	Sat. Boric Acid	$2.79x10^{-5}$	$4.23x10^{-6}$	3

Table A.5: *Hydronium effective diffusivities in hydrogels crosslinked for various times as depicted in* ***Figure 2.2****.*

Membrane	Crosslinking Type - Time (hrs.)	Crosslinker	Effective Diffusivity (cm^2/s)	+/- Error	Number of Replicates
10% PVA	Chemical - 4.5 hrs.	Sat. Boric Acid	$2.79x10^{-5}$	$4.23x10^{-6}$	3
10% PVA / 2% Alg	Chemical - 4.5 hrs.	2% $CaCl_2$ in Sat. Boric Acid	$9.41x10^{-6}$	$3.41x10^{-6}$	5
10% PVA / 2% Alg	Chemical - 6.5 hrs.	2% $CaCl_2$ in Sat. Boric Acid	$1.73x10^{-5}$	$3.98x10^{-6}$	3
10% PVA / 2% Alg	Chemical - 8 hrs.	2% $CaCl_2$ in Sat. Boric Acid	$1.55x10^{-5}$	$6.12x10^{-6}$	3
10% PVA / 2% Alg	Chemical - 4.5hrs	Sat. Boric Acid	$2.76x10^{-5}$	$1.42x10^{-5}$	3
10% PVA	Freeze / Thaw	-	$1.76x10^{-5}$	$2.58x10^{-6}$	4
10% PVA / 2% Alg	Freeze / Thaw	-	$1.77x10^{-5}$	$6.94x10^{-6}$	4

Table A.6: *Hydronium effective diffusivities in PVA and PVA / Alg hydrogels comparing cryogels and chemically crosslinked hydrogels in ionic solutions as depicted in* ***Figure 2.4****.*

Membrane	Crosslinking Type	Crosslinker	Ionic Strength (M)	Effective Diffusivity (cm^2/s)	+/- Error	Number of Replicates
10% PVA	Freeze / Thaw	-	0	$1.76x10^{-5}$	$2.58x10^{-6}$	4
10% PVA / 2% Alg	Freeze / Thaw	-	0	$1.77x10^{-5}$	$6.94x10^{-6}$	4
10% PVA	Freeze / Thaw	-	0.001	$2.74x10^{-5}$	$5.47x10^{-6}$	5
10% PVA / 2% Alg	Freeze / Thaw	-	0.001	$1.78x10^{-5}$	$2.32x10^{-6}$	3
10% PVA	Freeze / Thaw	-	0.01	$4.07x10^{-5}$	$5.39x10^{-6}$	5
10% PVA / 2% Alg	Freeze / Thaw	-	0.01	$2.78x10^{-5}$	$5.67x10^{-6}$	6
10% PVA	Freeze / Thaw	-	0.1	$3.77x10^{-5}$	$1.21x10^{-5}$	5
10% PVA / 2% Alg	Freeze / Thaw	-	0.1	$3.53x10^{-5}$	$4.60x10^{-6}$	6
10% PVA	Freeze / Thaw	-	0.5	$4.00x10^{-5}$	$2.27x10^{-6}$	6

10% PVA / 2% Alg	Freeze / Thaw	-	0.5	3.13×10^{-5}	9.32×10^{-6}	3
10% PVA	Freeze / Thaw	-	1	2.81×10^{-5}	1.19×10^{-5}	3
10% PVA / 2% Alg	Freeze / Thaw	-	1	2.55×10^{-5}	8.04×10^{-6}	3
10% PVA	Chemical	Sat. Boric Acid	0	2.79×10^{-5}	4.23×10^{-6}	3
10% PVA / 2% Alg	Chemical	2% $CaCl_2$ in Sat. Boric Acid	0	9.41×10^{-6}	3.41×10^{-6}	5
10% PVA	Chemical	Sat. Boric Acid	0.001	1.80×10^{-5}	2.84×10^{-6}	6
10% PVA / 2% Alg	Chemical	2% $CaCl_2$ in Sat. Boric Acid	0.001	1.54×10^{-5}	4.64×10^{-6}	3
10% PVA	Chemical	Sat. Boric Acid	0.01	2.42×10^{-5}	5.29×10^{-6}	3
10% PVA / 2% Alg	Chemical	2% $CaCl_2$ in Sat. Boric Acid	0.01	2.17×10^{-5}	4.65×10^{-6}	5
10% PVA	Chemical	Sat. Boric Acid	0.1	3.62×10^{-5}	1.08×10^{-5}	4
10% PVA / 2% Alg	Chemical	2% $CaCl_2$ in Sat. Boric Acid	0.1	2.71×10^{-5}	3.66×10^{-6}	4
10% PVA	Chemical	Sat. Boric Acid	0.5	3.28×10^{-5}	3.29×10^{-6}	3
10% PVA / 2% Alg	Chemical	2% $CaCl_2$ in Sat. Boric Acid	0.5	3.22×10^{-5}	5.58×10^{-6}	3
10% PVA	Chemical	Sat. Boric Acid	1	3.16×10^{-5}	5.61×10^{-6}	4
10% PVA / 2% Alg	Chemical	2% $CaCl_2$ in Sat. Boric Acid	1	3.19×10^{-5}	3.92×10^{-6}	6

A.10 Hydrogel Swelling

Swelling experiments were conducted as outlined in the methods section and water content was calculated based on the weight of the gel before and after swelling. A negative percent swelling indicates the percent contracted. **Table A.7** presents all this data.

Table A.7: *Water content and % swelling data obtained from 10% PVA and 10% PVA / 2% Alg hydrogels equilibrated in DI water, 0.1 M KCl, and 1 M KCl. The average values for each membrane type and ionic strength from this table are listed in* ***Table 2.1****.*

Membrane Type	Crosslinking Method	Ionic Strength (M)	Water Content (%)	% Swelling
10% PVA	Freeze / Thaw	0.1	93.7	-5
10% PVA	Freeze / Thaw	1	87.8	-19
10% PVA	Freeze / Thaw	1	87.8	-18
10% PVA	Freeze / Thaw	0	94.0	-2
10% PVA	Freeze / Thaw	0	94.2	-8
10% PVA	Freeze / Thaw	0.1	93.5	-4
10% PVA	Freeze / Thaw	1	87.8	-18
10% PVA	Freeze / Thaw	0	94.0	-4
10% PVA	Freeze / Thaw	0.1	93.5	0
10% PVA	Chemical	0.1	95.4	38
10% PVA	Chemical	0.1	94.5	9
10% PVA	Chemical	0	96.0	35
10% PVA	Chemical	1	87.8	-5
10% PVA	Chemical	0	95.4	20
10% PVA	Chemical	1	87.4	0
10% PVA	Chemical	0.1	95.4	37
10% PVA	Chemical	1	87.2	-8
10% PVA	Chemical	0	95.8	36
10% PVA / 2% Alg	Freeze / Thaw	1	88.0	-7
10% PVA / 2% Alg	Freeze / Thaw	0	94.9	6
10% PVA / 2% Alg	Freeze / Thaw	0.1	93.5	-6

10% PVA / 2% Alg	Freeze / Thaw	0.1	93.3	7
10% PVA / 2% Alg	Freeze / Thaw	1	87.7	-5
10% PVA / 2% Alg	Freeze / Thaw	0.1	93.2	-6
10% PVA / 2% Alg	Freeze / Thaw	0	94.6	8
10% PVA / 2% Alg	Freeze / Thaw	1	88.6	-2
10% PVA / 2% Alg	Freeze / Thaw	0	94.9	5
10% PVA / 2% Alg	Chemical	0	94.3	17
10% PVA / 2% Alg	Chemical	0.1	93.4	17
10% PVA / 2% Alg	Chemical	1	87.6	0
10% PVA / 2% Alg	Chemical	1	87.2	2
10% PVA / 2% Alg	Chemical	0.1	93.8	21
10% PVA / 2% Alg	Chemical	0	94.3	18
10% PVA / 2% Alg	Chemical	0	94.3	20
10% PVA / 2% Alg	Chemical	0.1	93.7	18
10% PVA / 2% Alg	Chemical	1	87.2	0

A.11 NMR Spectra

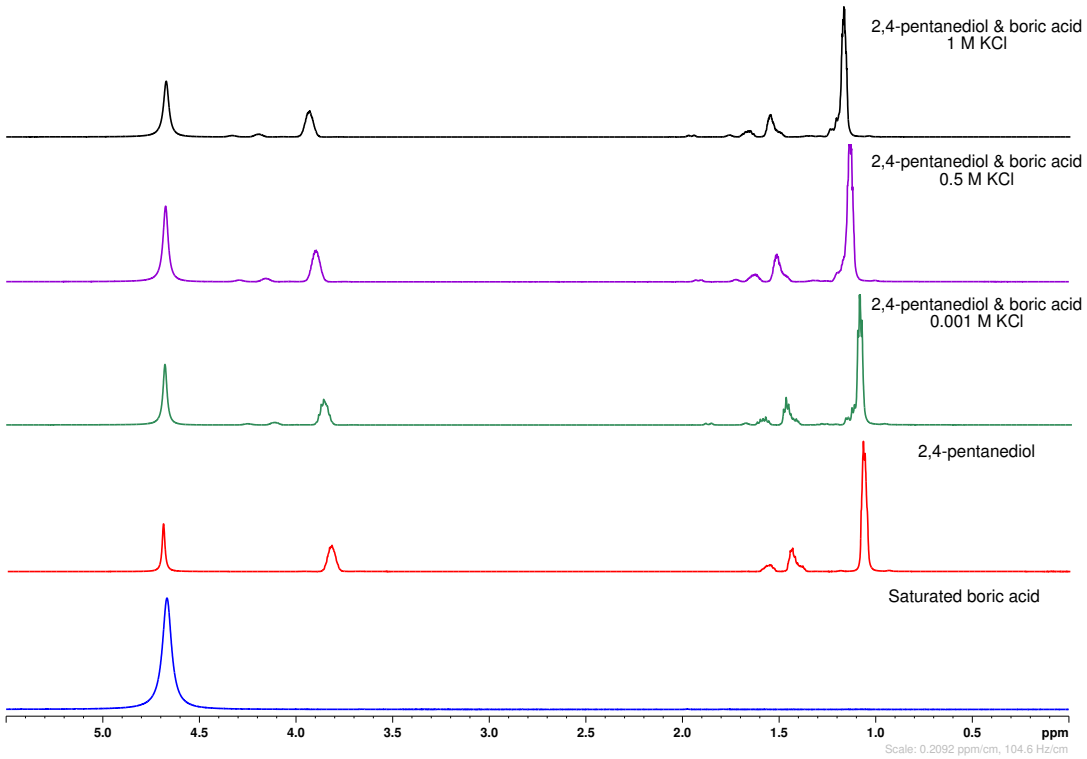

Figure A.9: *1H NMR spectra of samples of 2,4-pentanediol, boric acid, and KCl in D_2O.*

1H NMR analysis showed no formation of additional peaks after the addition of boric acid to 2,4-pentandiol as expected from the results reported by Shibayama et al.[4] There is also a noticeable but slight shift in each spectra as the ionic strength increases, but the difference in peak shift is within instrumental error, so no conclusions can be made. The results of the 1H NMR experiments were inconclusive and showed no indication of an interaction between the diol-borate complex and potassium chloride.

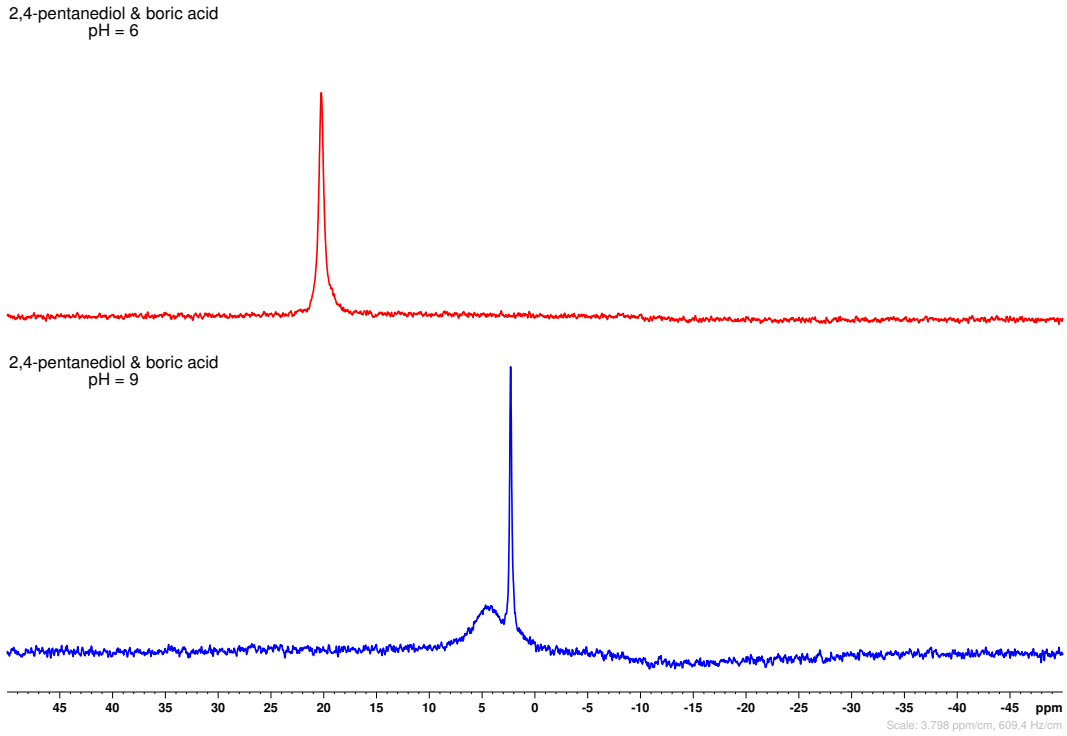

Figure A.10: *11B NMR of 2,4-pentanediol and boric acid in acidic and basic conditions.*

11B NMR experiments were run under acidic and basic conditions to confirm the formation of a PVA-borate complex. The top spectra in **Figure A.10**, the acidic condition, was inconclusive since there was no way to decern between the free boric acid peak and the diol-borate complex since both molecules are 3-coordinate complexes. The bottom spectra in **Figure A.10** shows two distinct peaks, the peak circled in red indicates the presence of a 4-coordinate PVA-borate complex.[5] The shift in the free boric acid peak between acidic and basic conditions is consistent with studies done by Sinton.[5]

A.12 FTIR Spectra

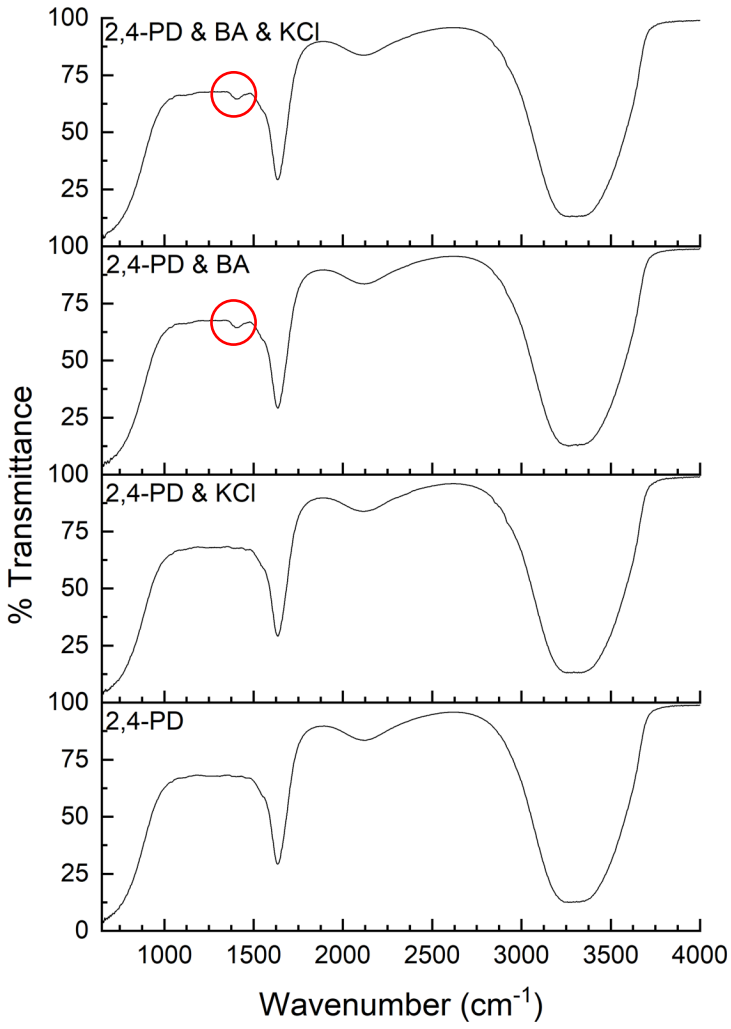

Figure A.11: *FTIR analysis of samples prepared with 2,4-pentanediol as a substitute for PVA. 2,4-PD is 2,4-pentanediol, BA is boric acid, and KCl is potassium chloride. Red circles indicate the peak identifying the presence of the B-O bond .*

FTIR characterization was done to determine if there was an interaction between the PVA-borate complex and potassium chloride. FTIR experiments were done with 2,4-pentanediol as a substitute for PVA. Red circles on **Figure A.11** indicate the peak identifying the presence of the B-O bond at 1400 cm^{-1} which could be either free boric acid, or a part of the diol-borate complex.[6] If KCl was interacting with either 2,4-pentanediol or the diol-borate complex, we would expect another peak to appear, but no additional peaks appear after KCl is introduced, indicating that there was no interaction.

A.13 Raman Spectra

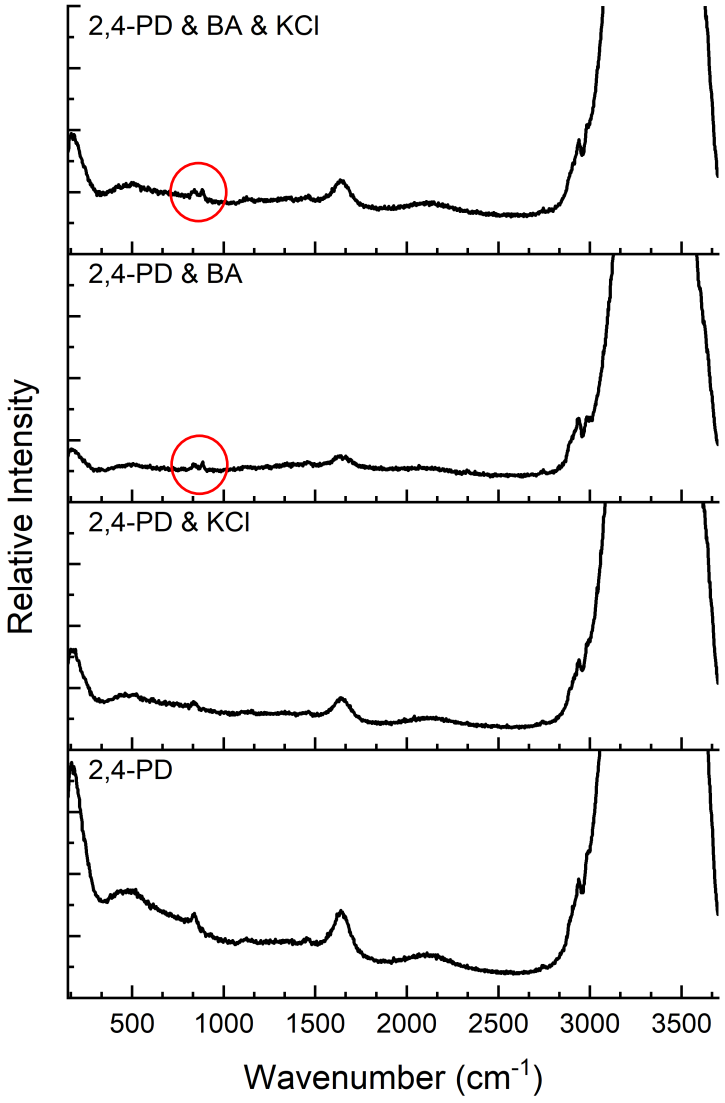

Figure A.12: *Raman spectroscopy spectra collected using 2,4-pentanediol as a substitute for PVA. 2,4-PD is 2,4-pentanediol, BA is boric acid, and KCl is potassium chloride. Red circles indicate the peaks associated with the presence a PVA-borate complex.7*

Raman spectroscopy was done as an additional effort to determine if potassium chloride was interacting with the PVA-borate complex, and as done previously, 2,4-pentanediol was used as a substitute for PVA in these experiments. The red circles in **Figure A.12** identify the formation of a second peak at 880 cm^{-1} which indicates the formation of the PVA-borate complex.[7] There seems to be no additional peaks or shift in the spectra after the addition of KCl, therefore there appears to be no interaction.

A.14 Statistical Analysis

Error bars were calculated using a 95% confidence interval. Since sample sizes were small (≤ 6), a t-distribution was used to describe experimental variability:

$$CI = \mu \pm t_{\frac{\alpha}{2},\nu}\left(\frac{\sigma}{\sqrt{n}}\right)$$

Equation A-3

Where α is the confidence level (0.05), ν is the degrees of freedom, σ is the standard deviation of the sample, and n is the sample size. Values for $t_{\frac{\alpha}{2},\nu}$ were determined using a t-distribution table.

Anova tables were generated in R. A type II Anova analysis was chosen due to the hierarchal unbalanced data sets being analyzed. Data was scaled by $1x10^5$ for analysis.

Table A.8: *3-way Type II Anova analysis on data presented in* ***Table A.6*** *after a transformation of 0.5. The effects of hydrogel blend, crosslinking method, and ionic strength on hydronium diffusivity were analyzed.*

	Sum of Squares	DF	F-value	p-value
Membrane (A)	0.8271	1	53.7533	<0.0001
Crosslinker (B)	0.3665	1	23.8180	<0.0001
Ionic Strength (C)	4.6999	5	61.0881	<0.0001
A:B	0.0030	1	0.1952	0.65986
A:C	0.2344	5	3.0466	0.01453
B:C	0.5040	5	6.5506	<0.0001
A:B:C	0.6940	5	9.0200	<0.0001
Error	1.2002	78		

Additional analysis was done to determine what drove the three-way interaction. The interaction plots generated for that analysis are shown in **Figure A.13 - A.15**.

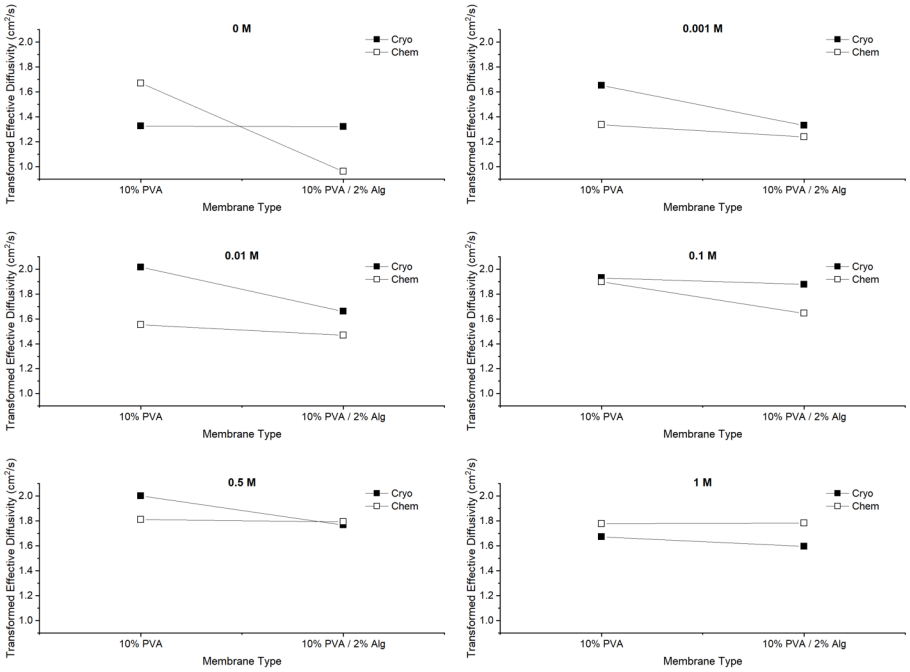

Figure A.13: *Two-way interaction plots depicting the interaction between membrane type and crosslinking method at each tested ionic strength.*

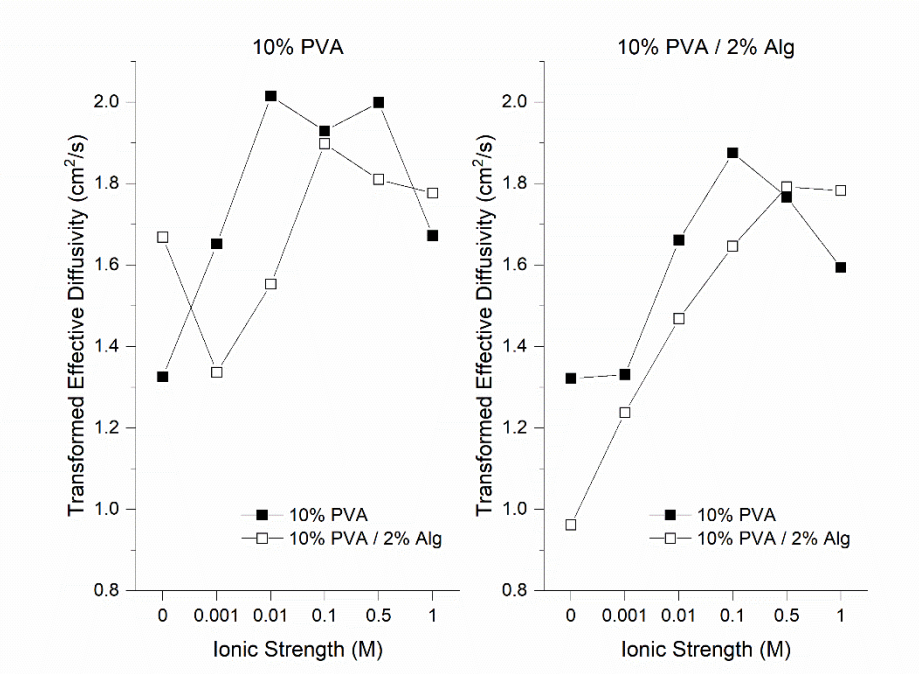

Figure A.14: *Two-way interaction plot depicting the interaction between ionic strength and membrane type with each membrane type.*

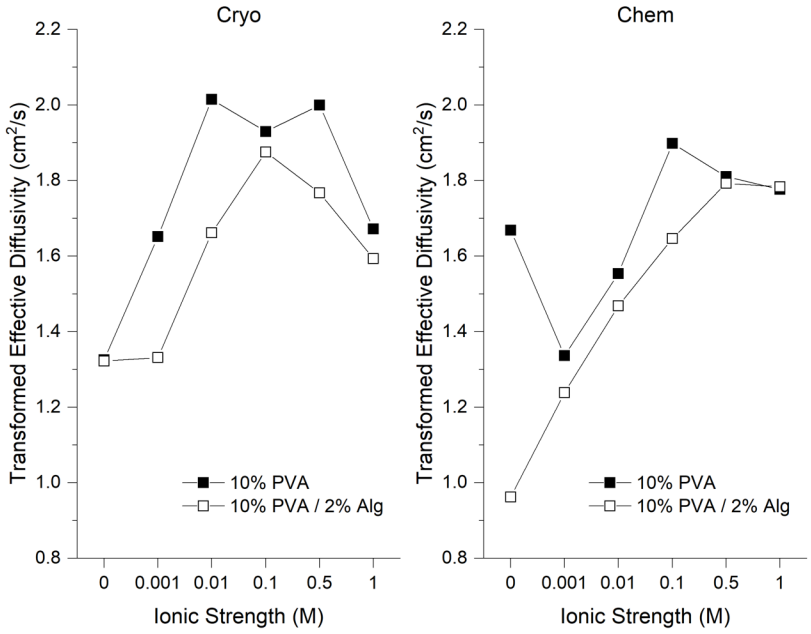

Figure A.15: *Two-way interaction between ionic strength and membrane type with each crosslinking method.*

Table A.9: *Further analysis of the effect of ionic strength on hydronium diffusivity in 10% PVA cryogels was analyzed.*

	Sum of Squares	DF	F-value	p-value
Ionic Strength	18.7819	5	13.608	<0.0001
Error	6.0728	22		

Table A.10: *Further analysis of the effect of ionic strength on hydronium diffusivity in 10% PVA chemically crosslinked hydrogels was analyzed.*

	Sum of Squares	DF	F-value	p-value
Ionic Strength	10.3837	5	15.208	<0.0001
Error	2.3215	17		

Table A.11: *Further analysis of the effect of ionic strength on hydronium diffusivity in 10% PVA / 2% Alg cryogels was analyzed.*

	Sum of Squares	DF	F-value	p-value
Ionic Strength	10.8346	5	11.804	<0.0001
Error	3.4879	19		

Table A.12: *Further analysis of the effect of ionic strength on hydronium diffusivity in 10% PVA / 2% Alg chemically crosslinked hydrogels was analyzed.*

	Sum of Squares	DF	F-value	p-value
Ionic Strength	18.9897	5	40.152	<0.0001
Error	1.8918	20		

Table A.13: *Tukey tests of the data presented in* ***Table A.3,*** *excluding 10% PVA / 2% Alg. The effect of PVA composition on hydronium diffusivity was analyzed, and p-values were adjusted using the single-step method.*

Compositions compared	Estimate	Standard Error	t-value	p-value
10 – 7	-0.04667	0.13720	-0.340	0.99674
15 – 7	-0.62187	0.13119	-4.740	0.00246
20 – 7	-0.23333	0.14668	-1.591	0.52471
30 – 7	-0.12917	0.13720	-0.941	0.87535
15 – 10	-0.57520	0.12051	-4.773	0.00232
20 – 10	-0.18667	0.13720	-1.361	0.65934
30 – 10	-0.08250	0.12702	-0.649	0.96370
20 – 15	0.38853	0.13119	2.962	0.06558
30 – 15	0.49270	0.12051	4.089	0.00819
30 – 20	0.10417	0.13720	0.759	0.93778

Table A.14: *1-way Type II Anova analysis on data presented in* ***Table A.5****. The effect of crosslinking time on hydronium effective diffusivity in 10% PVA / 2% Alg hydrogels was analyzed.*

	Sum of Squares	DF	F-value	p-value
Crosslinking Time	1.37796	2	11.591	0.004333
Error	0.47553	8		

Table A.15: *1-way Type II Anova analysis on data presented in* ***Table A.1****. The effect of the number of freeze-thaw cycles on hydronium effective diffusivity in 10% PVA hydrogels was analyzed.*

	Sum of Squares	DF	F-value	p-value
Number of cycles	0.9078	3	1.0898	0.3857
Error	3.8875	14		

Table A.16: *1-way Type I Anova analysis on data presented in* ***Table A.7****. The effect of crosslinking method on hydrogel water content in 10% PVA hydrogels was analyzed.*

	DF	Sum of Squares	Mean Square	F-value	p-value
Crosslinking Method	1	4.194	4.194	12.454	0.003337
Ionic Strength	2	196.012	98.006	291.046	<0.001
Error	14	4.714	0.337		

Table A.17: *1-way Type 1 Anova analysis on data presented in* ***Table A.7****. The effect of crosslinking method on hydrogel water content in 10% PVA / 2% Alg hydrogels was analyzed.*

	DF	Sum of Squares	Mean Square	F-value	p-value
Crosslinking Method	1	0.479	0.479	4.5679	0.0507
Ionic Strength	2	162.057	81.028	772.9250	<0.0001
Error	14	1.468	0.105		

A.15 XRD Analysis

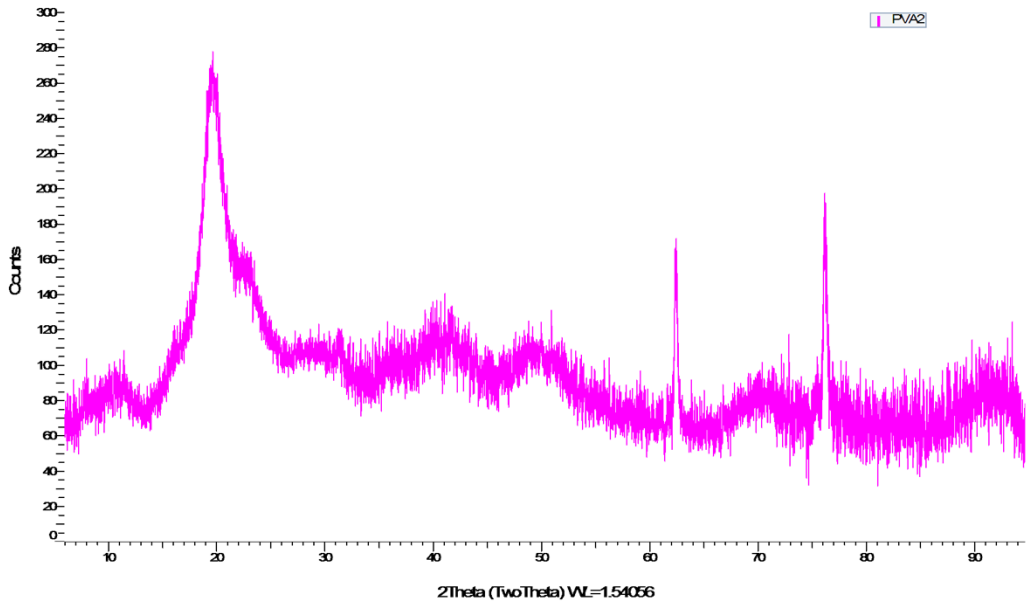

Figure A.16*: XRD spectra of a 10% PVA cryogel equilibrated in DI water.*

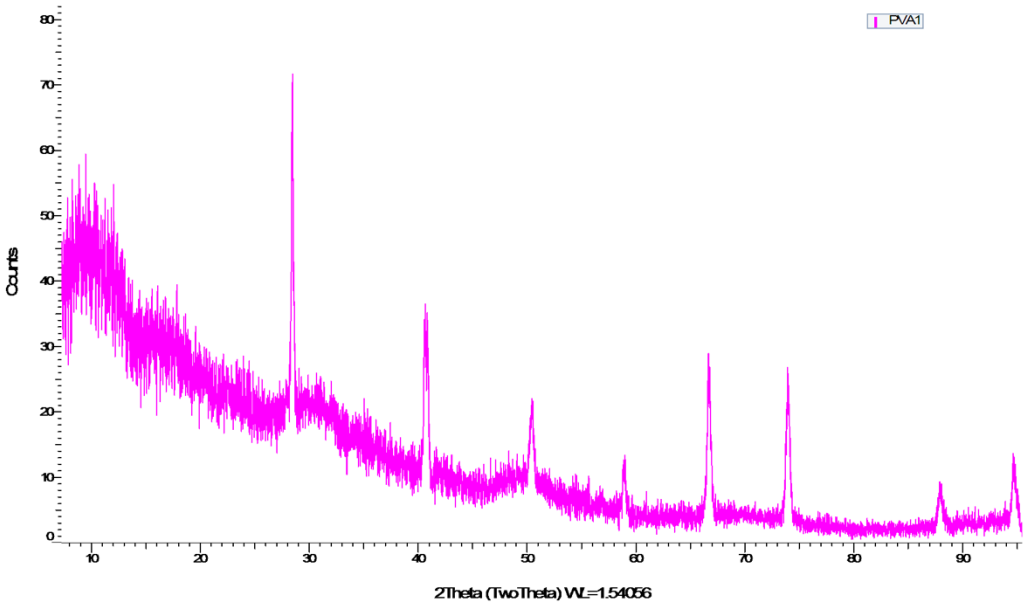

Figure A.17: *XRD spectra of a 10% PVA cryogel equilibrated in 1 M KCl.*

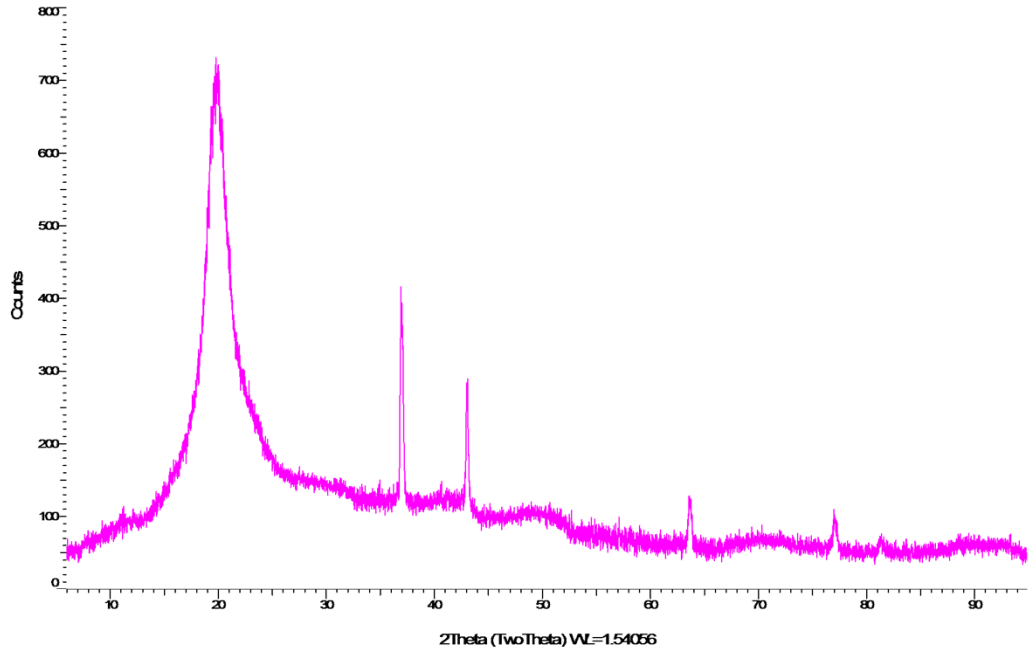

Figure A.18: *XRD spectra of 10% PVA chemically crosslinked hydrogel equilibrated in DI water.*

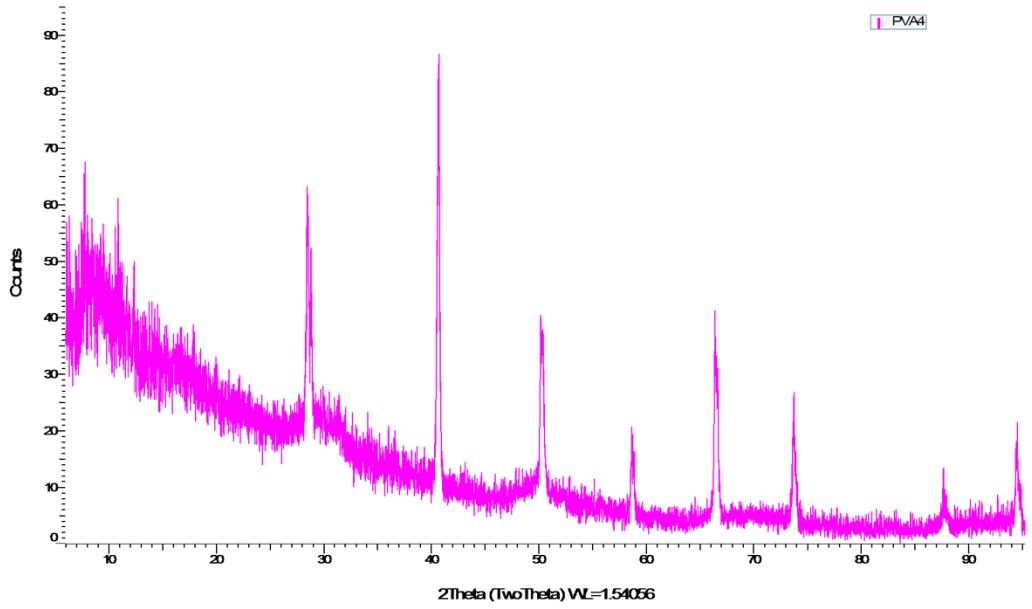

Figure A.19: *XRD spectra of a 10% PVA chemically crosslinked hydrogel equilibrated in 1 M KCl.*

The XRD spectra shown in **Figure A.16 and A.18** show the presence of crystalline regions in 10% PVA hydrogels. Absence of crystalline domains in **Figure A.17** and **A.19** are likely due to competing crystallization during hydrogel drying due to potassium chloride crystallization.

A.16 $D_{e,H+,gel}$ Relationship with High Molecular Weight and Solvent Ionic Strength

At high ionic strengths (> 0.1M), $D_{e_{(H_3O^+,\,gel)}}$ values are at a maximum. At these high salt concentrations, the effect of polymer volume fraction on diffusivity becomes apparent as shown in **Figure A.20**.

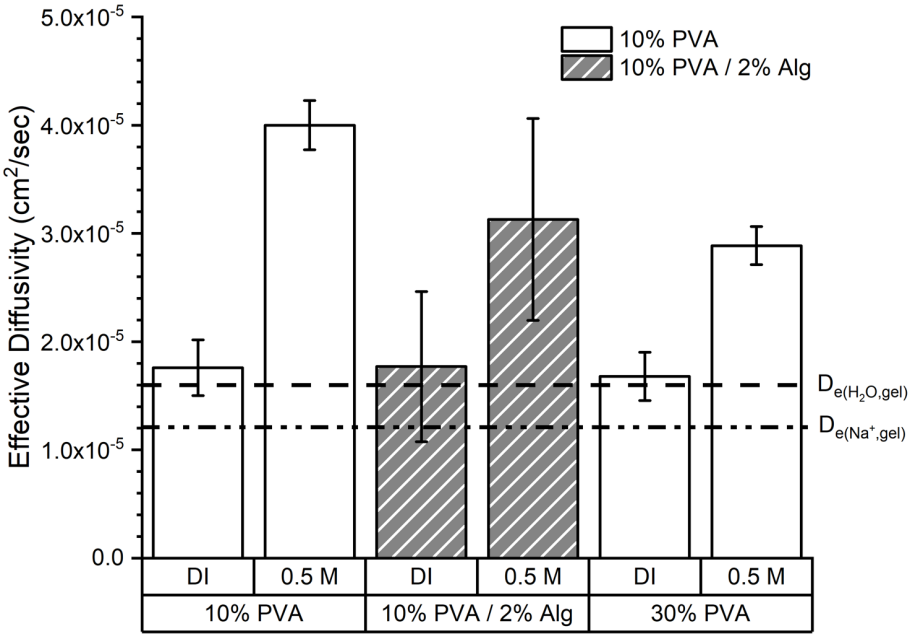

Figure A.20: *Hydronium effective diffusivity in cryogels compared between 0.5 M KCl and DI water systems. Error bars represent a 95% confidence interval.*

Table A.18: *Hydronium effective diffusivities of cryogels depicted in* ***Figure A.20****.*

Membrane	Crosslinking Type	Ionic Strength (M)	Effective Diffusivity (cm^2/s)	+/- Error	Number of Replicates
10% PVA	Freeze / Thaw	0	$1.76x10^{-5}$	$2.58x10^{-6}$	4
10% PVA	Freeze / Thaw	0.5	$4.00x10^{-5}$	$2.27x10^{-6}$	6
10% PVA / 2% Alg	Freeze / Thaw	0	$1.77x10^{-5}$	$6.94x10^{-6}$	4
10% PVA / 2% Alg	Freeze / Thaw	0.5	$3.13x10^{-5}$	$9.32x10^{-6}$	3
30% PVA	Freeze / Thaw	0	$1.68x10^{-5}$	$2.24x10^{-6}$	4
30% PVA	Freeze / Thaw	0.5	$2.89x10^{-5}$	$1.76x10^{-6}$	3

A.17 Model Sensitivity Analysis

Theory Development

To estimate hydronium diffusion through PVA membranes, the scaling law developed by Lustig and Peppas[8] was employed to normalize the diffusion coefficient. Calculations were only completed for 10% PVA hydrogels due to equation limitations for single component hydrogels. Swelling experiments, requisite for estimating parameters for the model, were performed to determine the swelling behavior of the hydrogels after crosslinking.

Membranes were cast and crosslinked as described in the methods section of the manuscript. The volume of each hydrogel was calculated using the known cross-sectional area of each casting mold and measuring the average equilibrated thickness of the membranes from five spatial points after swelling. The polymers were dried in a vacuum oven at 40 ˚C until no weight change was observed. The following parameters were calculated using this data, where subscripts α, β, and γ denote water, polymer, and solute respectively.

$$\nu_{\beta,i} = \frac{V_p}{V_{g,i}}$$

Equation A-4

$\nu_{\beta,i}$ is the polymer volume fraction before (r) or after (s) swelling, V_p is the volume of the dry crosslinked polymer, and $V_{g,i}$ is the gel volume after crosslinking and before or after swelling.[1]

The volume degree of swelling can be calculated by:[1]

$$Q = \frac{1}{\nu_{\beta,s}}$$

Equation A-5

To determine structural influences on diffusion, the following parameters were calculated. $\overline{M_c}$ is the number average molecular weight between crosslinks:[2]

$$\frac{1}{\overline{M_c}} = \frac{2}{\overline{M_n}} - \frac{\left(\frac{\bar{v}}{V_1}\right) \cdot \left[\ln\left(1-\nu_{\beta,s}\right) + \nu_{\beta,s} + \chi_{\alpha,\beta} \cdot \nu_{\beta,s}^2\right]}{\nu_{\beta,r} \cdot \left[\left(\frac{\nu_{\beta,s}}{\nu_{\beta,r}}\right)^{\frac{1}{3}} - \frac{1}{2} \cdot \left(\frac{\nu_{\beta,s}}{\nu_{\beta,r}}\right)\right]}$$

Equation A-6

When $\overline{M_n}$ is the number average molecular weight (85,000 g/mol, ThermoFisher) of the polymer, $\bar{\nu}$ is the specific volume of the polymer repeating unit (0.788 cm^{-3}/g),[2] $\chi_{\alpha,\beta}$ is a Flory interaction parameter for PVA-water systems (0.494 at 30 ˚C).[2] The number of links between repeating units per polymer chain, N, can be calculated:

$$N = 2 \cdot \left(\frac{\overline{M_c}}{M_r}\right)$$

Equation A-7

Where M_r is the molecular weight of the repeating unit (44 g/mol for PVA).[1] The mesh size of the swelled polymer gel can be calculated by the equation:[9]

$$\xi = Q^{\frac{1}{3}} \cdot (C_n \cdot N)^{\frac{1}{2}} \cdot l$$

Equation A-8

Where C_n is the Flory characteristic ratio (8.3 for PVA), l is the (C - C) bond length across the polymer chains (1.54 Å for PVA).[9]

With structural and physical parameters calculated, the normalized diffusion coefficient can be determined using the scaling law as laid out by Lustig and Peppas:[8]

$$\widehat{D} = \frac{D_{\gamma,\alpha\beta}}{D_{\gamma,\alpha}} \cong \left[1 - \frac{r}{\xi}\right] \cdot e^{\left[-\frac{Y}{(Q-1)}\right]}$$

Equation A-9

$\widehat{D}$ is the normalized diffusion coefficient, $D_{\gamma,\alpha\beta}$ is the diffusion coefficient of the solute through the hydrogel, $D_{\gamma,\alpha}$ is the diffusion coefficient of the solute through water, r is the Stokes hydrodynamic radius of the solute (2.82 Å H_3O^+,[10] 3.58 Å Na^+,[10] 1.30 Å H_2O,[11] and Y is a structural parameter (assumed to equal 1 as an approximation).[8]

Previous work by Wraight[12] used sodium as a surrogate for hydronium. The size and charge of a sodium ion is comparable to hydronium, allowing for the estimation of diffusive properties of hydronium through a hydrogel without the enhanced transport provided by the Grotthuss mechanism. Diffusion coefficients used as parameters in **Equation A-9** where hydronium ($D_{\gamma,\alpha} = D_e$ = 9.3 × 10^{-5} cm^2/s),[12] sodium ($D_{\gamma,\alpha} = D_e$ = 1.33 × 10^{-5} cm^2/s),[12] and water ($D_{\gamma,\alpha} = D_e$ = 1.73 × 10^{-5} cm^2/s).[11] Additional models relevant to solute diffusion in hydrogels have been reported by Masaro and Zhu.[13]

Overall Results

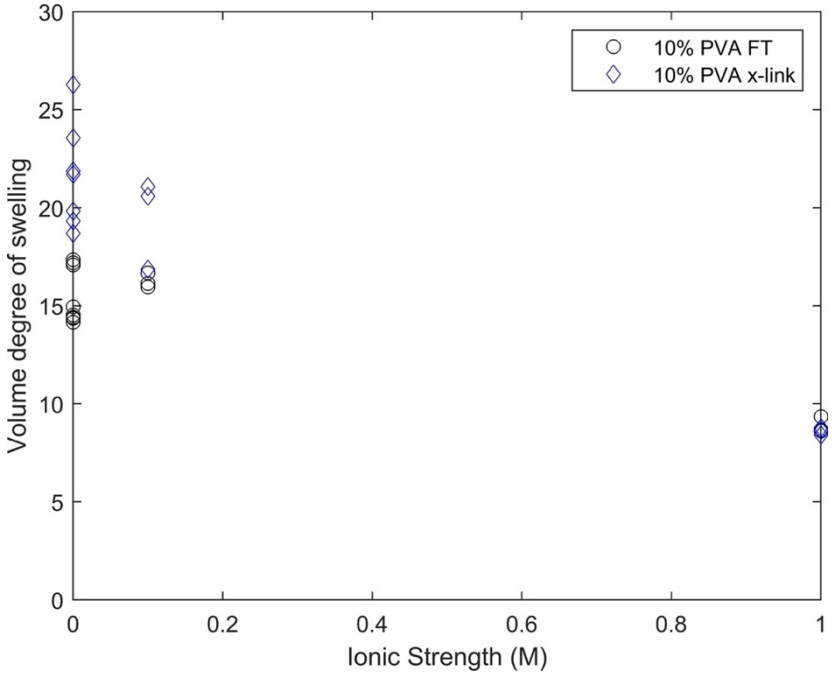

Figure A.21: *A plot of volume degree of swelling versus ionic strength. Note that more variability is observed at lower ionic strength.*

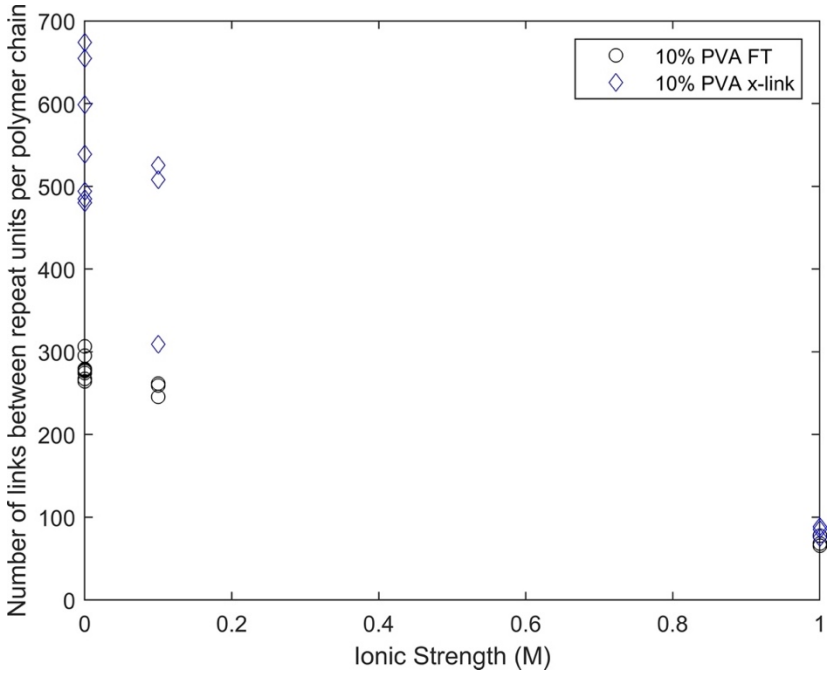

Figure A.22: *A plot of ionic strength versus the number of links between repeating units per polymer chain is shown below. Note that there was a significant difference between cryogels and chemically crosslinked gels at low ionic strength, but these differences were lost at higher ionic strengths.*

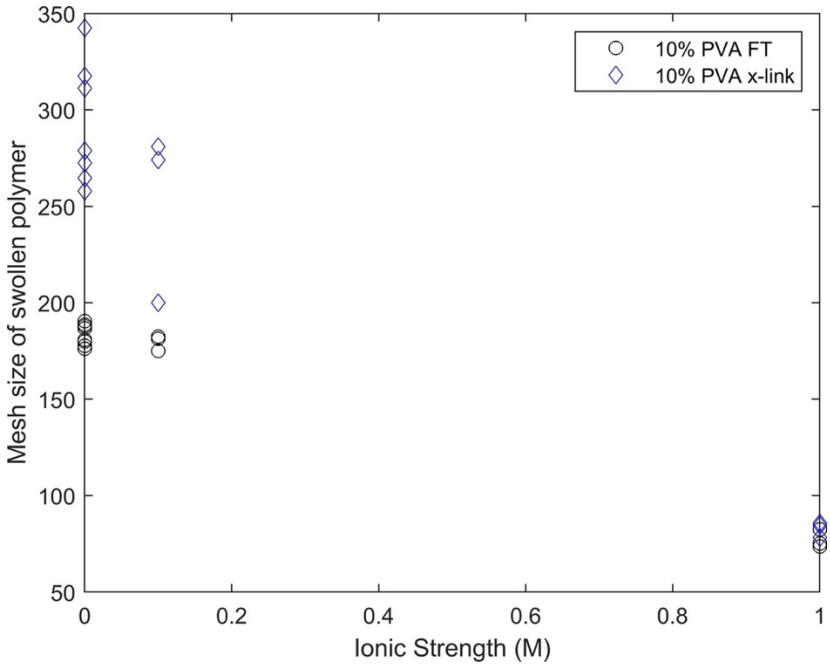

Figure A.23: *A plot of ionic strength versus the mesh size of the swelled polymer gel. Note that like the previous plot, there are significant difference between cryogels and chemically crosslinked hydrogels at low ionic strength, but these differences are lost at higher ionic strengths.*

Hydronium diffusion through hydrogels at 0 M KCl is calculated from the model to be 8.54×10^{-5} cm^2/s for cryogels and 8.77×10^{-5} cm^2/s for chemically crosslinked hydrogels. Measured diffusivity of hydronium through hydrogels was 1.76×10^{-5} cm^2/s for cryogels and 2.79×10^{-5} cm^2/s for chemically crosslinked 10% PVA hydrogels. Because of this large difference, a sensitivity analysis was performed below to examine factors within the model that may change the results to be more in line with measured values.

Sensitivity analysis for 0 M KCl

Changing Y parameter

First, we'll see how the diffusion coefficient of species in the hydrogel changes with changes in Y between 0 and 2. The default value for Y is 1.

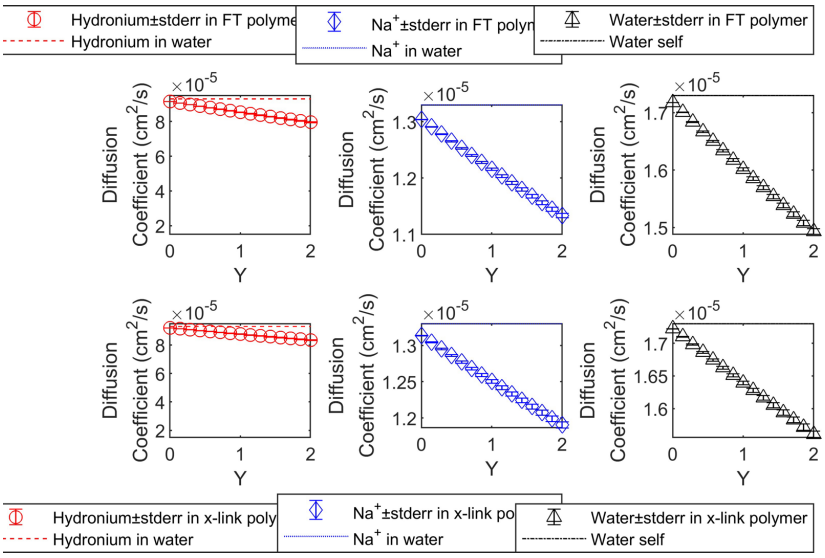

Figure A.24*: Calculated theoretical diffusion coefficient of various species plotted against the Y parameter. Results for cryogels in the top row and results for chemically crosslinked hydrogels on the bottom.*

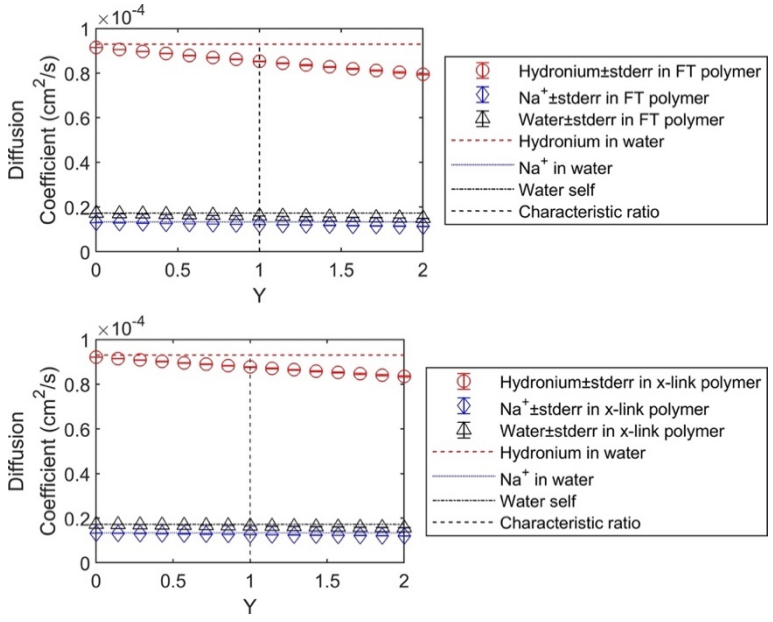

Figure A.25: *Calculated theoretical diffusion coefficients of various species plotted against the Y parameter. Same values as in* ***Figure A.24****, but collected into one graph per crosslinking method for scale reference.*

The diffusion coefficients appear to be somewhat sensitive (±Δ 7% for cryogels, ±Δ 5% for chemically crosslinked hydrogels) to changes in Y parameter over the ranges 0-2.

Changing Flory characteristic ratio C_n

As consequence of altering the Flory characteristic ratio, Cn, the xi parameter (mesh size) will also change, which may impact diffusion rates. We'll fix Y parameter at 1 for iterating the Flory characteristic ratio between 0.5 and 2 times the current value.

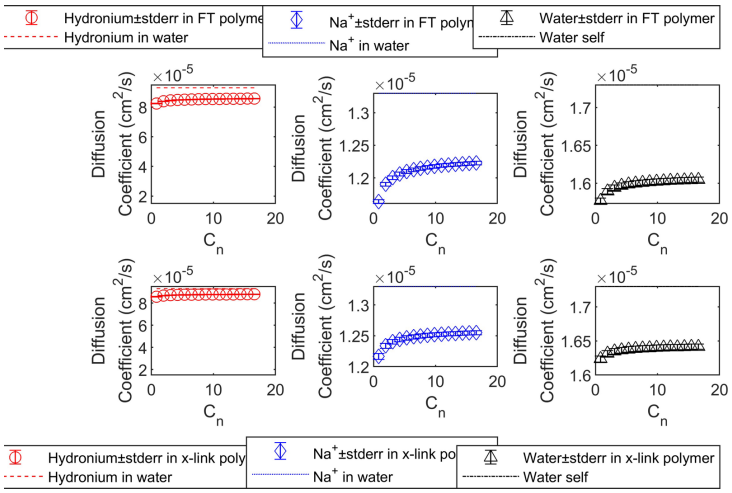

Figure A.26: *Calculated theoretical diffusion coefficient of various species plotted against the Flory characteristic ratio. Results for cryogels in the top row and results for chemically crosslinked hydrogels on the bottom.*

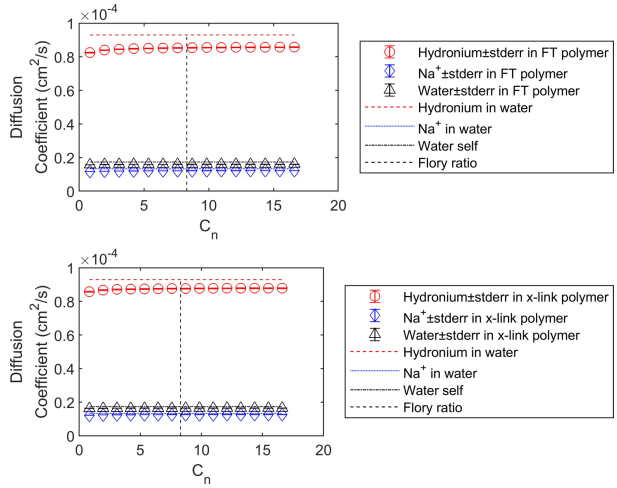

Figure A.27: *Calculated theoretical diffusion coefficients of various species plotted against the Flory characteristic ratio. Same values as in* ***Figure A.26****, but collected into one graph per crosslinking method for scale reference.*

The diffusion coefficients appear to somewhat sensitive (-Δ 4% to + Δ 0.4% for cryogels, - Δ 3% to +Δ 0.2% for chemically crosslinked hydrogels) over the range of C_n values tested. The larger C_n grows the larger ξ becomes. As ξ increases, $\left[1-\frac{r}{\xi}\right] \rightarrow 1$ and the diffusion coefficient approaches $D_{\gamma,\alpha\beta} \cong D_{\gamma,\alpha} \cdot e^{\left[-\frac{Y}{(Q-1)}\right]}$

Changing Flory interaction parameter $\chi_{\alpha,\beta}$

The Flory interaction parameter influences $\overline{M_c}, N, \xi$ (defined previously), which ultimately influences the diffusion coefficient. We'll iterate the Flory interaction parameter between 0 and 0.523 (the instability point).

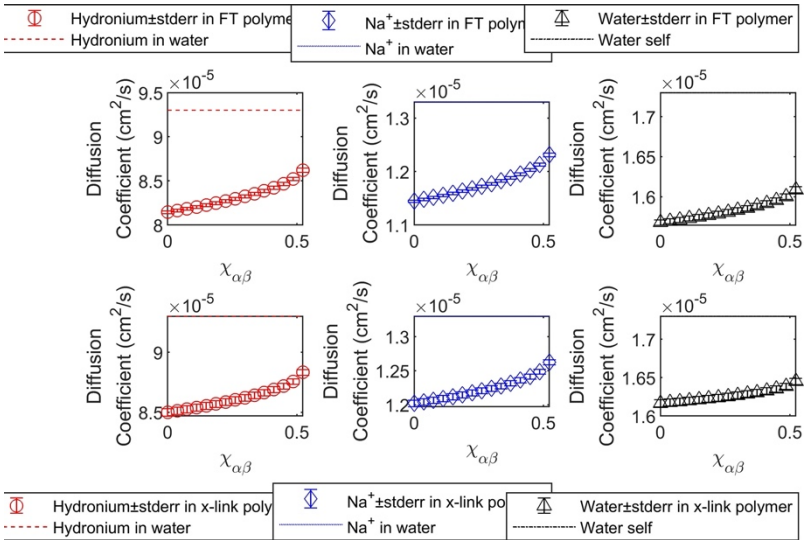

Figure A.28: *Calculated theoretical diffusion coefficient of various species plotted against the Flory interaction parameter. Results for cryogels in the top row and results for chemically crosslinked hydrogels on the bottom.*

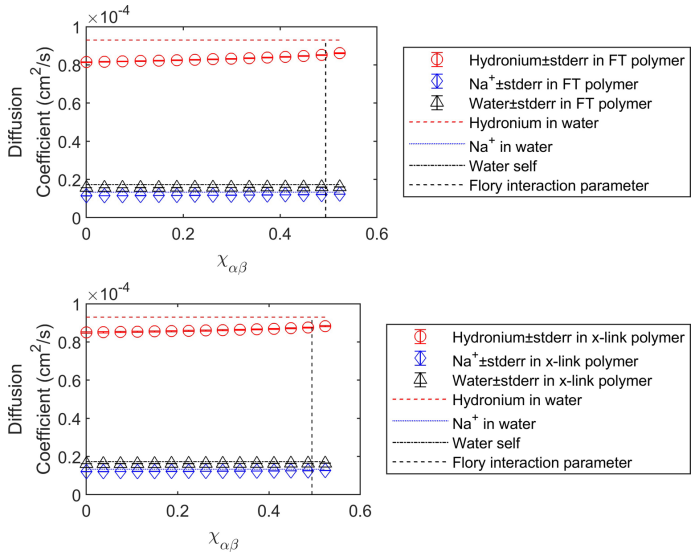

Figure A.29: *Calculated theoretical diffusion coefficients of various species plotted against the Flory interaction parameter. Same values as in* ***Figure A.28****, but collected into one graph per crosslinking method for scale reference.*

Diffusion appears to be somewhat sensitive (-Δ 5% to +Δ 1% for cryogels, -Δ 4% to +Δ 0.7% for chemically crosslinked hydrogels) over the range of $\chi_{\alpha,\beta}$ values tested.

Changing specific volume of polymer repeating unit $\bar{\nu}$

We'll iterate the specific volume of the polymer repeating unit between 0 and 10 times the current value.

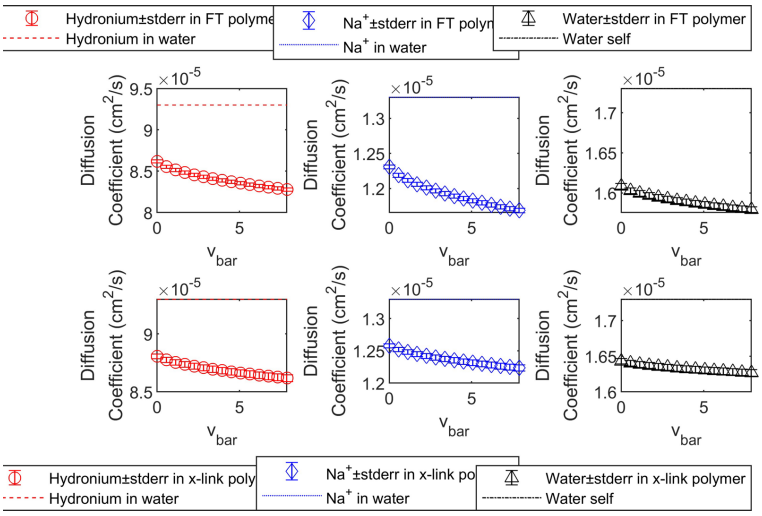

Figure A.30: *Calculated theoretical diffusion coefficient of various species plotted against the specific volume of the polymer repeating unit. Results for cryogels in the top row and results for chemically crosslinked hydrogels on the bottom.*

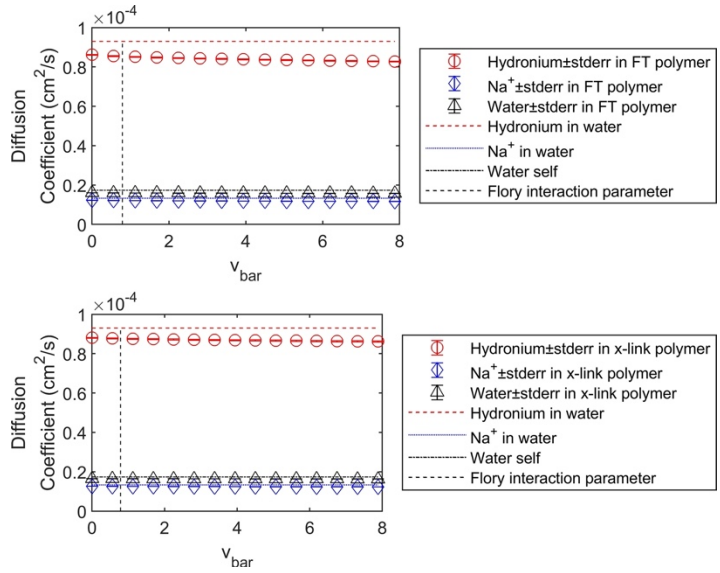

Figure A.31: *Calculated theoretical diffusion coefficients of various species plotted against the specific volume of the polymer repeating unit. Same values as in* ***Figure A.30****, but collected into one graph per crosslinking method for scale reference.*

The diffusion coefficients appear to somewhat insensitive (-Δ 5% to +Δ 1% for cryogels, -Δ 2% to +Δ 0.4% for chemically crosslinked hydrogels) over the range of $\bar{\nu}$ values tested.

Changing Stokes hydrodynamic radius *r*

Hydrodynamic radius is likely very different from an Eigen ($H_9O_4^+$) or Zundel ($H_5O_2^+$) cation than for the "traditional" hydronium ion (H_3O^+). How does a change in hydrodynamic radius impact diffusion? A range of 0.1 to 8 Angstrom, since Kadhim and Gamaj[14] reported H+ hydrodynamic radius as 0.3 Angstroms, while Nightingale[10] reported 2.82 Angstroms for hydronium ion.

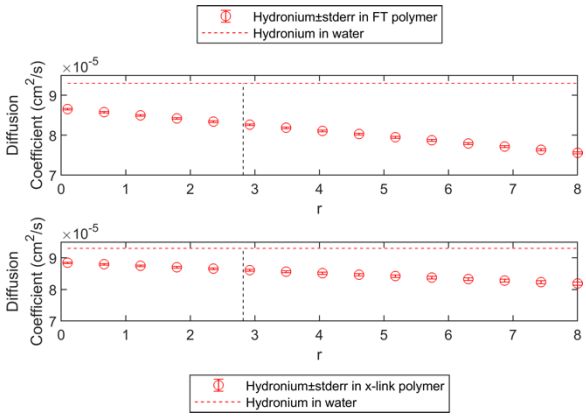

Figure A.32: *Calculated theoretical diffusion coefficient of hydronium plotted against the Stokes hydrodynamic radius. Results for cryogels in the top row and results for chemically crosslinked hydrogels on the bottom.*

If $\frac{r}{\xi}$ is set to 0, diffusivity increases by ~0.25 × 10^{-5} cm^2/s.

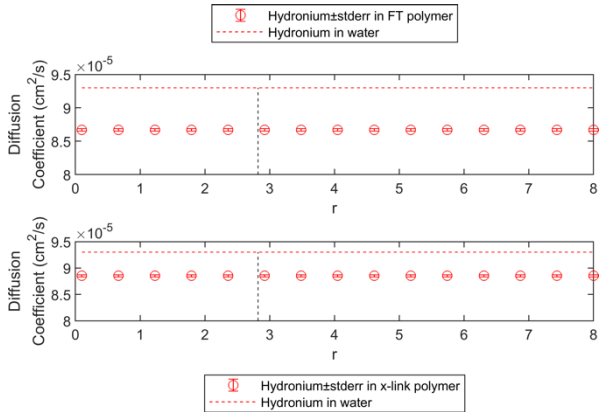

Figure A.33: *Calculated theoretical diffusion coefficients of hydronium in 0.01 M KCl plotted against the Stokes hydrodynamic radius.* $\frac{r}{\xi}$ *was set to zero.*

The change in diffusivity observed after varying Stokes radius was the largest (-Δ 12% to +Δ 1% for cryogels, -Δ 7% to +Δ 0.9% for chemically crosslinked hydrogels). Ignoring the hydrodynamic radius effects and mesh size completely results in a +Δ 1.5% for cryogels and a +Δ 0.9% for chemically crosslinked hydrogels.

Final summary of sensitivity analysis for 0 M KCl

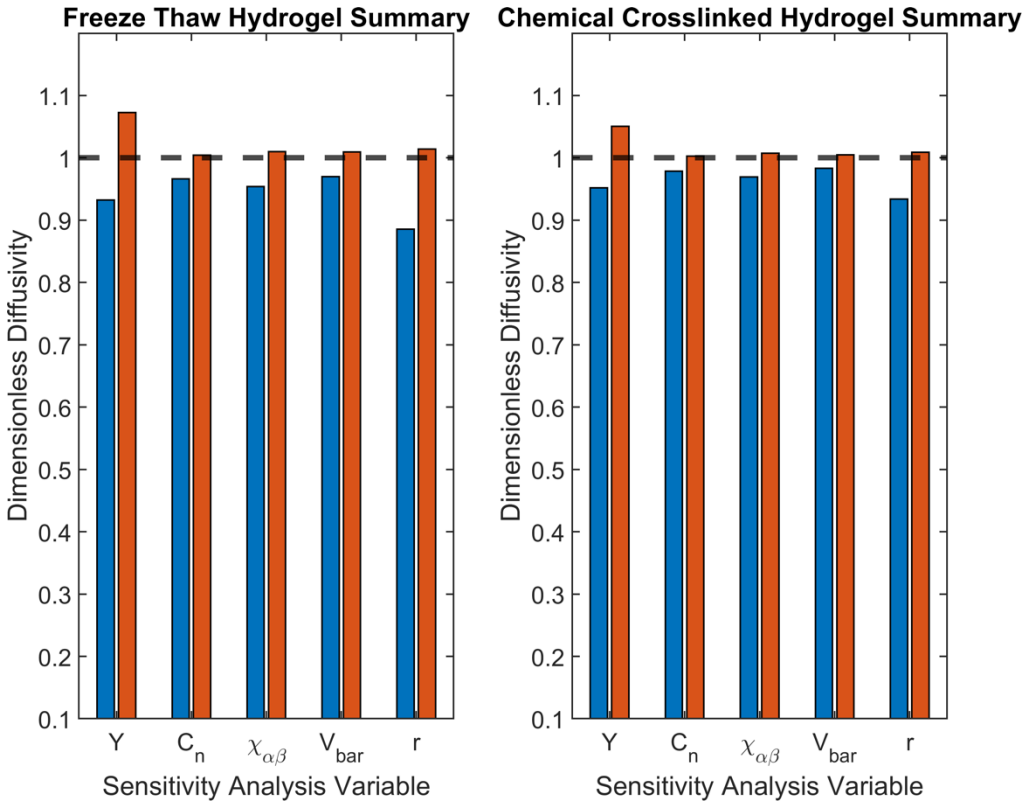

Figure A.34: *Summary of the sensitivity analysis for cryogels and chemically crosslinked hydrogels in DI water. The red bars indicate the maximum dimensionless diffusivity calculated per parameter over the values tested. The blue bars indicated the minimum dimensionless diffusivity calculated. Values closer to 1 are closer to the original prediction.*

Sensitivity analysis for 0.1 M KCl

Measured diffusivity of hydronium through hydrogels at 0.1 M KCl was 3.77×10^{-5} cm ^{2}/s for cryogels and 3.62×10^{-5} cm^2/s for chemically crosslinked 10% PVA hydrogels. As with 0 M KCl a large difference exists between measured and predicted diffusivities.

Changing Y parameter

As before, changes in Y between 0 and 2.

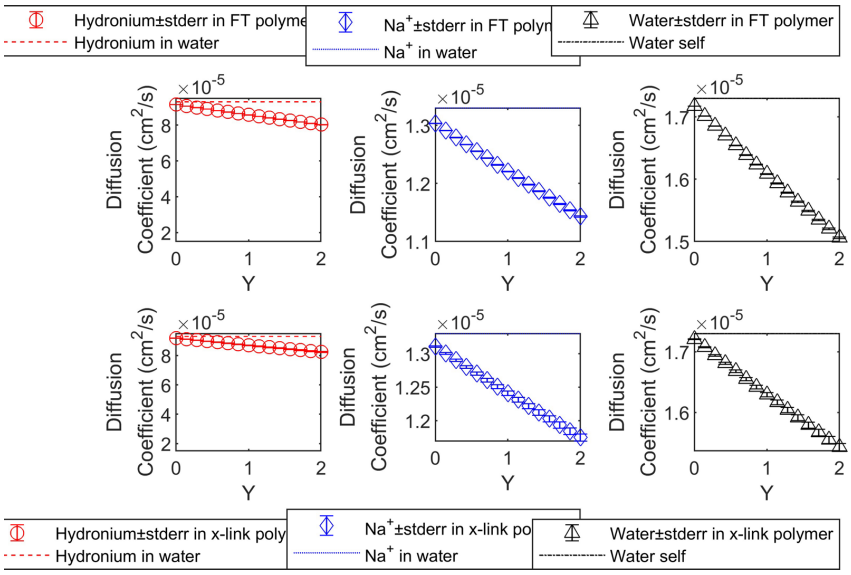

Figure A.35: *Calculated theoretical diffusion coefficient of various species in 0.1 M KCl plotted against the Y parameter. Results for cryogels in the top row and results for chemically crosslinked hydrogels on the bottom.*

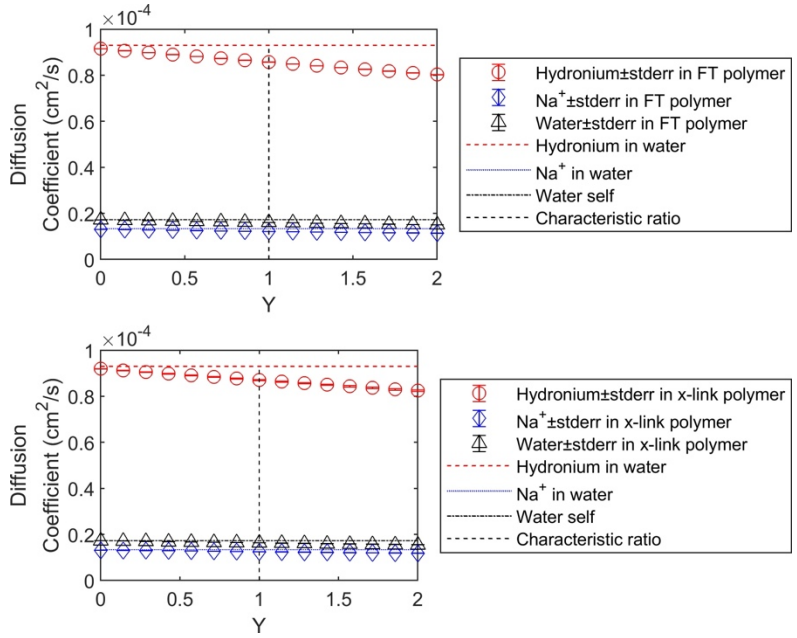

Figure A.36: *Calculated theoretical diffusion coefficients of various species in 0.1 M KCl plotted against the Y parameter. Same values as in* ***Figure A.35****, but collected into one graph per crosslinking method for scale reference.*

The diffusion coefficients appear to be somewhat sensitive (±Δ7% for cryogels, ±Δ5% for chemically crosslinked hydrogels) to changes in the Y parameter over the ranges evaluated.

Changing Flory characteristic ratio C_n

As before, we'll fix Y parameter at 1 for iterating the Flory characteristic ratio between 0.5 and 2 times thecurrent value.

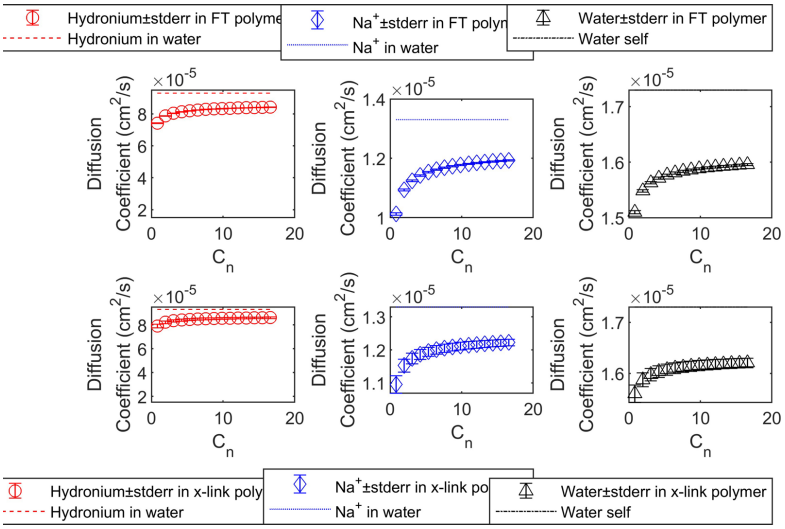

Figure A.37: *Calculated theoretical diffusion coefficient of various species in 0.1 M KCl plotted against the Flory characteristic ratio. Results for cryogels in the top row and results for chemically crosslinked hydrogels on the bottom.*

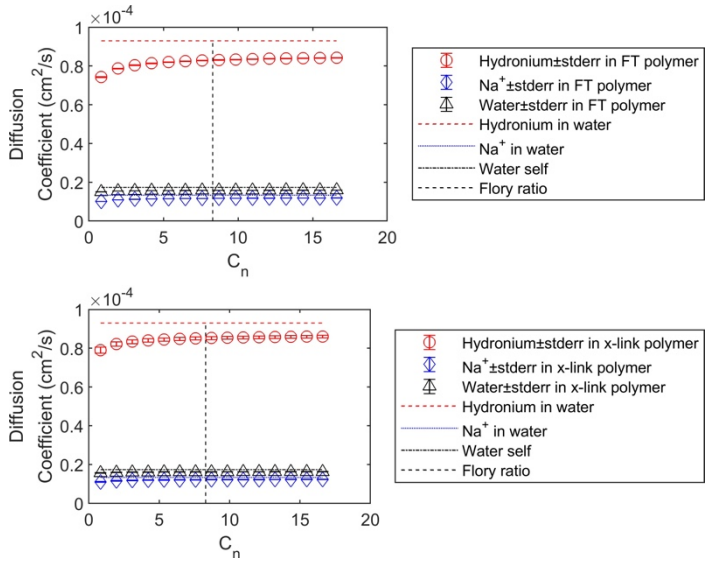

Figure A.38: *Calculated theoretical diffusion coefficients of various species in 0.1 M KCl plotted against the Flory characteristic ratio. Same values as in* ***Figure A.37****, but collected into one graph per crosslinking method for scale reference.*

The diffusion coefficients appear to be somewhat sensitive (-Δ13% to -Δ1.8% for cryogels, -Δ9.3% to -Δ1.2% forchemically crosslinked hydrogels) to changes in C_n over the ranges evaluated and are larger and more consistently negative than for the same conditions at 0M KCl.

Changing Flory interaction parameter $\chi_{\alpha,\beta}$

As before, we'll iterate the Flory interaction parameter between 0 and 0.523 (the instability point).

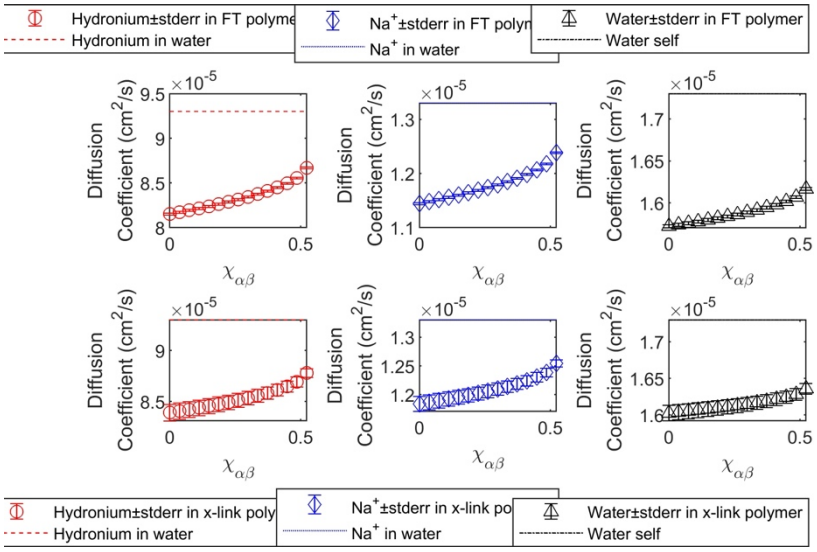

Figure A.39: *Calculated theoretical diffusion coefficient of various species in 0.1 M KCl plotted against the Flory interaction parameter. Results for cryogels in the top row and results for chemically crosslinked hydrogels on the bottom.*

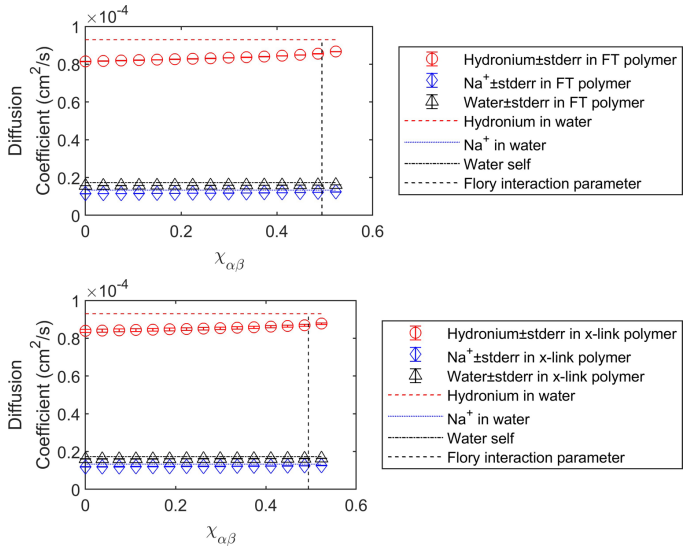

Figure A.40: *Calculated theoretical diffusion coefficients of various species in 0.1 M KCl plotted against the Flory interaction parameter. Same values as in* ***Figure A.39****, but collected into one graph per crosslinking method for scale reference.*

Diffusion coefficient appears to be somewhat sensitive (-Δ4.9% to +Δ1.1% for cryogels, -Δ4.4% to +Δ0.9% for chemically crosslinked hydrogels) to changes in $\chi_{\alpha,\beta}$ over the ranges evaluated and is about the same for the same conditions at 0M KCl.

Changing specific volume of polymer repeating unit $\bar{\nu}$

We'll iterate the specific volume of the polymer repeating unit between 0 and 10 times the current value.

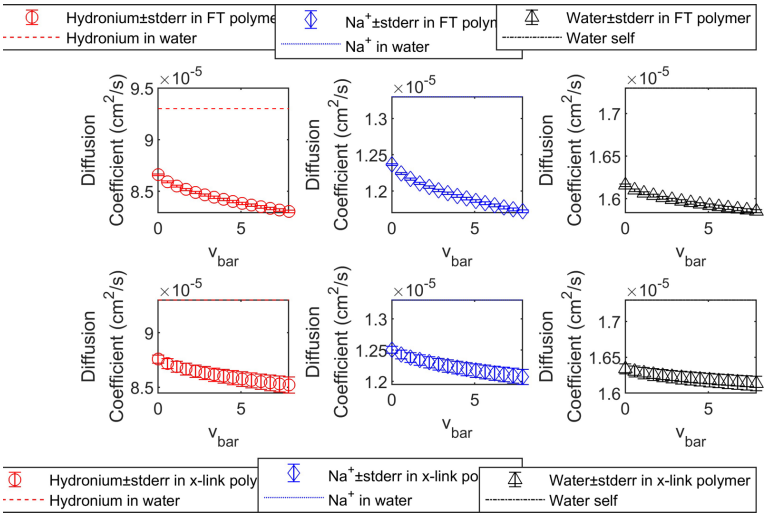

Figure A.42: *Calculated theoretical diffusion coefficient of various species in 0.1 M KCl plotted against the specific volume of the polymer repeating unit. Results for cryogels in the top row and results for chemically crosslinked hydrogels on the bottom.*

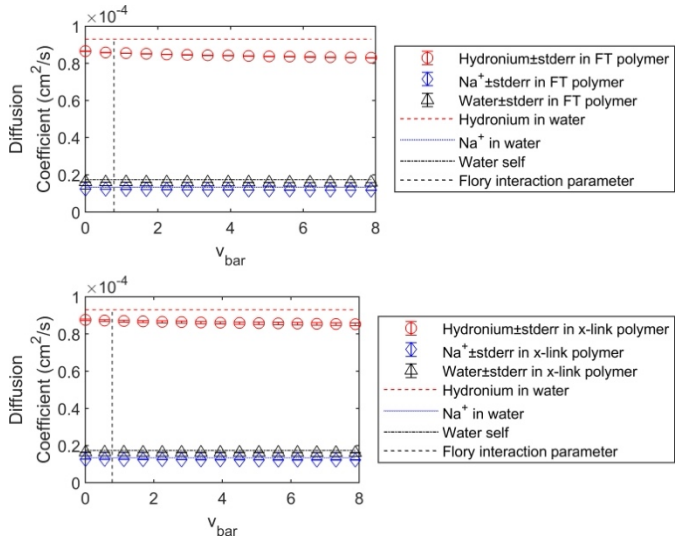

Figure A.41*: Calculated theoretical diffusion coefficients of various species in 0.1 M KCl plotted against the specific volume of the polymer repeating unit. Same values as in* ***Figure A.42****, but collected into one graph per crosslinking method for scale reference.*

The diffusion coefficients appear to be somewhat sensitive (-Δ3.1% to +Δ1.0% for cryogels, -Δ2.1% to +Δ0.6% for chemically crosslinked hydrogels) to changes in $\bar{\nu}$ over the ranges evaluated and are about the same for the same conditions at 0M KCl.

Changing Stokes hydrodynamic radius *r*

As before we'll chose a range of values from 0.1 to 8 Angstrom for the Stokes hydrodynamic radius.

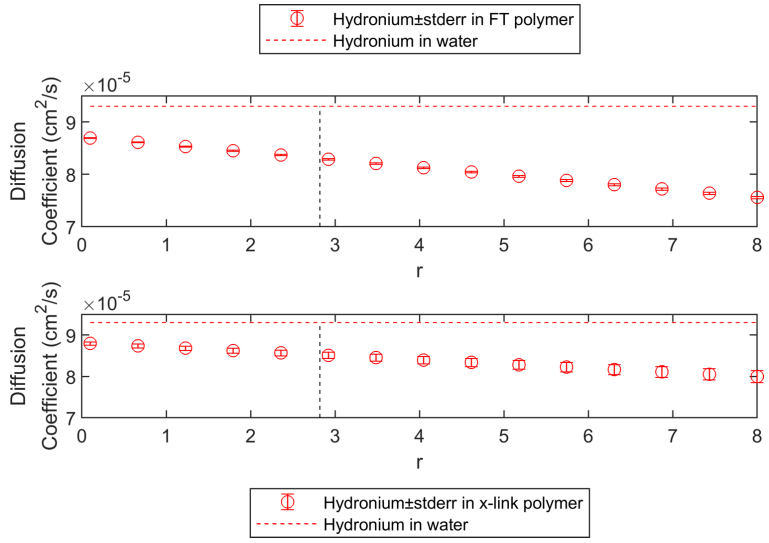

Figure A.43: *Calculated theoretical diffusion coefficient of hydronium in 0.1 M KCl plotted against the Stokes hydrodynamic radius. Results for cryogels in the top row and results for chemically crosslinked hydrogels on the bottom.*

Neglecting $\frac{r}{\xi}$ completely gives:

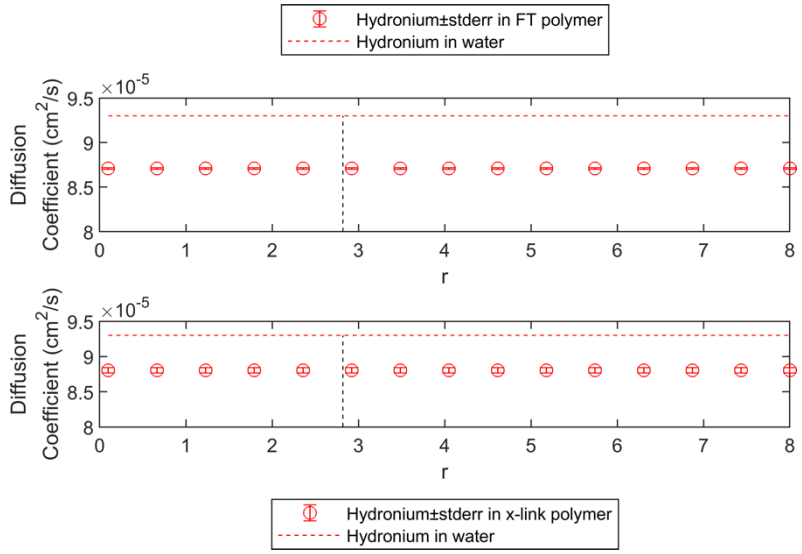

Figure A.44*: Calculated theoretical diffusion coefficients of hydronium in 0.1 M KCl plotted against the Stokes hydrodynamic radius.* $\frac{r}{\xi}$ *was set to zero.*

The diffusion coefficients appear to be somewhat sensitive (-Δ11.8% to +Δ1.4% for cryogels, -Δ8.1% to +Δ1.0%for chemically crosslinked hydrogels) to changes in *r* over the ranges evaluated and are about the same for the same conditions at 0M KCl.

Final summary of sensitivity analysis for 0.1 M KCl

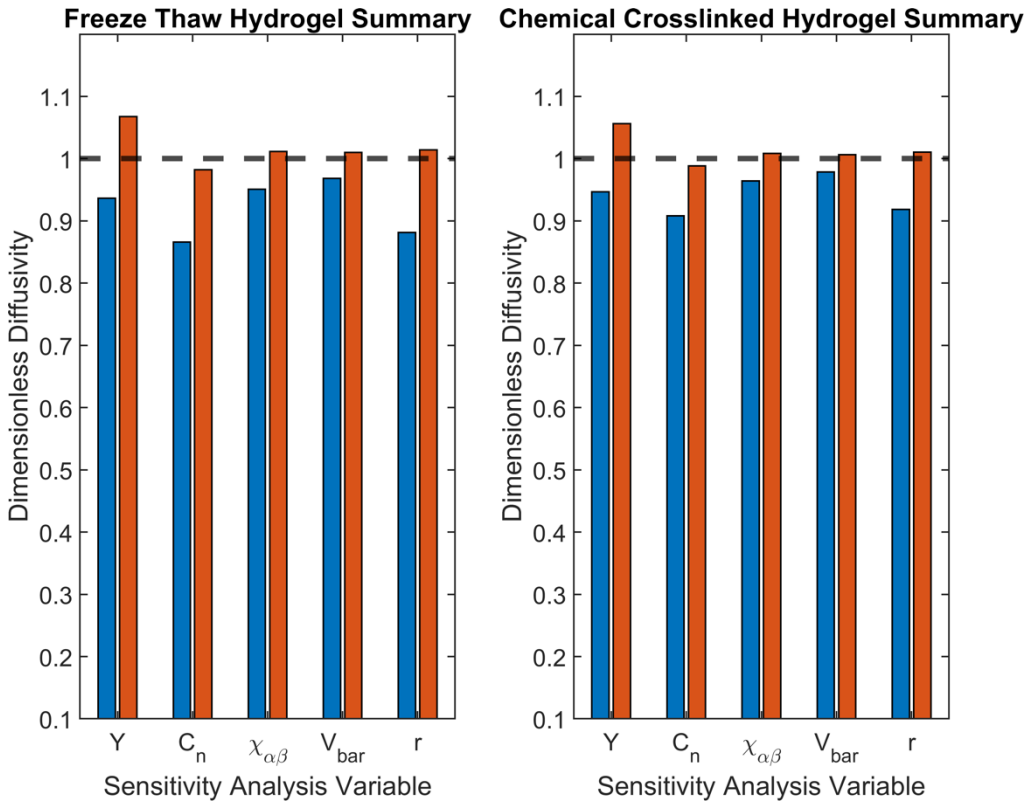

Figure A.45: *Summary of the sensitivity analysis for cryogels and chemically crosslinked hydrogels in 0.1 M KCl. The red bars indicate the maximum dimensionless diffusivity calculated per parameter over the values tested. The blue bars indicated the minimum dimensionless diffusivity calculated. Values closer to 1 are closer to the original prediction.*

Rankings were a little different with 0.1M KCl compared to 0M KCl. The magnitude of model changes for eachparameter are in the order C_n ~ r > Y > $\chi_{\alpha,\beta}$ ~ $\bar{\nu}$ and is not symmetric in both directions.

Sensitivity Analysis for 1 M KCl

The measured hydronium diffusivity in 10% PVA cryogels was $2.55\text{x}10^{-5}\text{cm}^2/\text{s}$ and for chemically crosslinked hydrogels was $3.16\text{x}10^{-5}\text{cm}^2/\text{s}$. As before for both 0 and 0.1M KCl, the model overpredicted diffusion coefficients.

Changing Y parameter

For Y between 0 and 2.

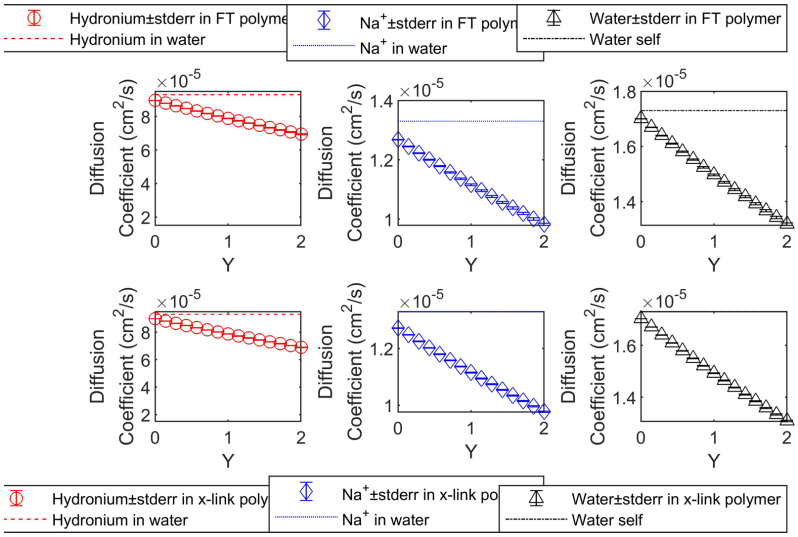

Figure A.46: *Calculated theoretical diffusion coefficient of various species in 1 M KCl plotted against the Y parameter. Results for cryogels in the top row and results for chemically crosslinked hydrogels on the bottom.*

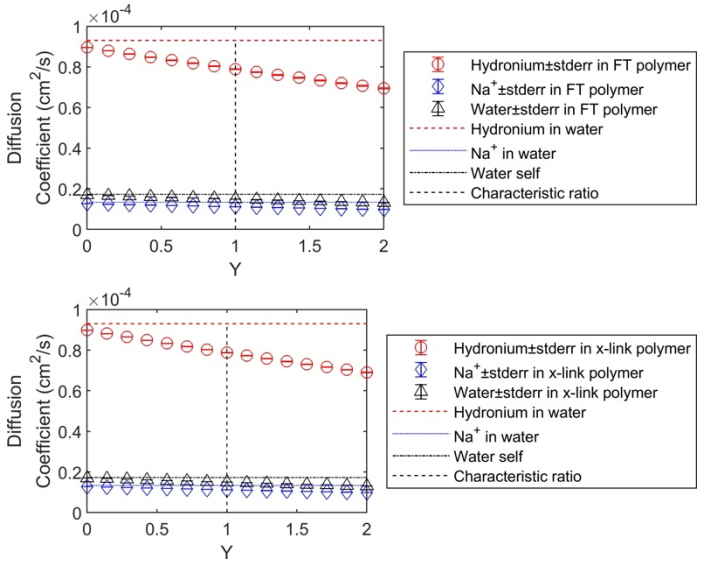

Figure A.47: *Calculated theoretical diffusion coefficients of various species in 1 M KCl plotted against the Y parameter. Same values as in* ***Figure A.46****, but collected into one graph per crosslinking method for scale reference.*

Diffusion coefficient appears to be sensitive (-Δ11.9% to +Δ13.5% for cryogels, -Δ12.3% to +Δ14.1% for chemically crosslinked hydrogels) to changes in Y parameter over the ranges evaluated.

Changing Flory characteristic ratio *Cn*

As before, we'll fix Y parameter at 1 for iterating the Flory characteristic ratio between 0.5 and 2 times thecurrent value.

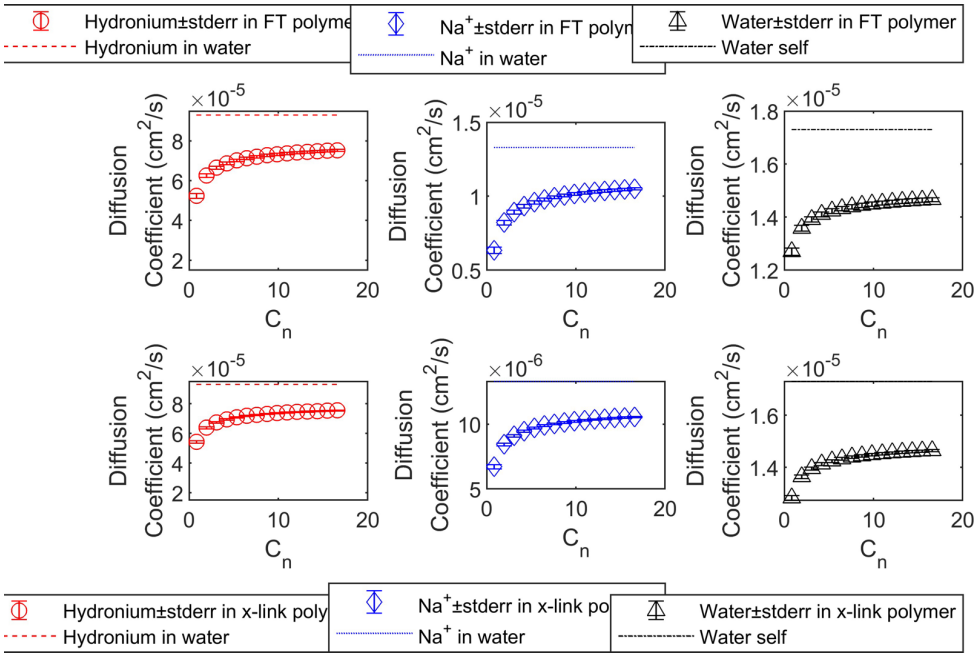

Figure A.48: *Calculated theoretical diffusion coefficient of various species in 1 M KCl plotted against the Flory characteristic ratio. Results for cryogels in the top row and results for chemically crosslinked hydrogels on the bottom.*

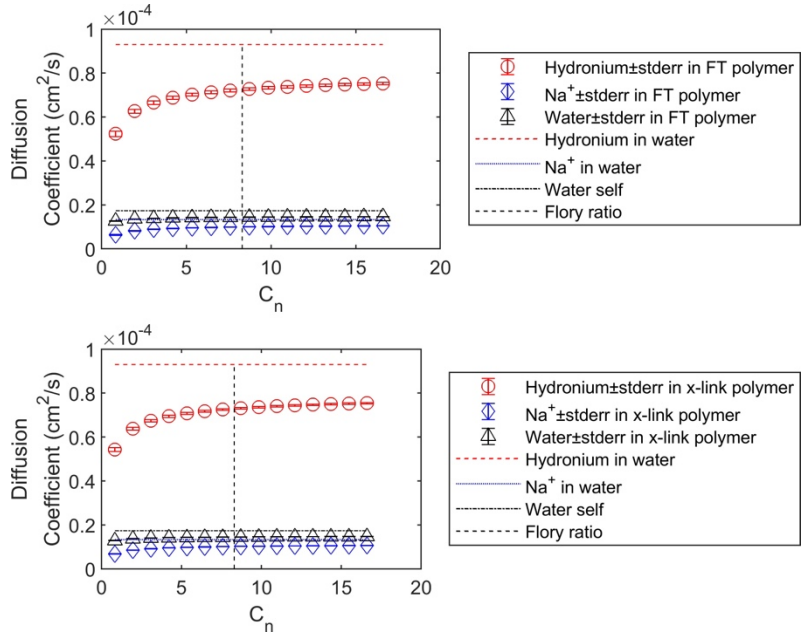

Figure A.49: *Calculated theoretical diffusion coefficients of various species in 1 M KCl plotted against the Flory characteristic ratio. Same values as in* ***Figure A.48****, but collected into one graph per crosslinking method for scale reference.*

Diffusion coefficient appears to be sensitive (-Δ36.6% to -Δ4.6% for cryogels, -Δ31.1% to -Δ4.4% for chemically crosslinked hydrogels) to changes in C_n over the ranges evaluated.

Changing Flory interaction parameter $\chi_{\alpha,\beta}$

As before, we'll iterate the Flory interaction parameter between 0 and 0.523 (the instability point).

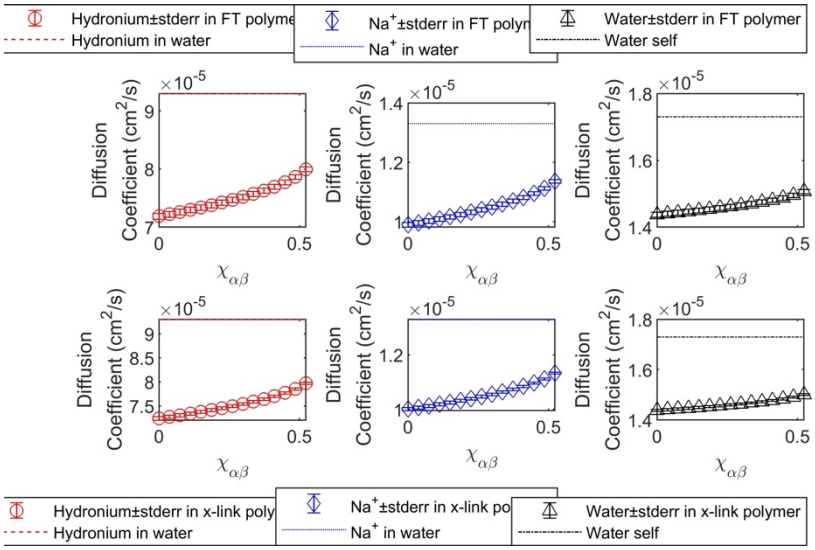

Figure A.50: *Calculated theoretical diffusion coefficient of various species in 1 M KCl plotted against the Flory interaction parameter. Results for cryogels in the top row and results for chemically crosslinked hydrogels on the bottom.*

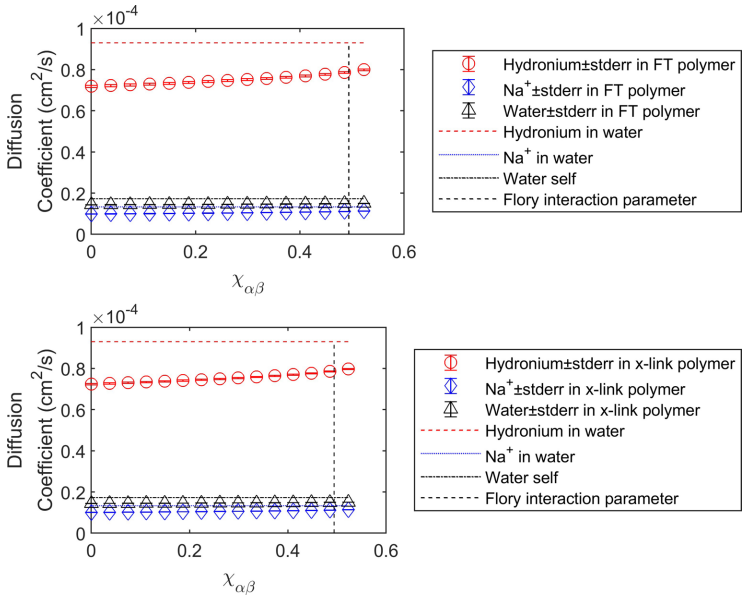

Figure A.51: *Calculated theoretical diffusion coefficients of various species in 1 M KCl plotted against the Flory interaction parameter. Same values as in* ***Figure A.50****, but collected into one graph per crosslinking method for scale reference.*

Diffusion coefficient appears to be sensitive (-Δ8.9% to +Δ1.4% for cryogels, -Δ8.0% to +Δ1.2% for chemically crosslinked hydrogels) to changes in $\chi_{\alpha,\beta}$ over the ranges evaluated.

Changing specific volume of polymer repeating unit $\bar{\nu}$

We'll iterate the specific volume of the polymer repeating unit between 0 and 10 times the current value.

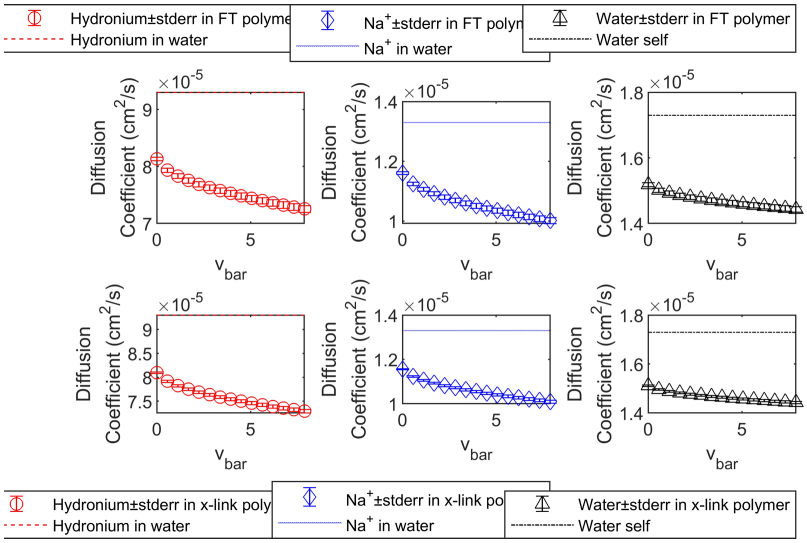

Figure A.52: *Calculated theoretical diffusion coefficient of various species in 1 M KCl plotted against the specific volume of the polymer repeating unit. Results for cryogels in the top row and results for chemically crosslinked hydrogels on the bottom.*

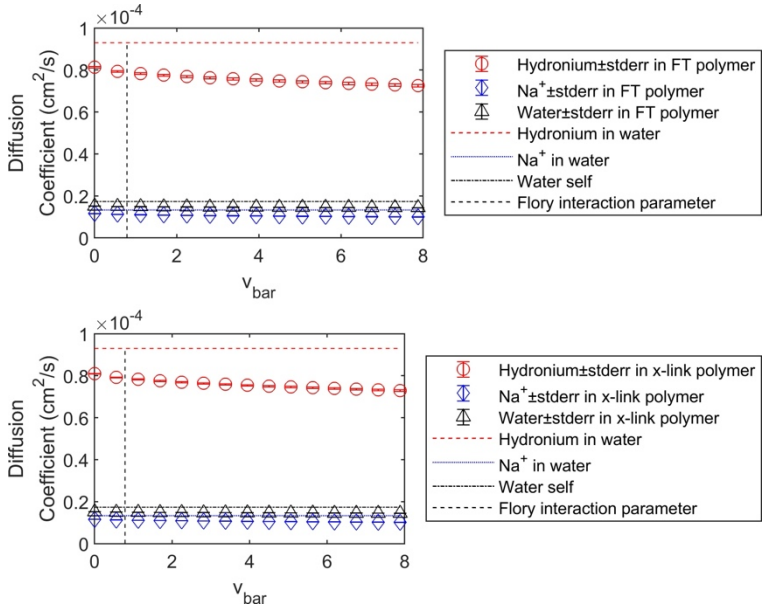

Figure A.53: *Calculated theoretical diffusion coefficients of various species in 1 M KCl plotted against the specific volume of the polymer repeating unit. Same values as in* ***Figure A.52****, but collected into one graph per crosslinking method for scale reference.*

The diffusion coefficients appear to be sensitive (-Δ8.0% to +Δ3.1% for cryogels, -Δ7.4% to +Δ2.8% for chemically crosslinked hydrogels) to changes in $\bar{\nu}$ over the ranges evaluated.

Changing Stokes hydrodynamic radius *r*

r values vary from 0.1 to 8 Angstrom.

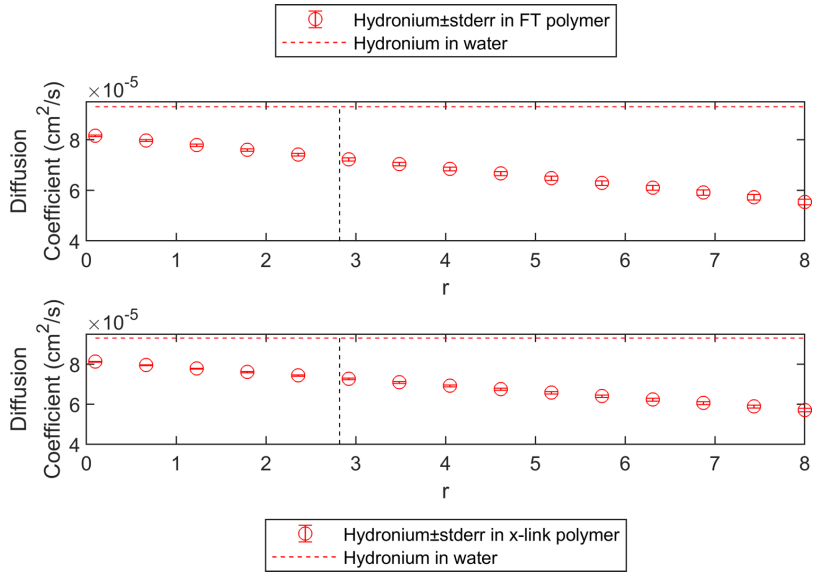

Figure A.54: *Calculated theoretical diffusion coefficient of hydronium in 1 M KCl plotted against the Stokes hydrodynamic radius. Results for cryogels in the top row and results for chemically crosslinked hydrogels on the bottom.*

Neglecting $\frac{r}{\xi}$ completely yields:

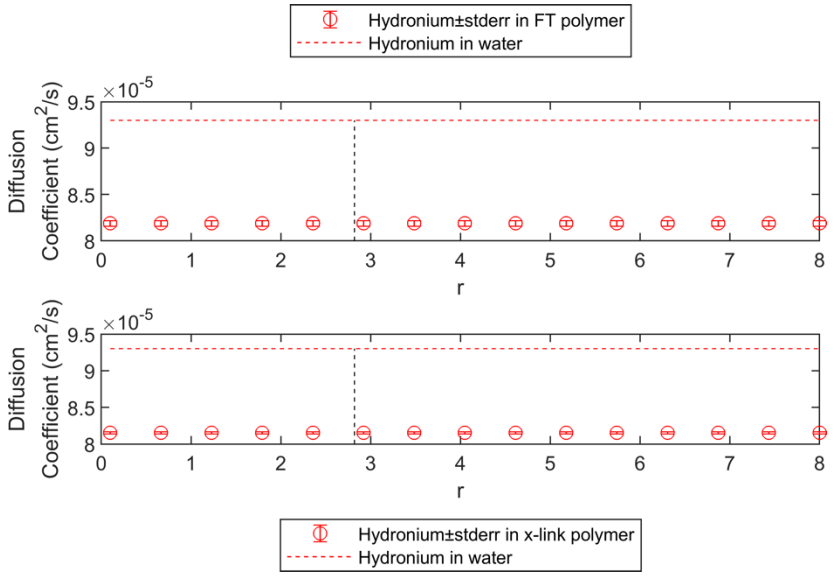

Figure A.55: *Calculated theoretical diffusion coefficients of hydronium in 1 M KCl plotted against the Stokes hydrodynamic radius.* $\frac{r}{\xi}$ *was set to zero.*

The diffusion coefficient appears to be very sensitive (-Δ29.8% to +Δ3.3% for cryogels, -Δ27.5% to +Δ3.1% forchemically crosslinked hydrogels) to changes in r over the ranges evaluated.

Final summary of sensitivity analysis for 1 M KCl

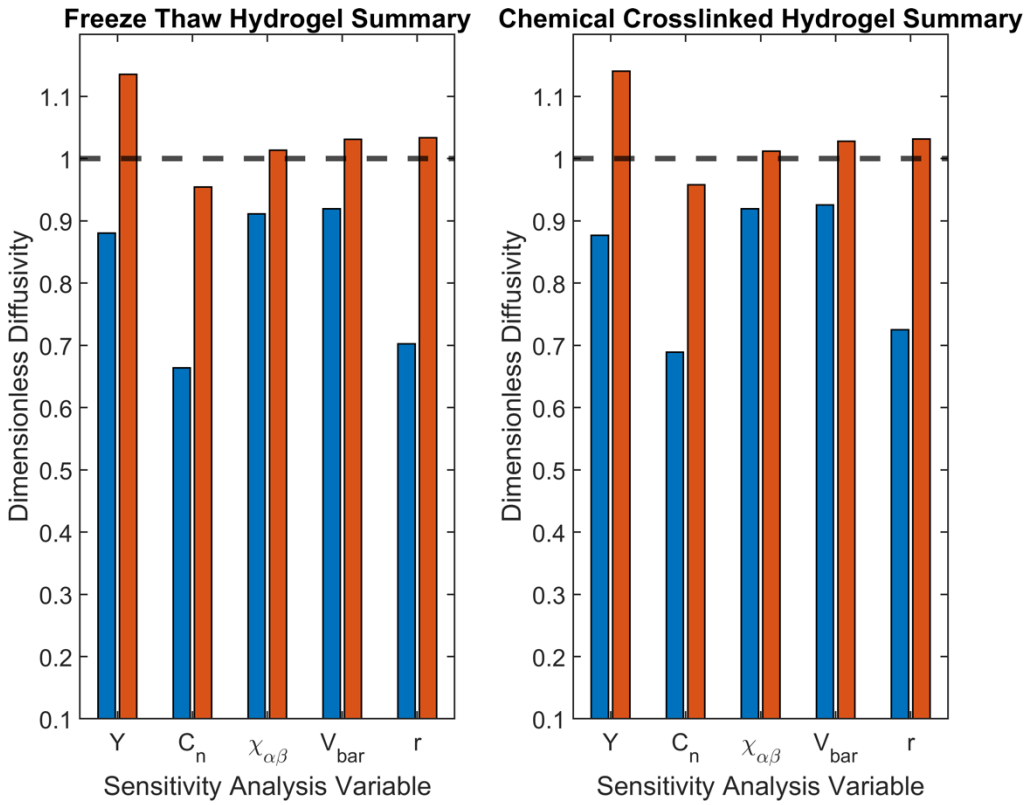

Figure A.56: *Summary of the sensitivity analysis for cryogels and chemically crosslinked hydrogels in 1 M KCl. The red bars indicate the maximum dimensionless diffusivity calculated per parameter over the values tested. The blue bars indicated the minimum dimensionless diffusivity calculated. Values closer to 1 are closer to the original prediction.*

Ranking magnitudes are a little different with 1M KCl compared to 0.1M KCl, but are in the same order. The magnitude of model changes for each parameter are in the order Cn > r > Y > $\chi_{\alpha,\beta} \sim \bar{\nu}$ and is not symmetric in both directions.

Reference

(1) Meadows, D. L.; Peppas, N. A. Solute Diffusion in Swollen Membranes Iii. Non-Equilibrium Thermodynamic Aspects of Solute Diffusion in Polymer Network Membranes. *null* **1984**, *31* (1–6), 101–119. https://doi.org/10.1080/00986448408911144.

(2) Peppas, N. A.; Merrill, E. W. Poly(Vinyl Alcohol) Hydrogels: Reinforcement of Radiation-Crosslinked Networks by Crystallization. *Journal of Polymer Science: Polymer Chemistry Edition* **1976**, *14* (2), 441–457. https://doi.org/10.1002/pol.1976.170140215.
(3) Thermo Fischer Scientific. Personal Correspondence, 2020.
(4) Shibayama, M.; Sato, M.; Kimura, Y.; Fujiwara, H.; Nomura, S. 11B n.m.r. Study on the Reaction of Poly(Vinyl Alcohol) with Boric Acid. *Polymer* **1988**, *29* (2), 336–340. https://doi.org/10.1016/0032-3861(88)90343-6.
(5) Sinton, S. W. Complexation Chemistry of Sodium Borate with Poly(Vinyl Alcohol) and Small Diols: A Boron-11 NMR Study. *Macromolecules* **1987**, *20* (10), 2430–2441. https://doi.org/10.1021/ma00176a018.
(6) Wang, P.-H.; Chang, Y.-R.; Lee, D.-J. Shape Stable Poly(Vinyl Alcohol) Hydrogels with Immobilized Activated Sludge at Repeated Dry-Rewet Cycles. *Bioresource Technology* **2019**, *289*, 121662. https://doi.org/10.1016/j.biortech.2019.121662.
(7) Itou, T.; Kitai, H.; Shimazu, A.; Miyazaki, T.; Tashiro, K. Clarification of Cross-Linkage Structure in Boric Acid Doped Poly(Vinyl Alcohol) and Its Model Compound As Studied by an Organized Combination of X-Ray Single-Crystal Structure Analysis, Raman Spectroscopy, and Density Functional Theoretical Calculation. *J. Phys. Chem. B* **2014**, *118* (22), 6032–6037. https://doi.org/10.1021/jp5026569.
(8) Lustig, S. R.; Peppas, N. A. Solute Diffusion in Swollen Membranes. IX. Scaling Laws for Solute Diffusion in Gels. *J. Appl. Polym. Sci.* **1988**, *36* (4), 735–747. https://doi.org/10.1002/app.1988.070360401.
(9) Gudeman, L. F.; Peppas, N. A. Preparation and Characterization of PH-Sensitive, Interpenetrating Networks of Poly(Vinyl Alcohol) and Poly(Acrylic Acid). *J. Appl. Polym. Sci.* **1995**, *55* (6), 919–928. https://doi.org/10.1002/app.1995.070550610.
(10) Nightingale, E. R. Phenomenological Theory of Ion Solvation. Effective Radii of Hydrated Ions. *J. Phys. Chem.* **1959**, *63* (9), 1381–1387. https://doi.org/10.1021/j150579a011.
(11) Masaro, L.; Ousalem, M.; Baille, W. E.; Lessard, D.; Zhu, X. X. Self-Diffusion Studies of Water and Poly(Ethylene Glycol) in Solutions and Gels of Selected Hydrophilic Polymers. *Macromolecules* **1999**, *32* (13), 4375–4382. https://doi.org/10.1021/ma990211s.
(12) Wraight, C. A. Chance and Design—Proton Transfer in Water, Channels and Bioenergetic Proteins. *Biochim. Biophys. Acta BBA - Bioenerg.* **2006**, *1757* (8), 886–912. https://doi.org/10.1016/j.bbabio.2006.06.017.
(13) Masaro, L.; Zhu, X. X. Physical Models of Diffusion for Polymer Solutions, Gels and Solids. *Prog. Polym. Sci.* **1999**, *24* (5), 731–775. https://doi.org/10.1016/S0079-6700(99)00016-7.
(14) Kadhim, M. J.; Gamaj, M. I. Estimation of the Diffusion Coefficient and Hydrodynamic Radius (Stokes Radius) for Inorganic Ions in Solution Depending on Molar Conductivity as Electro-Analytical Technique-A Review. *J. Chem. Rev.* **2020**, *2* (3), 182–188. https://doi.org/10.22034/jcr.2020.106910.

Appendix B - CAH Diffusion Data and Statistics

Table B.1: *Average effective diffusivity of each CAH at all ionic strengths tested. Error represents a 95% confidence interval.*

Species	Ionic Strength (M)	Diffusion Coefficient (cm^2/s)	+/- Error	Number of Replicates
TCE	0	1.03×10^{-5}	2.36×10^{-6}	3
TCE	0.001	2.90×10^{-5}	1.50×10^{-5}	3
TCE	0.01	3.35×10^{-5}	1.18×10^{-5}	3
DCE	0	3.86×10^{-5}	1.55×10^{-5}	4
DCE	0.001	5.15×10^{-5}	2.85×10^{-5}	3
DCE	0.01	1.14×10^{-4}	7.22×10^{-5}	3
VC	0	4.47×10^{-5}	2.42×10^{-5}	4
VC	0.001	5.59×10^{-5}	1.94×10^{-5}	3
VC	0.01	9.25×10^{-5}	6.82×10^{-5}	3

Table B.2: *Type II two-way ANOVA table of the data presented in* ***Table B.1****.*

	Sum of Squares	DF	F-value	p-value
CAH species	107.989	2	22.9216	< 0.001
Ionic Strength	125.181	2	26.5707	< 0.001
Interaction	32.166	4	3.4137	0.02778
Residuals	47.113	20		

Table B.3: *Two sample t-tests using were calculated for means comparisons and p-values were adjusted using Holm's correction in R.*

Data Set 1	Data Set 2	p-value
TCE (0 M)	TCE (0.01 M)	0.009
DCE (0 M)	DCE (0.01 M)	0.029
VC (0 M)	VC (0.01 M)	0.124
TCE (0 M)	DCE (0 M)	0.029
TCE (0.01 M)	DCE (0.01 M)	0.045
DCE (0 M)	VC (0 M)	1.00
DCE (0.001 M)	VC (0.001 M)	1.00
DCE (0.01 M)	VC (0.01 M)	1.00

Appendix C - Reaction-Diffusion Model and Cluster Slurm file

C.1 Reaction-Diffusion Model

```
% Carson Silsby 12/17/21
% This is the Current Running file
% Modified version of 'dmacBeadDegAqProEDIT5'
% Modifed from original work by Jonny Counts
% Set to run on uidaho supercomputer as a function
% It will be called with a series of bead radii and cell concentrations

% The function allows input of a bead radius (dm) and runs 2000 space
% steps (or whatever m is set as) and 160000000 time steps (or whatever
% n is set as) for a bead of radius R (as input by user).
% The cell concentration (cells/mL) is input by the user (unit*10^pwr).
% Function outputs a *.mat and *.fig file of all time and spacial data

% TCE Parameters from Haest et al.
function CAHcode_V11_working(R,unit,pwr,scales)
%% Converts character arrays from command line to numbers
R = str2double(R);
unit = str2double(unit);
pwr = str2double(pwr);
scales = str2double(scales);
%% Defining adjustable parameters
% Diffusivity in Hydrogel
    % Contaminant diffusivity in DI water
DeTCE = scales*(11E-6)*3600*24*.01;   % Convert from cm^2/s to dm^2/day
% 0.01 M -> 33.5E-6 cm^2/s % Measured De at 0.01 M KCl
DeDCE = scales*(6.90E-6)*3600*24*.01; % Convert from cm^2/s to dm^2/day
% 0.01 M -> 136E-6 cm^2/s % Scaled based on TCE increase from 0 - 0.01 M
DeVC = scales*(4.04E-6)*3600*24*.01;  % Convert from cm^2/s to dm^2/day
% 0.01 M -> 145E-6 cm^2/s % Scaled based on TCE increase from 0 - 0.01 M
    % Proton diffusivity in 0.01M KCl (near grounwater salinity)
DePro = (2.78E-5)*3600*24*.01;        % Convert from cm^2/s to dm^2/day
% Aqueous diffusivity
DeTCEa=9.971e-6*3600*24*.01; % DeTCE from Wilke-Chang correlation at 25∞C
DeDCEa=1.125e-5*3600*24*.01; % DeDCE;%1.125x10^-5 cm2/s
DeVCa=1.309e-5*3600*24*.01;  % DeVC;
DeProa=9.31e-5*3600*24*.01;  % from Agmon(1995) - "The Grotthus Mechanism"

% Solubility of TCE in water is 1.1g/L, c-DCE in water is 3.5 g/L, and VC
% in water is 2.7 g/L (might need these in calculations, various online
% sources)

%% Defining constants
% Step counts (vary by input arguments)
m = 2000;               % Number of spatial steps
nodes = m+1;            % Number of nodes where concentration is calculated
stability = 0.49;       % Stability criteria
n = 40*m^2;             % Number of time steps to be iterated
dr = R/m;               % Radius step size (dm)

% Physical parameters
cellsmL = 10^pwr;          % Sets order of magnitude for cell count
```

```
Xm = cellsmL*unit*1000;     % (cells/L)
Co = 1*(10^-7)*1000;        % Concentration (mM) of protons in bulk solution

% Calulating stability for each diffusing species to determine step size
dtTCE = (stability*dr*dr)/DeTCE;   % Stability criteria set for TCE
dtDCE = (stability*dr*dr)/DeDCE;   % Stability criteria set for DCE
dtVC = (stability*dr*dr)/DeVC;     % Stability criteria set for VC
dtPro = (stability*dr*dr)/DePro;   % Stability criteria set for Pro
dtvec=[dtTCE dtDCE dtVC dtPro];    % Vector of calculated dt
dt = min(dtvec);                   % Assigns dt value to minimum of set
                                   % (Time step in days)

% Preallocating matrix for radii
rr=zeros(nodes,1);
% Calculating radii to be evaluated and setting up matrix
for k=1:nodes
    rr(k)=(k-1)*dr;
end

% TCE Parameters
    % Constants from McCarty et al. (1998) -- 'Full-Scale Evaluation of
    % In Situ Cometabolic Degredation of Trichloroethylene in Groundwater
    % Through Toluene Injection'
ktce = 1.56E-10*Xm*dt;      % kmax_tce (mM/cell*day) *Xm * dt
Kstce = 4.19E-3;            % Ks_tce (mM)
Kitce = 37E-2;              % KCI_tce (mM)
EC50tce = 1.01;             % EC_50,tce (mM)
btce = 8.83;                % b_tce (exponential constant for inhibition)
Tcesat = 0.011415;          % Concentration of TCE (mM) in the aquifer
                            % equal to 1500 ppb TCE
tcePwr = btce*log(10);      % Power to raise C_tce to for rate calculation
EC50TCEpwr=1/EC50tce^tcePwr;

% DCE Parameters
kdce = 2.08E-11*Xm*dt;        % kmax,dce (mM/cell*day) *Xm * dt
Ksdce = 99.7E-3;              % Ks_dce (mM)
Kidce = 4.79E-3;              % KCI_dce (mM)
EC50dce = 1.27;               % EC_50,dce (mM)
bdce = 10.4;                  % b_dce (exponential constant for inhibition)
dcePwr=bdce*log(10);          % Power to raise Ctce to for rate calculation
EC50DCEpwr=1/EC50dce^dcePwr;  %
KDT=Ksdce/Kitce;              % Define this ratio to eliminate a divide

% VC Parameters
    % Some parameters are from Heurst et al. Some are repeated values from
    % DCE. There is no EC50 or bvc term for VC degradation, since no
    % inhibition was observed at high concentrations by Haest et al.
    % (personal communication).
kvc = 5E-13*Xm*dt;     % kmax_dce (mM/cell*day)
Ksvc = 2.6E-3;         % Ks_vc (mM)
KVD=Ksvc/Kidce;        % Defined for faster computation
KVT=Ksvc/Kitce;        % Def...

% pH inhibition constants - Lacroiz et al. 2014
pH0 = 7.0;        % initial pH
pHopt_T = 6.99;   % optimal pH for dehalogentation
```

```
pHopt_D = 6.60;
pHopt_V = 6.50;
sig_T = 1.10;     % empirical parameter (sigma)
sig_D = 0.97;
sig_V = 0.67;
N_T = 2.09;       % empirical parameter (N)
N_D = 5.28;
N_V = 2.75;
% pH inhibition: r = rmax*f(pH)

%% Build matrices for differential coefficients (finite diff. method)
% Preallocating space
dcm = zeros(nodes,1); % Derivative coefficients at r - del r
dcr = zeros(nodes,1); % Derivative coefficients at r
dcp = zeros(nodes,1); % Derivative coefficients at r + del r

% Cacluate derivative coefficients for R = k
for k = 2:nodes-1
    rk = (k-1)*dr;
    dcm(k) = dt*(1/dr^2 - 1/(rk*dr));
    dcr(k) = -2*dt/dr^2;
    dcp(k) = dt*(1/dr^2 + 1/(rk*dr));
end
% Calculate derivative coefficients at R = 0
% At the center node there is no dcm, just dcr and dcp
dcr(1) = -2*dt/dr^2;
dcp(1) = 2*dt/dr^2;

% Calculate derivative coefficients at r = R
    % At r = R TCE concentration is fixed at TCE saturation
    % The boundary node for DCE, VC, and Pro is calculated at all t:
dcmBdce = 2*dt*DeDCE/dr^2;
dcrBdce = -2*dt*(DeDCEa/(R*dr) + DeDCE/dr^2 +DeDCEa/R^2);
dcmBvc = 2*dt*DeVC/dr^2;
dcrBvc = -2*dt*(DeVCa/(R*dr) + DeVC/dr^2 + DeVCa/R^2);
dcmBpro = 2*dt*DePro/dr^2;
dcrBpro = -2*dt*(DeProa/(R*dr) + DePro/dr^2 + DeProa/R^2);

% Concentration of DCE and VC is zero in bulk (similar to h(T-Tinf) in heat
% transfer

%% Define vectors for concentrations
% Preallocating space for CAH concentrations
CAH = [zeros(nodes,3),ones(nodes,1)*Co]; % [TCE,DCE,VC,Pro]
% The T,D,V,P matricies are calculated from the TCE,DCE,VC,Pro matricies at
% each time step.  Then the T,D,V,P matricies are copied into the
% TCE,DCE,VC,Pro matricies to start another time step.
delCAH = CAH; % [T,D,V,P]

CAH(nodes,1) = Tcesat; % [TCE] = T_sat at r = R at all time t

% Define arrays for recording the time history at nr locations
rt = [0.1;0.5;0.75;0.9;1.0];% fractional time recording positions 0 to 1=R
nr = length(rt); % number of radial locations to be recorded
% nr must equal five for current version
```

```
mtr = zeros(nr,1); % node numbers for recording data
for k = 1:nr
    mtr(k) = floor(rt(k)*m);
end
mtr(nr) = nodes; % Sets the final value in mtr to nodes
mtr(1) = 1; % Sets the first value in mtr to 1
ntr = n; % Number of time points to record
nStp = 1; % Set spacial step counter to 1
if ntr > 2000
    nStp = ceil(n/1000.0);
    ntr = floor(n/nStp);
end
tt = zeros(ntr,1); % Allocates space for time array
% Calculates exact tt values to be evaluated.
for k = 1:ntr
    tt(k) = (k-1)*dt*nStp;
end

% Creates array of zeros of size [ntr x nr]
tTCE = zeros(ntr,nr);
tDCE = zeros(ntr,nr);
tVC = zeros(ntr,nr);
tPro = zeros(ntr,nr);
% Preallocate for an array to define whether at steady state or not
% (@ SS(i) = 1 if at steady state -> see for loop)
SS = zeros(5,4);
SS(5,1) = 1; % Set SS to 1 at R = 1 for TCE since C_TCE = T_sat is constant

%% Time loop
% 1) Calculates the rate of each species based on concentration at each
%    spacial point.
% 2) Use rates and derivative coefficients to calculate the new
%    concentrations.
% 3) Add delCAH(T,D,V,P) to CAH(TCE,DCE,VC,Pro) for new CAH values
% 4) Save selected points in the time history array.
% 5) Check if steady state has been reached
tCount = 0;    % Seting intial time to 0
for mt = 1:n
    %% 1.1) Evaluate differential change in central knot
        % rate * dt for each species
        rateTCE_max = ktce*CAH(1,1) /...
                      ((Kstce + CAH(1,1)) * ...
                      (1 + EC50TCEpwr*CAH(1,1)^tcePwr));
        rateTCE = rateTCE_max *...
                  exp(-abs(pHopt_T - (-log10(CAH(1,4)/1000)))^N_T/sig_T^2);
        rateDCE_max = kdce*CAH(1,2) /...
                      ((Ksdce + KDT*CAH(1,1) + ...
                        CAH(1,2))*(1 + EC50DCEpwr*CAH(1,2)^dcePwr));
        rateDCE = rateDCE_max *...
                  exp(-abs(pHopt_D - (-log10(CAH(1,4)/1000)))^N_D/sig_D^2);
        rateVC_max = kvc*CAH(1,3) /...
                     (Ksvc + KVD*CAH(1,2) + KVT*CAH(1,1) + CAH(1,3));
        rateVC = rateVC_max *...
                 exp(-abs(pHopt_V - (-log10(CAH(1,4)/1000)))^N_V/sig_V^2);
        % Rate of proton generation for each species equal to the sum of
        % the rate of degredation for each species since protons are
```

```
    % generated at each reaction step with a 1:1 molar ratio.
    ratePro = rateTCE + rateDCE + rateVC;

    % 2.1) Calculating differential change for each species using the
    %      forward difference method and diffusion coefficients.
    delCAH(1,1) = DeTCE * (dcr(1)*CAH(1,1) + dcp(1)*CAH(2,1)) -...
                  rateTCE;
    delCAH(1,2) = DeDCE * (dcr(1)*CAH(1,2) + dcp(1)*CAH(2,2)) +...
                  rateTCE - rateDCE;
    delCAH(1,3) = DeVC * (dcr(1)*CAH(1,3) + dcp(1)*CAH(2,3)) -...
                  rateVC + rateDCE;
    delCAH(1,4) = DePro * (dcr(1)*CAH(1,4) + dcp(1)*CAH(2,4)) +...
                  ratePro;

%% 1.2) Evaluate differential change in all interior knots
for k=2:nodes-1
    rateTCE_max = ktce*CAH(k,1) /...
                  ((Kstce + CAH(k,1)) * ...
                   (1 + EC50TCEpwr*CAH(k,1)^tcePwr));
    rateTCE = rateTCE_max *...
              exp(-abs(pHopt_T - (-log10(CAH(k,4)/1000)))^N_T/sig_T^2);

    rateDCE_max = kdce*CAH(k,2) /...
                  ((Ksdce + KDT*CAH(k,1) + CAH(k,2)) *...
                   (1 + EC50DCEpwr*CAH(k,2)^dcePwr));
    rateDCE = rateDCE_max *...
              exp(-abs(pHopt_D - (-log10(CAH(k,4)/1000)))^N_D/sig_D^2);

    rateVC_max = kvc*CAH(k,3) /...
                 (Ksvc + KVD*CAH(k,2) + KVT*CAH(k,1) + CAH(k,3));
    rateVC = rateVC_max *...
             exp(-abs(pHopt_V - (-log10(CAH(k,4)/1000)))^N_V/sig_V^2);

    ratePro = rateTCE + rateDCE + rateVC;

    % 2.2)
    delCAH(k,1) = DeTCE * (dcm(k)*CAH(k-1,1) + dcr(k)*CAH(k,1)+...
           dcp(k)*CAH(k+1,1)) - rateTCE;
    delCAH(k,2) = DeDCE * (dcm(k)*CAH(k-1,2) + dcr(k)*CAH(k,2)+...
           dcp(k)*CAH(k+1,2)) + rateTCE - rateDCE;
    delCAH(k,3) = DeVC * (dcm(k)*CAH(k-1,3) + dcr(k)*CAH(k,3) +...
           dcp(k)*CAH(k+1,3)) - rateVC + rateDCE;
    delCAH(k,4) = DePro * (dcm(k)*CAH(k-1,4) + dcr(k)*CAH(k,4) +...
           dcp(k)*CAH(k+1,4)) + ratePro;
end
%% 1.3) Evaluate differential change in outer boundry knot
    rateTCE_max = ktce*CAH(nodes,1) / ((Kstce + CAH(nodes,1)) *...
                                       (1 + EC50TCEpwr*CAH(nodes,1)...
                                        ^tcePwr));
    rateTCE = rateTCE_max *...
              exp(-abs(pHopt_T -...
                       (-log10(CAH(nodes,4)/1000)))^N_T/sig_T^2);

    rateDCE_max = kdce*CAH(nodes,2) / ((Ksdce + KDT*CAH(nodes,1) +...
                                        CAH(nodes,2)) *...
```

```
                                            (1 + EC50DCEpwr*CAH(nodes,2)...
                                             ^dcePwr));
    rateDCE = rateDCE_max *...
              exp(-abs(pHopt_D -...
                       (-log10(CAH(nodes,4)/1000)))^N_D/sig_D^2);

    rateVC_max = kvc*CAH(nodes,3) /(Ksvc+KVD*CAH(nodes,2) +...
                                    KVT*CAH(nodes,1) + CAH(nodes,3));
    rateVC = rateVC_max *...
             exp(-abs(pHopt_V -...
                      (-log10(CAH(nodes,4)/1000)))^N_V/sig_V^2);

    ratePro = rateTCE + rateDCE + rateVC;

    % 2.3)
    delCAH(nodes,2) = dcmBdce*CAH(nodes-1,2) + dcrBdce*CAH(nodes,2)...
                      + rateTCE - rateDCE;
    delCAH(nodes,3) = dcmBvc*CAH(nodes-1,3) + dcrBvc*CAH(nodes,3) -...
                      rateVC + rateDCE;
    delCAH(nodes,4) = dcmBpro*CAH(nodes-1,4) + dcrBpro*CAH(nodes,4)...
                      + ratePro + (dt*2*DeProa*Co*dr/R)*((1/(R*dr))...
                      + (1/(dr*dr)));

%% 3) Add differentials to old values
for k = 1:nodes
    CAH(k,:) = CAH(k,:) + delCAH(k,:);
end
%% Check if concentration value is less than zero
Tmin = min(CAH(:,1));
Dmin = min(CAH(:,2));
Vmin = min(CAH(:,3));
if   Tmin<0 || Dmin<0 || Vmin<0 % tests if the concentration is less
                                % than zero and if so, steps out of
                                % this for loop (resulting in TCE,
                                % DCE, and VC staying at its
                                % originally assigned value)
    return
end


if mod(mt,nStp)==0
    tCount=tCount+1;
 %% 4) Save time path points
    for k = 1:nr      % loop over selected points to save
        ri = mtr(k);  % radial index
        tTCE(tCount,k) = CAH(ri,1);
        tDCE(tCount,k) = CAH(ri,2);
        tVC(tCount,k) = CAH(ri,3);
        tPro(tCount,k) = -log10(CAH(ri,4)/1000);
    end
 %% 5) Determine if any CAH species is at steady state
    % Takes the derivative of CAHs using change variables T, D, V,
    % and Pro at each spacial point at time t
    dVCdt_1 = diff(nonzeros(tVC(:,1))) ./...
              diff(tt(1:length(nonzeros(tVC(:,1)))));
    dVCdt_2 = diff(nonzeros(tVC(:,2))) ./...
```

```
          diff(tt(1:length(nonzeros(tVC(:,2)))));
dVCdt_3 = diff(nonzeros(tVC(:,3))) ./...
          diff(tt(1:length(nonzeros(tVC(:,3)))));
dVCdt_4 = diff(nonzeros(tVC(:,4))) ./...
          diff(tt(1:length(nonzeros(tVC(:,4)))));
dVCdt_5 = diff(nonzeros(tVC(:,5))) ./...
          diff(tt(1:length(nonzeros(tVC(:,5)))));
dTCEdt_1 = diff(nonzeros(tTCE(:,1))) ./...
           diff(tt(1:length(nonzeros(tTCE(:,1)))));
dTCEdt_2 = diff(nonzeros(tTCE(:,2))) ./...
           diff(tt(1:length(nonzeros(tTCE(:,2)))));
dTCEdt_3 = diff(nonzeros(tTCE(:,3))) ./...
           diff(tt(1:length(nonzeros(tTCE(:,3)))));
dTCEdt_4 = diff(nonzeros(tTCE(:,4))) ./...
           diff(tt(1:length(nonzeros(tTCE(:,4)))));
dTCEdt_5 = diff(nonzeros(tTCE(:,5))) ./...
           diff(tt(1:length(nonzeros(tTCE(:,5)))));
dDCEdt_1 = diff(nonzeros(tDCE(:,1))) ./...
           diff(tt(1:length(nonzeros(tDCE(:,1)))));
dDCEdt_2 = diff(nonzeros(tDCE(:,2))) ./...
           diff(tt(1:length(nonzeros(tDCE(:,2)))));
dDCEdt_3 = diff(nonzeros(tDCE(:,3))) ./...
           diff(tt(1:length(nonzeros(tDCE(:,3)))));
dDCEdt_4 = diff(nonzeros(tDCE(:,4))) ./...
           diff(tt(1:length(nonzeros(tDCE(:,4)))));
dDCEdt_5 = diff(nonzeros(tDCE(:,5))) ./...
           diff(tt(1:length(nonzeros(tDCE(:,5)))));
dProdt_1 = diff(nonzeros(tPro(:,1))) ./...
           diff(tt(1:length(nonzeros(tPro(:,1)))));
dProdt_2 = diff(nonzeros(tPro(:,2))) ./...
           diff(tt(1:length(nonzeros(tPro(:,2)))));
dProdt_3 = diff(nonzeros(tPro(:,3))) ./...
           diff(tt(1:length(nonzeros(tPro(:,3)))));
dProdt_4 = diff(nonzeros(tPro(:,4))) ./...
           diff(tt(1:length(nonzeros(tPro(:,4)))));
dProdt_5 = diff(nonzeros(tPro(:,5))) ./...
           diff(tt(1:length(nonzeros(tPro(:,5)))));

% Saves values into species specific matrices
dTCEdt = [dTCEdt_1,dTCEdt_2,dTCEdt_3,dTCEdt_4,dTCEdt_5];
dDCEdt = [dDCEdt_1,dDCEdt_2,dDCEdt_3,dDCEdt_4,dDCEdt_5];
dVCdt = [dVCdt_1,dVCdt_2,dVCdt_3,dVCdt_4,dVCdt_5];
dProdt = [dProdt_1,dProdt_2,dProdt_3,dProdt_4,dProdt_5];

% Starts check for each species at each time spacial point
% Tolerance can be changed as needed
for i = 1:5

    % Check if trichloroethylene is at steady state
    if isempty(dTCEdt) == 1
    % If not empty checks if at SS
    elseif length(dTCEdt(:,i)) > 1
        if dTCEdt(length(dTCEdt(:,i)),i) < 1E-5...
           && dTCEdt(length(dTCEdt(:,i))-1,i) > 1E-5
           SS(i,1) = 1; % SS_TCE
        end
```

```
            end

            % Check if cis-dichloroethylene is at steady state
            if isempty(dDCEdt) == 1
            % If not empty checks if at SS
            elseif length(dDCEdt(:,i)) > 1
                if dDCEdt(length(dDCEdt(:,i)),i) < 1E-5...
                   && dDCEdt(length(dDCEdt(:,i))-1,i) > 1E-5
                   SS(i,2) = 1; % SS_DCE
                end
            end

            % Check if vinyl chloride is at steady state
            if isempty(dVCdt) == 1
            % If not empty checks if at SS
            elseif length(dVCdt(:,i)) > 1
                if dVCdt(length(dVCdt(:,i)),i) < 1E-5...
                   && dVCdt(length(dVCdt(:,i))-1,i) > 1E-5
                   SS(i,3) = 1; % SS_VC
                end
            end

            % Check if pH is at steady state
            if isempty(dProdt) == 1
            % If not empty checks if at SS
            elseif length(dProdt(:,i)) > 1
                if dProdt(length(dProdt(:,i)),i) > -1E-5...
                   && dProdt(length(dProdt(:,i))-1,i) < -1E-5
                   SS(i,4) = 1; % SS_Pro
                end
            end

        end % end of for loop (steady state check)

        % Array for steady state determination
        % Exits time loop if all values of SS equal one.
        if SS(:) == 1;
        break
        end
    end % end of if loop (final save/check)
end  % end of time loop

%% Reconfigure final values in tx to remove unused space
tt = tt(1:(length(dVCdt(:,1))+1)); % Sets tt to size of dVCdt plus one
tTCE = nonzeros(tTCE);        % Removes all unused space in matrix (zeros)
tTCE = reshape(tTCE,length(tt),5); % Reconfig to five columns of equal size
tDCE = nonzeros(tDCE);
tDCE = reshape(tDCE,length(tt),5);
tVC = nonzeros(tVC);
tVC = reshape(tVC,length(tt),5);
tPro = nonzeros(tPro);
tPro = reshape(tPro,length(tt),5);

%% Ploting results
% Stops plot from opening a window
```

```
figure('Visible','off');

subplot(3,2,1)
hold off;
plot(rr,CAH(:,1));
xlabel("dimensionless radius"); ylabel("CAH conc. (mM)");
hold on;
plot(rr,CAH(:,2));
plot(rr,CAH(:,3));
legend("TCE","cDCE","VC");

hold off
subplot(3,2,2)
plot(tt,tTCE(:,1),'b');
xlabel("time(days)"); ylabel("TCE conc. (mM)");
hold on;
plot(tt,tTCE(:,2),'r');
plot(tt,tTCE(:,3),'c');
plot(tt,tTCE(:,4),'k');
plot(tt,tTCE(:,5),'g');
labelstring = {num2str(rt(1)),num2str(rt(2)),num2str(rt(3)),...
               num2str(rt(4)),num2str(rt(5))};
legend(labelstring);

hold off;
subplot(3,2,3)
plot(tt,tDCE(:,1),'b');
xlabel("time(days)"); ylabel("cDCe conc. (mM)");
hold on;
plot(tt,tDCE(:,2),'r');
plot(tt,tDCE(:,3),'c');
plot(tt,tDCE(:,4),'k');
plot(tt,tDCE(:,5),'g');
labelstring = {num2str(rt(1)),num2str(rt(2)),num2str(rt(3)),...
               num2str(rt(4)),num2str(rt(5))};
legend(labelstring);

hold off;
subplot(3,2,4)
plot(tt,tVC(:,1),'b');
xlabel("time(days)"); ylabel("VC conc. (mM)");
hold on;
plot(tt,tVC(:,2),'r');
plot(tt,tVC(:,3),'c');
plot(tt,tVC(:,4),'k');
plot(tt,tVC(:,5),'g');
labelstring = {num2str(rt(1)),num2str(rt(2)),num2str(rt(3)),...
               num2str(rt(4)),num2str(rt(5))};
legend(labelstring);
hold off;

subplot(3,2,5)
plot(tt,tPro(:,1),'b');
xlabel("time(days)"); ylabel("pH");
hold on;
plot(tt,tPro(:,2),'r');
```

```
plot(tt,tPro(:,3),'c');
plot(tt,tPro(:,4),'k');
plot(tt,tPro(:,5),'g');
labelstring = {num2str(rt(1)),num2str(rt(2)),num2str(rt(3)),...
               num2str(rt(4)),num2str(rt(5))};
legend(labelstring);
hold off;

%% Write and saves datafiles and figures

% Generates todays date for *.mat file name
filedate = datetime('today');
% Creates a folder named 'CAH_Cluster_Results' to save data to
mkdir('CAH_Cluster_Results')
% Sets path to save data to folder just created in the current directory
pathname = fullfile(cd,'CAH_Cluster_Results','/');

% Sets variable type for file names (n,m,data,R,unit,pwr,scales)
formatSpec = "%d,%c,%d,%c,%s,%c,%0.4f,%c,%d,%c,%0.4f,%c,%d,%s";

% Generates *.mat file name
matfile = fullfile(pathname,erase(sprintf(formatSpec, n, "-", m, "-",...
          filedate, "-",R, "-",unit, "-",pwr, "-",scales,".mat"),','));
% Saves *.mat file in designated path
save(matfile);

% Generates *.fig file name
figfile = fullfile(pathname,erase(sprintf(formatSpec, n, "-", m, "-",...
          filedate, "-",R, "-",unit, "-",pwr, "-",scales, ".fig"),','));
% Saves *.fig file in designated path
savefig(figfile);

close all  % closes figure window
```

C.2 How to Submit Jobs to the RCDS Cluster

This SOP is for compiled MATLAB code only. IBEST servers can run MATLAB, but those procedures are not discussed here.

IBEST servers use Linux, so any compiled MATLAB code used on this server must be compiled on a Linux machine. If compiled on windows or a MAC, the application will not run.

For additional tutorials go to: https://www.hpc.uidaho.edu/compute/Tutorials/

Any questions about the servers can be sent to comp-core@uidaho.edu

Prerequisite software for access to the IBEST servers: Microsoft (bitvise ssh client), Mac (Terminal)

1. Log into IBEST servers
    a. Using a command line terminal type:
    ssh ADusername@fortyfour.ibest.uidaho.edu
        i. Replace "ADusername" with your UIdaho username
        ii. fortyfour is the head node, so if you plan on submitting multiple jobs using Slurm, this is the node to use. If you wish to run a single job, use the standalone server "trillian" since it is the only standalone server with MATLAB Runtime installed (as of December 2021). To log into trillian, replace "fortyfour" in the above command to "trillian".
    b. If this is your first-time logging into any server, you will be asked if you want to "continue connecting."
        i. Type "yes" then press [ENTER]
        ii. Then type your password and press [ENTER]
    c. Move files from your local computer to the IBEST servers:
        i. If using a windows computer, download bitvise.
            1. This program allows you to transfer files from your local computer to the server and also will open a terminal window that allows access to both.
        ii. If using a Mac, download cyberduck.
            1. This program allows you to transfer files from your local computer to the server directly from an app.
2. Identifying key files and running the compiled code in a single job.
    a. When you compile your MATLAB code, a folder is created with three additional folders inside. The only one you need to interact with is the folder labeled "for_redistribution_files_only".
        i. This folder includes the compiled application with your code (a *.exec file in Linux), a readme file, a shell (*.sh) file with which you can run the application, and icon pictures.
            1. Move the *.exec and *.sh files to the IBEST server as discussed previously in step 1c.
    b. Once all files are in the current directory you will need to modify the app, *.sh, and *.csv files so that the server reads them properly.
        i. To make the app and *.sh file executable run these commands:

1. chmod +x filename.sh
2. chmod +x filename.app

ii. When transferring *.csv files from another operating system to linux, numbers in a *.csv file will have a "^M" character, which can cause many errors in the code.

1. First check if "^M" character is present in the *.csv file.
    a. cat -v filename.csv
2. If the "^M" is present, type
    a. vi filename.csv [ENTER]
    b. :e ++ff=dos [ENTER]
    c. :set ff=unix [ENTER]
    d. :wq [ENTER]

c. Once the application, *.sh, and *.csv file are in your current directory and in the proper format, you can run the application for a single iteration by typing:

./ShellFileName.sh /usr/local/MATLAB/MATLAB_Runtime/v910 R units pwr scales

i. R, units, pwr, and scales are individual input arguments of the CAH code function. Put a space between each variable.

1. These variables should be typed here as numbers or variables (e.g., $variable)

ii. The runtime version must correspond to the version of MATLAB used to compile the code. MATLAB_R2021a corresponds to v910 of MATLAB runtime.

3. Running compiled code on the cluster nodes using the ***fortyfour*** server.
    a. Use the cluster (fortyfour) if you want to run multiple iterations using the same application.
    b. The cluster uses a scheduling software called Slurm to organize the computational requirements of each job and node.
    c. Go to the tutorials page linked above for a tutorial on using Slurm to run applications. Multiple options are available and can be used to fit your computational needs.
    d. Unlike in the standalone server, you will need to create a separate *.slurm file to run your application.
        i. Start each *.slurm file with: #!/bin/bash

1. Must be on the first line of the script file or you will get an error.

ii. You can specify options within Slurm to tell the software how you want to run your application. Here are some examples:
    1. For jobs with multiple iterations (example of 20 iterations):
        a. #SBATCH – array=1-20
        b. If you only want to run 2 iterations at a time (20 iterations, but only 2 iterations will run at one time):
            i. #SBATCH – array=1-20%2
    2. To allocate how many nodes will be used per job (usually just one)
        a. #SBATCH --cpus-per-task=1
    3. To tell Slurm to only choose nodes with MATLAB Runtime and ceph installed:
        a. #SBATCH -C "matlab_runtime&ceph"
    4. To tell Slurm to only choose nodes with a set memory allocation (20 GB in this example):
        a. #SBATCH --mem=20G
    5. To tell Slurm to only run jobs on the long partition (The long partition has no time limit. The default partition will time out after 7 days):
        a. #SLURM -p long

iii. You can use the function readarray to read in a *.csv file with variable inputs and cycle through them using the indexing variable ${SLURM_ARRAY_TASK_ID}.
    1. NOTE: Linux uses 0 indexing so an index of 1 will actually give you the second value in an array, so modify your *.csv file accordingly.

iv. At the end of the *.slurm file, you will use the same line of code from 2b to run the application.
    1. The input variables can be sequentially organized using the array task ID variable mentioned in 3d.iii.

e. To begin a job, type: sbatch filename.slurm into the command line
    i. See the example *.slurm file in the next section (**Appendix C.3**).

C.3 Cluster Job Submission File Example

The file detailed below can be saved as a *.slurm file to be run on the IBEST serves as described in the SOP in **Appendix C.2**.

```
#!/bin/bash

# Allocates 1 core per task
#SBATCH --cpus-per-task=1

# Will run through 200 tasks
#SBATCH --array=1-200
#SBATCH -C "matlab_runtime&ceph"
#SBATCH --requeue
#SBATCH --mem=20G
#SBATCH -p long

source /usr/modules/init/bash
module load matlab-runtime

# Data read from current directory. Made in matlab for random distribution
readarray -t r_extra < r_extra.csv
readarray -t pwr_extra < pwr_extra.csv

# Displays the input bead radius and exponentail power
echo ${pwr_extra[${SLURM_ARRAY_TASK_ID}]}
echo ${r_extra[${SLURM_ARRAY_TASK_ID}]}
# Displays the node that the iteration is started on
hostname

# run app: ./run_CAH_Code_TEST.sh <PathToRuntime> <Variables(R units pwr scales)>
# This script *.sh and the app must be in the current directory
./run_CAH_Code.sh /usr/local/MATLAB/MATLAB_Runtime/v910
${r_extra[${SLURM_ARRAY_TASK_ID}]} 1 ${pwr_extra[${SLURM_ARRAY_TASK_ID}]} 1
```

C.4 Data Collection and Analysis Code

```
% Carson Silsby 1/3/21
% Based on 'ComparisonDiffusionChangesv2.m' created by Dr. James Moberly
close all; clear all; clc;
format long
%% Import Data
MY = open('160000000-2000-19-Jan-2022-0.0297-1-1.554800e-01-1.mat');
close all
.
.
.
BQO = open('160000000-2000-18-May-2022-0.0025-1-9.600000e+00-1.mat');
close all

%% Convert [H+] to pH
```

```
MY.pH = -log10(MY.CAH(:,4)/1000);
.
.
.
BQO.pH = -log10(BQO.CAH(:,4)/1000);

%% Calculating Flux Out and Degradation at Steady State
% Provides a list of structure arrays where data is stored. List should
% match named variables above.
MatrixID={'MY'...'BQO'};

%% Pull in Terms for Rate Laws
% TCE rate law parameters
EC50TCEpwr = MY.EC50TCEpwr;
Kstce = MY.Kstce;
Kitce = MY.Kitce;
tcePwr = MY.tcePwr;
% DCE rate law parameters
Ksdce = MY.Ksdce;
KDT = MY.KDT;
EC50DCEpwr = MY.EC50DCEpwr;
dcePwr = MY.dcePwr;
% VC rate law parameters
Ksvc = MY.Ksvc;
KVD = MY.KVD;
KVT = MY.KVT;
% pH inhibtion function constants
pH0 = MY.pH0;
pHopt_T = MY.pHopt_T;
pHopt_D = MY.pHopt_D;
pHopt_V = MY.pHopt_V;
sig_T = MY.sig_T;
sig_D = MY.sig_D;
sig_V = MY.sig_V;
N_T = MY.N_T;
N_D = MY.N_D;
N_V = MY.N_V;

%% Preallocate Empty Matricies for Flux Out of the Bead
FTCEin = zeros(length(MatrixID),1);
FDCEout = zeros(length(MatrixID),1);
FVCout = zeros(length(MatrixID),1);
FVCcon = zeros(length(MatrixID),1);
FDCEcon = zeros(length(MatrixID),1);
FProtout = zeros(length(MatrixID),1);
R = zeros(length(MatrixID),1);
unit = zeros(length(MatrixID),1);
pwr = zeros(length(MatrixID),1);
scales = zeros(length(MatrixID),1);
MinpH = zeros(length(MatrixID),1);
pH1 = zeros(length(MatrixID),1);

%% Calcualting Fluxes of Each CAH and Protons
for m = 1:length(MatrixID)
   % Define variables from each *.mat file
   Matrixpick = char(MatrixID(m));
```

```
    R(m) = eval(strcat(Matrixpick,'.R'));
    rr = eval(strcat(Matrixpick,'.rr'));
    TCE = eval(strcat(Matrixpick,'.CAH(:,1)'));
    DCE = eval(strcat(Matrixpick,'.CAH(:,2)'));
    VC = eval(strcat(Matrixpick,'.CAH(:,3)'));
    Pro = eval(strcat(Matrixpick,'.CAH(:,4)'));
    pH = eval(strcat(Matrixpick,'.pH'));
    pH1(m) = pH(end);
    dt = eval(strcat(Matrixpick,'.dt'));
    ktce = eval(strcat(Matrixpick,'.ktce'))/dt;
    kdce = eval(strcat(Matrixpick,'.kdce'))/dt;
    kvc = eval(strcat(Matrixpick,'.kvc'))/dt;
    deltar = eval(strcat(Matrixpick,'.dr'));
    unit(m) = eval(strcat(Matrixpick,'.unit'));
    pwr(m) = eval(strcat(Matrixpick,'.pwr'));
    scales(m) = eval(strcat(Matrixpick,'.scales'));
    rateTCE = zeros(length(rr),1);
    rateDCE = zeros(length(rr),1);
    rateVC = zeros(length(rr),1);
    ratePro = zeros(length(rr),1);
    Ftcein = zeros(length(rr),1);
    Fdceconsume = zeros(length(rr),1);
    Fvcconsume = zeros(length(rr),1);
    Fprotgen = zeros(length(rr),1);

    % Calculate rates and flux of each CAH and protons
    for r = 1:length(rr)
     radius = rr(r);
     rateTCE(r) = ktce*TCE(r) /...
                  ((Kstce + TCE(r))*(1+EC50TCEpwr*TCE(r)^tcePwr)) *...
                  exp(-abs(pHopt_T - pH(r))^N_T/sig_T^2);
     rateDCE(r) = kdce*DCE(r) / ((Ksdce+KDT*TCE(r)+DCE(r))*...
                  (1+EC50DCEpwr*DCE(r)^dcePwr))* ...
                  exp(-abs(pHopt_D - pH(r))^N_D/sig_D^2);
     rateVC(r) = kvc*VC(r) / (Ksvc + KVD*DCE(r) + KVT*TCE(r) + VC(r)) *...
                 exp(-abs(pHopt_D - pH(r))^N_D/sig_D^2);
     ratePro(r) = rateTCE(r) + rateDCE(r) + rateVC(r);

     % Rate TCE is consumed at R = r
     Ftcein(r) = rateTCE(r)*4*pi()*(radius^2)*deltar;
     % Rate DCE is consumed at R = r
     Fdceconsume(r) = rateDCE(r)*4*pi()*(radius^2)*deltar;
     % Rate VC is consumed at R = r
     Fvcconsume(r) = rateVC(r)*4*pi()*(radius^2)*deltar;
     % Rate Protons are generated at R = r
     Fprotgen(r) = ratePro(r)*4*pi()*(radius^2)*deltar;
    end

    % Total amounts fluxed at steady state (mM/day)
    FTCEin(m) = sum(Ftcein); % TCE consumed = DCE generated
    FDCEcon(m) = sum(Fdceconsume); % DCE consumed = VC generated
    FVCcon(m) = sum(Fvcconsume); % VC consumed = Ethylene generated
    FDCEout(m) = FTCEin(m) - FDCEcon(m); % DCE generated - DCE consumed
    FVCout(m) = FDCEcon(m) - FVCcon(m); % VC generated - VC consumed
    FProtout(m) = sum(Fprotgen); % Protons generated
end
```

```
%% Compiling and Archiving Data
DataOut = [R pwr pH1 FVCcon./FTCEin FDCEcon./FTCEin...
           FDCEout./FTCEin FVCout./FTCEin];

DataOut = sortrows(DataOut,[1,2]);

% Save variables listed in DataOut.csv
writematrix(DataOut,'DataOut.csv')

% For Diffusion limited (Goldilocks Scenario A) - saving APJ
% r = 0.08943 dm pwr = 10.6
Difflim = [APJ.CAH(:,1),APJ.CAH(:,2),APJ.CAH(:,3),APJ.pH,APJ.rr./APJ.R];
% For Reaction limited (Goldilocks Scenario B) - saveing AAU
% r = 0.00491 dm pwr = 0.66665
Reaclim = [AAU.CAH(:,1), AAU.CAH(:,2),AAU.CAH(:,3),AAU.pH,AAU.rr./AAU.R];
% For Balanced (Goldilocks Scenario C) - saving AFA
% r = 0.0526 dm pwr = 6.5543
Balanced = [AFA.CAH(:,1),AFA.CAH(:,2),AFA.CAH(:,3),AFA.pH,AFA.rr./AFA.R];

% Saving data for Goldilocks scenarios
writematrix(Difflim,'Difflim.csv')
writematrix(Reaclim,'Reaclim.csv')
writematrix(Balanced,'Balanced.csv')

%% Plot Point Distribtuion
figure(1)
scatter(R,pwr)
```

Appendix D - R Code Used for Statistical Analysis

R was used for statistical analysis of the data presented in Chapter 2 and Chapter 3.

D.1 Chapter 2 Statistical Analysis

Reads in data from csv file (data initially stored in ORIGIN)

data <- read.csv("/Users/CarsonSilsby/Desktop/Grad_school/Classes/STAT507/Fig6Data.csv", header = TRUE)

data

protonF6 <- data.frame(data)

rm(data)

Open required packages

library(car)

library(phia)

```
library(afex)
library(multcomp)
library(emmeans)

# Denotes membrane type, crosslinking method, and ionic strength as factors
# 1 = 10% PVA, 2 = 10% PVA / 2% Alg
protonF6$Membrane <- as.factor(protonF6$Membrane)
# Cryo = Freeze / Thaw, Chem = Chemical
protonF6$Treatment <- as.factor(protonF6$Treatment)
# Ionic strength in units of Molarity
protonF6$Ionic.Strength <- as.factor(protonF6$Ionic.Strength)
# Multiply De by 1E5 to rescale for R (without - calculates residuals to be 0)
protonF6$De <- protonF6$De*1e5

# Creates a linear model for the given data
protonF6.lm <- lm(De ~ Membrane + Treatment + Ionic.Strength + Membrane:Treatment + Membrane:Ionic.Strength + Treatment:Ionic.Strength + Membrane:Treatment:Ionic.Strength, data=protonF6)

# Creates a type 2 ANOVA table
Anova(protonF6.lm,type="II")

# Test model assumptions
x11()
par(mfrow=c(2,2))
plot(protonF6.lm)
par(mfrow=c(1,1))

# Box Cox analysis
x11()
boxcox(De ~ Membrane*Treatment*Ionic.Strength, data=protonF6, lambda=seq(-2.00, 2.00, length = 50))
```

```
# Transform data with near optimal option: 0.5
protonF6$transDe <- sqrt(protonF6$De)

# Redo ANOVA analysis with transformed data
protonF6.lm2 <- lm(transDe ~ Membrane + Treatment + Ionic.Strength + Membrane:Treatment + Membrane:Ionic.Strength + Treatment:Ionic.Strength + Membrane:Treatment:Ionic.Strength, data=protonF6)
Anova(protonF6.lm2,type="II")

# Reassess model assumptions
x11()
par(mfrow=c(2,2))
plot(protonF6.lm2)
par(mfrow=c(1,1))

## Generate interaction plots
x11()
interaction.plot(protonF6$Treatment,protonF6$Ionic.Strength,protonF6$transDe,type="b")
x11()
interaction.plot(protonF6$Membrane,protonF6$Treatment,protonF6$transDe,type="b")
x11()
interaction.plot(protonF6$Membrane,protonF6$Ionic.Strength,protonF6$transDe,type="b")

## Compare Membrane and Treatment at different ionic strengths
protonF6_0.001M   <- subset(protonF6, Ionic.Strength == "0.001")
protonF6_0.01M   <- subset(protonF6, Ionic.Strength == "0.01")
protonF6_0.1M   <- subset(protonF6, Ionic.Strength == "0.1")
protonF6_0.5M   <- subset(protonF6, Ionic.Strength == "0.5")
protonF6_1M   <- subset(protonF6, Ionic.Strength == "1")
x11()
```

```
par(mfrow=c(3,2))

interaction.plot(protonF6_0.001M$Membrane,protonF6_0.001M$Treatment,protonF6_0.001M$De,type="b",main="0.001 M")

interaction.plot(protonF6_0.01M$Membrane,protonF6_0.01M$Treatment,protonF6_0.01M$De,type="b",main="0.01 M")

interaction.plot(protonF6_0.1M$Membrane,protonF6_0.1M$Treatment,protonF6_0.1M$De,type="b",main="0.1 M")

interaction.plot(protonF6_0.5M$Membrane,protonF6_0.5M$Treatment,protonF6_0.5M$De,type="b",main="0.5 M")

interaction.plot(protonF6_1M$Membrane,protonF6_1M$Treatment,protonF6_1M$De,type="b",main="1 M")


## Compare Treatment and Ionic Strength at different membrane types

protonF6_PVA   <- subset(protonF6, Membrane == "1")

protonF6_PVA_Alg   <- subset(protonF6, Membrane == "2")

x11()

par(mfrow=c(1,2))

interaction.plot(protonF6_PVA$Ionic.Strength,protonF6_PVA$Treatment,protonF6_PVA$De,type="b",main="PVA")

interaction.plot(protonF6_PVA_Alg$Ionic.Strength,protonF6_PVA_Alg$Treatment,protonF6_PVA_Alg$De,type="b",main="PVA-Alg")


## Compare Membrane and Ionic Strength with different crosslinking methods

protonF6_Chem <- subset(protonF6, Treatment == "Chem")

protonF6_Cryo <- subset(protonF6, Treatment == "Cryo")

x11()

par(mfrow=c(1,2))

interaction.plot(protonF6_Chem$Ionic.Strength,protonF6_Chem$Membrane,protonF6_Chem$De,type="b",main="Chem")

interaction.plot(protonF6_Cryo$Ionic.Strength,protonF6_Cryo$Membrane,protonF6_Cryo$De,type="b",main="Cryo")


par(mfrow=c(1,1))
```

```
## ANOVA tables determining significance of ionic strength on PVA and PVA/Alg hydrogels
# Cryogels
protonF6_PVA_Cryo <- subset(protonF6_PVA, Treatment =="Cryo")
protonF6_PVA_Cryo.lm <- lm(De ~ Ionic.Strength, data=protonF6_PVA_Cryo)
Anova(protonF6_PVA_Cryo.lm,type="II")
protonF6_PVA_Alg_Cryo <- subset(protonF6_PVA_Alg, Treatment =="Cryo")
protonF6_PVA_Alg_Cryo.lm <- lm(De ~ Ionic.Strength, data=protonF6_PVA_Alg_Cryo)
Anova(protonF6_PVA_Alg_Cryo.lm,type="II")

# Chemically crosslinked
protonF6_PVA_Chem <- subset(protonF6_PVA, Treatment =="Chem")
protonF6_PVA_Chem.lm <- lm(De ~ Ionic.Strength, data=protonF6_PVA_Chem)
Anova(protonF6_PVA_Chem.lm,type="II")
protonF6_PVA_Alg_Chem <- subset(protonF6_PVA_Alg, Treatment =="Chem")
protonF6_PVA_Alg_Chem.lm <- lm(De ~ Ionic.Strength, data=protonF6_PVA_Alg_Chem)
Anova(protonF6_PVA_Alg_Chem.lm,type="II")

# Cryo vs Chem
protonF6_PVA.lm <- lm(De ~ Treatment + Ionic.Strength + Treatment:Ionic.Strength,
data=protonF6_PVA)
Anova(protonF6_PVA.lm,type="II")
protonF6_PVA_Alg.lm <- lm(De ~ Treatment + Ionic.Strength + Treatment:Ionic.Strength,
data=protonF6_PVA_Alg)
Anova(protonF6_PVA_Alg.lm,type="II")

# Print versions for each package used and software
version
citation()
packageVersion('car')
citation(package = "car")
packageVersion('multcomp')
```

```
citation(package = "multcomp")
packageVersion('phia')
citation(package = "phia")
packageVersion('afex')
citation(package = "afex")
packageVersion('emmeans')
citation(package = "emmeans")
```

D.2 Chapter 3 Statistical Analysis

```
# Reads in data from csv file (data initially stored Compiled_Des_Carson.xlsx)
data <- read.csv("/Users/CarsonSilsby/Desktop/OneDrive - University of Idaho/NSF biobead/CAH-paper/CAH_De_Data.csv", header = TRUE)
data

Diff <- data.frame(data)
rm(data)

# Open required packages
library(multcomp)

# Denotes membrane type, diffusing species, and ionic strength as factors
# 1 = 10% PVA, 2 = 10% PVA / 2% Alg
Diff$Membrane <- as.factor(Diff$Membrane)
Diff$CAH <- as.factor(Diff$CAH)
# Ionic strength in units of Molarity
Diff$Ionic.Strength <- as.factor(Diff$Ionic.Strength)
# Multiply De by 1E5 to rescale for R (without - calculates residuals to be 0)
Diff$De <- Diff$De*1e5

# Creates a linear model for the given data
Diff.lm <- lm(De ~ CAH + Ionic.Strength + CAH:Ionic.Strength, data=Diff)
```

```
# Creates a type 2 ANOVA table
Anova(Diff.lm,type="II")

# Test model assumptions
x11()
par(mfrow=c(2,2))
plot(Diff.lm)
par(mfrow=c(1,1))

# Box Cox analysis
boxcox(De ~ CAH*Ionic.Strength, data=Diff, lambda=seq(-2.00, 2.00, length = 50))

## Create subsets for each group set
# TCE
Diff_TCE <- subset(Diff, CAH =="TCE")
Diff_TCE_0 <- subset(Diff_TCE, Ionic.Strength == "0")
Diff_TCE_001 <- subset(Diff_TCE, Ionic.Strength == "0.001")
Diff_TCE_01 <- subset(Diff_TCE, Ionic.Strength == "0.01")
# DCE
Diff_DCE <- subset(Diff, CAH =="DCE")
Diff_DCE_0 <- subset(Diff_DCE, Ionic.Strength == "0")
Diff_DCE_001 <- subset(Diff_DCE, Ionic.Strength == "0.001")
Diff_DCE_01 <- subset(Diff_DCE, Ionic.Strength == "0.01")
# VC
Diff_VC <- subset(Diff, CAH =="VC")
Diff_VC_0 <- subset(Diff_VC, Ionic.Strength == "0")
Diff_VC_001 <- subset(Diff_VC, Ionic.Strength == "0.001")
Diff_VC_01 <- subset(Diff_VC, Ionic.Strength == "0.01")
```

```
## 2 sample t-tests for relevant combinations
# TCE 0M to TCE 0.01M
t.test(Diff_TCE_0$De, Diff_TCE_01$De, var.equal = TRUE)
# DCE 0M to DCE 0.01M
t.test(Diff_DCE_0$De, Diff_DCE_01$De, var.equal = TRUE)
# VC 0M to VC 0.01M
t.test(Diff_VC_0$De, Diff_VC_01$De, var.equal = TRUE)
# TCE 0M to DCE 0M
t.test(Diff_TCE_0$De, Diff_DCE_0$De, var.equal = TRUE)
# TCE 0.01M to DCE 0.01M
t.test(Diff_TCE_01$De, Diff_DCE_01$De, var.equal = TRUE)
# DCE 0M to VC 0M
t.test(Diff_DCE_0$De, Diff_VC_0$De, var.equal = TRUE)
# DCE 0.001M to VC 0.001M
t.test(Diff_DCE_001$De, Diff_VC_001$De, var.equal = TRUE)
# DCE 0.01M to VC 0.01M
t.test(Diff_DCE_01$De, Diff_VC_01$De, var.equal = TRUE)

# Adjusting p-values using ...
pvals <- c(0.001179, 0.004149, 0.03096, 0.004579, 0.008988, 0.5234, 0.6072, 0.3944)
p.adjust(pvals, "holm")

# Print versions for each package used and software
version
citation()
packageVersion('multcomp')
citation(package = "multcomp")
```